Alma Mater Studiorum – Università di Bologna

DOTTORATO DI RICERCA IN

SCIENZE CARDIO NEFRO TORACICHE

Ciclo XXXIII

Settore Concorsuale: 06/D2 - ENDOCRINOLOGIA, NEFROLOGIA E SCIENZE DELL'ALIMENTAZIONE E DEL BENESSERE

Settore Scientifico Disciplinare: MED/14 - NEFROLOGIA

In vivo evaluation of renal function using intravital multiphoton microscopy on rats and mice with induced or spontaneous renal injury

Presentata da: Dott. Vincenzo Costanzo

Coordinatore Dottorato

Prof. Gaetano Domenico Gargiulo

Supervisore

Prof. Gaetano La Manna

Esame finale anno 2021

First of all, I would like to express my gratitude to Biogem research center (Ariano Irpino, AV) and to its President, Prof. Ortensio Zecchino for giving me the possibility to carry out my PhD project in this exciting work environment. I performed most of my experiments in the laboratory of translational nephrology at Biogem, where I had the opportunity to work and discuss with national and international researchers, improving my scientific knowledge, technical abilities and communication skills. This increased my motivations and ambitions and represents a good start for my scientific career in the research field.

I am also placed to thank Prof. Emmanuele F.M. Emanuele, President of "Fondazione Terzo Pilastro-Internazionale", for his unlimited support, which allowed the purchase of the innovative 2-photon microscopy. Thanks to this generous gift, it has been possible to investigate in real time the dynamic renal processes in health and diseases in animal models, opening the way for future studies that aim to find new pharmacological targets suitable for human renal diseases.

FONDAZIONE TERZO PILASTRO
INTERNAZIONALE

I also want to thank Prof. Gaetano La Manna, my supervisor, for his availability and reliability demonstrated during these years of my PhD. I feel honored and proud to have completed this important step of my scientific formation in the prestigious University of Bologna under his supervision.

I am also very grateful to Prof. Sebastian Frische for all the support I received during my period at Aarhus University (Aarhus, Denmark), Department of Biomedicine, as visiting researcher. I am so proud to have worked in his international research group where I acquired important skills that will be helpful for my scientific career.

A particular acknowledgment goes to University of Campania "Luigi Vanvitelli", Prof. Giovambattista Capasso and Prof. Francesco Trepiccione, who co-supervised my work activities at Biogem center. I started to work in the translational nephrology laboratory of Prof. Capasso since 2015, when I only was a master student. From the beginning they gave me trust and great opportunities, teaching me to be responsible and how to solve problems. I am honored to have carried out my PhD project in their cutting-edge laboratory, working on exciting international projects under their supervision.

In the end, I want to thank my family and my girlfriend, Emanuela, who always believed in me and encouraged me every day to do my best and not to give up. This thesis would not have been possible without their trust and support.

Index

ABSTRACT

Multiphoton microscopy is a powerful tool for the *in vivo* imaging of renal processes thanks to the improved tissue penetration and the high spatial and temporal resolution. Intravital imaging permits to evaluate dynamic processes and pathophysiological parameters in real time using non-invasive methods. In this way multiphoton microscopy overcomes the limitations represented by previous approaches, such as confocal microscopy, becoming the technique of choice for the study of renal function in living animals.

This project aims to use existing multiphoton microscopy approaches to evaluate *in vivo* many renal parameters in our animal models and, at the same time, to develop an original application for the assessment of single nephron glomerular filtration rate. In addition, a method for detection and quantification of renal fibrosis *ex vivo* was developed coupling multiphoton microscopy and machine learning-based segmentation software.

The linescan-based innovative methodology offered a great improvement in terms of temporal resolution and provided reliable values of single nephron glomerular filtration rate comparable with previous methods. The validation of this approach was carried out measuring renal filtration in low-dose dopamine and ischemic treated rats, which showed significantly higher and lower values of single nephron glomerular filtration rate, respectively, compared to the control group.

The dynamic process of renal glucose reabsorption was elucidated in GLUT2 cKO mice mimicking the Fanconi Bickel Syndrome. Intravital multiphoton microscopy of the renal tubules after the continuous infusion of fluorescent 2-NBDG demonstrated an impaired utilization of glucose in these mice compared to the control. Thus, the presence of GLUT2 transporter in renal proximal tubules is fundamental to ensure the physiological mechanism of glucose uptake.

Moreover, the high temporal resolution of intravital microscopy allowed to monitor over the time the beta-lactoglobulin uptake in mice proximal tubules, permitting to observe and clarify in detail the mechanism of renal protein reabsorption.

We also developed a novel approach based on second harmonic generation tool provided by the multiphoton microscopy and a machine learning-based segmentation software to detect and quantify renal fibrosis in kidney slices. This application provided great specificity and 3D reconstruction of the fibrotic signal detected as well as high reproducibility of the analysis due to an automatic machine learning algorithm, showing promising application as diagnostic and prognostic tool in human diseases.

These multiphoton applications highlighted the great potential of intravital microscopy to elucidate in real time the mechanisms involved in renal pathophysiology at cellular and subcellular resolution.

1. AIM OF THESIS

The kidney is a very complex organ constituted by more than 10 cell types and accomplish a multitude of fundamental processes. In the last decades many approaches and microscopy techniques have been developed and improved in order to understand the mechanisms underline renal physiology.

MPM represents the gold standard approach to study kidney pathophysiology in tissues and organs of living animals at cellular and subcellular resolution thanks to the higher tissue penetration and less phototoxicity. Recent advances regarding optics, new fluorescent dyes, transgenic animals and analysis methods allowed investigators to enhance MPM approaches, making the data analysis and interpretation of results more reliable.

In this project we aimed to use different MPM image techniques to study *in vivo* the main renal parameters in control and disease animal models.

The existing imaging method for the assessment of SNGFR developed by Kang et al. is limited in terms of temporal resolution when full frames are acquired, limiting the reliability of the measurements. For this purpose, we aimed to develop a new imaging approach in rats to improve the temporal resolution and accuracy of the SNGFR measurements. To demonstrate the efficiency of this original method, SNGFR was measured in control, low dopamine-treated and ischemic rats.

In addition, we performed experiments to elucidate *in vivo* the renal glucose uptake in conditional GLUT2 knock out mice. This mouse model was generated in our laboratory to mimic and study the human Fanconi-Bickel syndrome (FBS), a rare autosomal recessive disease characterized by hepatorenal glucose accumulation, disfunctions of proximal tubule and altered function of glucose. In order to complete the characterization of this murine model, we investigated in real time the tubular transport of glucose with MPM.

Moreover, we wanted to clarify *in vivo* the mechanism underlying the protein reabsorption across the renal proximal tubule. For this purpose, we imaged and quantified the constant uptake of beta-lactoglobulin in mice kidneys, showing the reliability of this technique.

Finally, we worked on the development of a method to quantify *ex vivo* the renal fibrosis using MPM. Interstitial tubular fibrosis, characterized by excessive deposition of extra-cellular matrix, is an important prognostic and diagnostic marker of kidney injury in many diseases, such as diabetes and systemic hypertension. By using MPM, we visualized the renal parenchyma through emission of autofluorescence and any collagen deposits (type I and III collagen) thanks to the "Second Harmonic Generation". After the acquisition of kidney sections, we proceeded with fibrosis quantification by using an algorithm of machine learning that permits to have more reproducible results.

2. ASSESSING A METHOD FOR SNGFR MEASUREMENT

2.1 INTRODUCTION

2.1.1 The glomerular filtration barrier

The first step in urine production is the ultrafiltration of blood plasma by renal glomeruli. This process leads to the formation of a fluid, called glomerular filtrate, which is collected in the Bowman's space to be further filtered into renal tubules. The glomerular filtrate has a solute composition similar to that in the plasma, but with reduced concentrations of proteins and high molecular weight substances, and it is free of blood cells. The amount of blood filtered per time by renal glomerulus is referred as glomerular filtration rate (GFR) and it provides a reliable parameter to measure how efficiently the kidney removes a substance from the circulation. In physiological conditions the kidneys filter about 120 mL/min of plasma, thus 180 L/day (1).

The selectively permeability of substances filtered by the glomerulus is guaranteed by the glomerular filtration barrier (GFB). GFB is a complex system composed by three elements: the endothelial cells, the glomerular basement membrane and the podocytes (Figure 1).

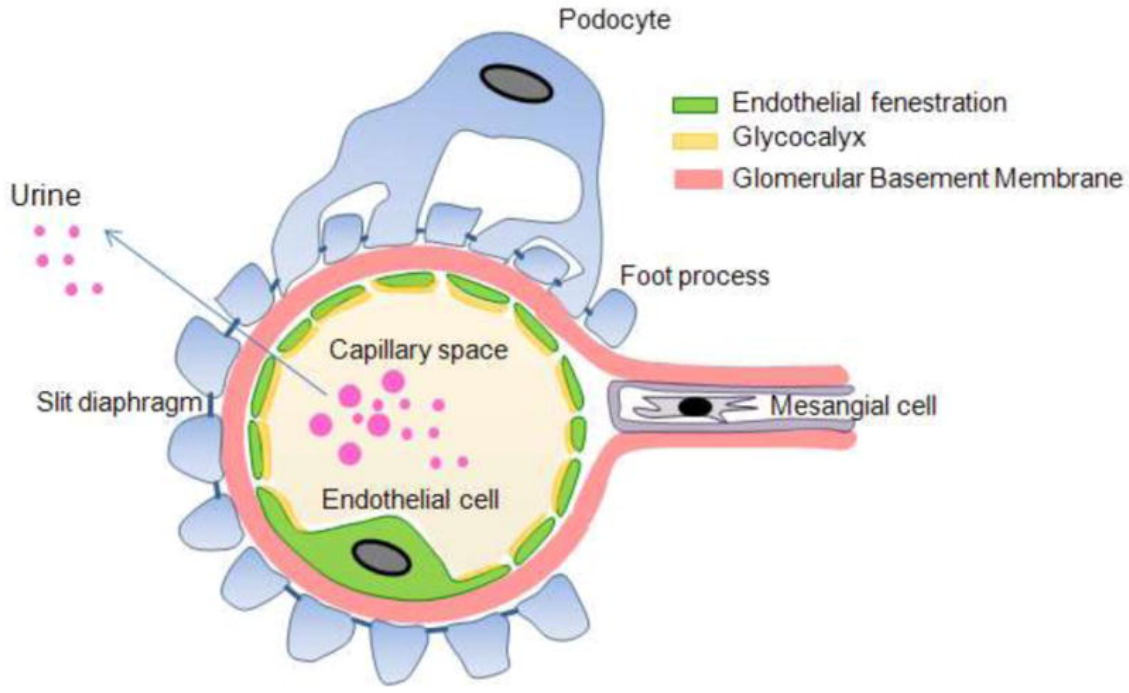

Figure 1. Representation of glomerular filtration barrier. The glomerular filtration barrier shows three main components: fenestrated endothelial cells, glomerular basement membrane and podocytes.
Arif et al., 2013.

The endothelial cells (EC) line around the vessels, working as barrier between blood and tissues. These cells are characterized by 60-70 nm fenestrations, transcellular holes localized in the cellular cytoplasm and specialized in the control of selectivity of GFB (2). The dimension of these fenestrations is not enough to restrict the passage of albumin and other plasma proteins, suggesting that glomerular capillary wall does not constitute a perfect barrier in restricting the substances. Instead, the presence of negative charged components in the glycocalyx of EC may be fundamental to regulate the permeability of GFB, allowing preferably the filtration of positive charged molecules (3, 4). Moreover, the EC may be useful to limit the filtration of cells components, including erythrocytes.

The glomerular basement membrane (GBM) is composed by extracellular matrix containing four main macromolecules: laminin, collagen IV, nidogen, and agrin (heparan sulfate proteoglycan). This membrane, which surrounds completely the endothelial cells separating the vessels from the urinary space, contributes to the permeability of the GFB. Since the high negative charge of GBM given by heparan sulfate proteoglycan, smaller size and positive charged substances move more readily into the filtrate than bigger and negative charged ones (5). Indeed, the plasma albumin is restricted by the GBM because of its negative charge. However, mutations of proteins constituting the GBM can cause severe diseases that lead to barrier abnormalities resulting in albumin and protein leakage and, in turn, kidney failure (6, 7).

Podocytes represent specialized epithelial cells of GFB that face the Bowman's capsule and the pre-urine. Podocytes have a big central cellular body, from which major processes split into numerous foot processes, which in turn project and lay on the GBM (8). The processes are connected each other by a 40 nm thin structure called slit-diaphragm, formed by nephrin, podocin and other proteins fundamental to maintain the glomerular filtration function. All these proteins form a signaling network involved in the regulation of podocytes structure and function (9). The architecture of podocytes is also characterized by actin cytoskeleton, which contributes to its morphology and function. The slit diaphragm allows the passage of water and small solutes but may selectively restrict the filtration of larger substances (10). Indeed, the negative charge of proteins covering the podocytes and the slit diaphragm, including the podoendin, help to limit the passage of large anionic molecules (11).

The filtration of substances through the GFB strongly depends by their molecular weight and radius. Small molecules, such as water, urea and glucose, filtered by the glomerulus show the same concentration as in plasma, while higher molecular weight substances including lysozyme or albumin pass more difficult in the ultrafiltrate. Electrical charge also contributes to the selectivity of renal filtration: as stated above, the negative charge of the GFB allows the cationic molecules to move more readily in the ultrafiltrate, restricting instead the anionic ones. The shape also affects the renal

permeability, since more rigid molecules seem to pass less easily compared to more deformable molecules, e.g. dextrans (12).

2.1.2 The determinants of glomerular filtration

The main driving force for the glomerular filtration is provided by the Starling forces, which regulate the fluid flow in the glomerular capillaries as well as in other vessels. The hydrostatic pressure in glomerular capillaries (PGC) and the oncotic pressure in Bowman's space (πBS) favor the ultrafiltration. On the other hand, the oncotic pressure in glomerular capillaries (πGC) and the hydrostatic pressure in Bowman's space (PBS) oppose ultrafiltration. Thus, the driving force favoring the renal ultrafiltration is the net hydrostatic force (PCG-PBS) minus the net oncotic force (πGC-πBS) (13)(Figure 2).

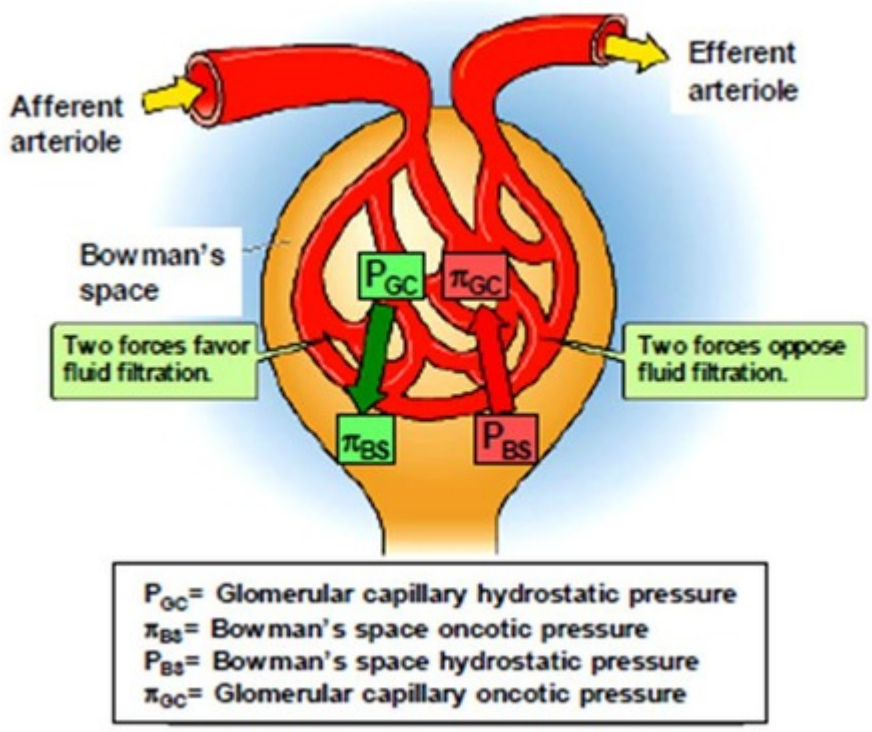

Figure 2. Forces regulating the ultrafiltration. The hydrostatic pressure in glomerular capillaries (PGC) and the oncotic pressure in Bowman's space (πBS) favor the ultrafiltration, while the oncotic pressure in glomerular capillaries (πGC) and the hydrostatic pressure in Bowman's space (PBS) oppose ultrafiltration. Adapted from Boron et al., 2012

An important parameter that affects the renal filtration is the renal blood flow (RBF), defined as the amount of blood arriving to the kidney per time unit. In physiological condition, the kidney receive

about 25% of the cardiac output, thus more than 1 L/min. The RBF is correlated to the renal plasma flow (RPF), which is the volume of plasma arriving to the kidney, and this value corresponds to about 600 mL/min. The RPF is strictly connected to renal filtration, since an increase of GFR is shown at higher value of RPF, while it decreases strongly with lowering of RPF (14). The GFR-RPF ratio describes the volume of formed filtrate derived from a certain amount of plasma entering in the glomerulus, a parameter known as filtration fraction (FF). Considering the physiological values of GFR and RPF, the FF in health is about 0,2 (14).

The GFR and RPF can undergo autoregulation mechanisms after a variation of body conditions, such as change of mean arterial pressure, allowing them to remain within acceptable limits. Two main mechanisms are involved in the renal autoregulation: myogenic response and tubule glomerular feedback (TGF). Myogenic response refers to the ability of smooth muscle cells to contract or relax according to the different changes in blood pressure: a good blood flow is preserved by the vessels contractions after a rise of blood pressure, permitting to increase the resistance of afferent arterioles (15, 16).

The TGF, instead, is a mechanism that involves the macula densa, a region of specialized epithelial cells of the thick ascending limb of loop of Henle (TAL). Together with mesangial and granular cells, macula densa form the juxtaglomerular apparatus (JGA), a complex machinery implicated in the regulation of blood pressure and release of renin. The macula densa cells, in particular, can detect an increased sodium load at the distal level thanks to NKCC2 transporter and they can compensate it increasing the arteriolar vasoconstriction and lowering the PGC and RPF. As a result, the GFR opposes to the initial raise in renal filtration, remaining within regular ranges (17, 18).

2.1.3 Assessing the renal function: GFR and SNGFR

The GFR, one of the most important renal parameters, provides a reliable measure of kidney function and it taken in account by clinicians to diagnose renal disorders or to monitor chronic renal diseases (13, 19).

Inulin is the ideal marker to estimate the renal function, since it is a substance freely filtered by the kidney and it is neither secreted nor reabsorbed by the tubules (20–22). However, it is rarely used in the clinical routine due to technical difficulties and high costs (23, 24). The clearance of creatinine, instead, is easy to calculate because it is physiologically released from the muscles and excreted by the kidney. Despite this method only requires the creatinine values in blood and urine and the day-urine output, it is not often used since creatinine is proportional to the muscle mass, causing a huge variability among patients (25). To overcome these drawbacks, the value of estimated GFR (eGFR)

is widely employed in order to monitor the progression of renal injury in many nephropathies (26, 27).

The measurement of eGFR considers many factors, such as serum creatinine, age and gender (19). According to the National Kidney Foundation's guidelines for clinical practice, a GFR higher than 90 mL/min/1.73m2 is considered normal, while values lower than 59 mL/min/1.73m2 indicate progressive renal failure (28)(Figure 3).

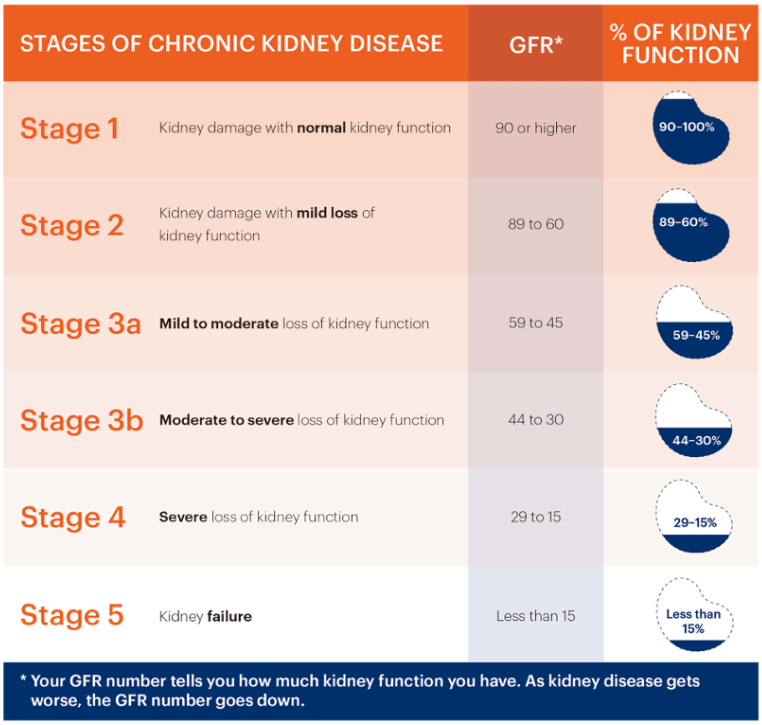

Figure 3. Staging of chronic kidney disease. Each stage indicates the specific kidney function and the corresponding GFR range. National Kidney Foundation's.

While GFR refers as the filtration function of all nephrons, the glomerular filtration rate of single nephrons (SNGFR) takes in account the individual filtration events in the kidney.

Since its discovery, the knowledge of SNGFR has become very important for researchers to evaluate the renal function, since it gives more precise information regarding the glomerulus dynamics and the determination of the mechanisms of tubular reabsorption and secretion (29). SNGFR is affected by many determinants: age (30), sex (31), number of kidneys (32), genetic background (33) and can vary according to different body conditions. In particular, SNGFR can increase after nephrons loss as a compensatory mechanism, allowing the stability of total GFR, or in consequence of the increased metabolic request (34). Indeed, in course of diabetic nephropathy whole-kidney GFR may remain stable thanks to the renal functional reserve provided by single nephrons even when extensive loss of

nephron mass is shown (<50%)(35). However, it is difficult to determine the exact relationship between nephrons loss and SNGFR changes, since the counting of human nephrons is challenging. SNGFR is influenced also by the examined site in the kidney: in fact, superficial nephrons have a lower filtration rate than deeper ones (30, 36). This proves the big morphological and functional diversity existing among nephrons. Moreover, changes in SNGFR have been observed after some conditions, such as extracellular fluid volume expansion (37) and protein-based diets (38). However, the mechanisms regulating SNGFR are not yet well known, and they could arise from the glomerular blood circulation or the macula densa cells (39). Higher SNGFR has been linked to old patients (more than 70 years), reflecting the compensatory mechanism after nephrons loss, and to patients having high body mass index (BMI) and taller than 190 cm. This could be due to the larger size of single nephrons, as shown by Denic et al (40). In addition, also other conditions have been related to SNGFR, such as patients with obesity or familiar story of end stage renal diseases showed higher SNGFR. Therefore, it is reasonable to think that these conditions represent risk factors for the development of chronic renal diseases (40, 41). There is not a gold standard method to evaluate SNGFR in humans: some investigators have recently developed an approach to calculate it, using kidney donors characteristics including total GFR, density of non-sclerotic glomeruli in biopsy samples and cortical volume of kidneys; in practice, SNGFR corresponds to the ratio between the total GFR and the total number of nephrons (34). The assessment of SNGFR in rodent models may help to provide new insights in the mechanism of glomerular filtration in health and in the adaptive changes following nephron loss.

2.1.4 Measurements of SNGFR with renal micro-puncture

Most of the knowledge regarding the renal pathophysiology has been obtained by micro-puncture studies. Many renal functions in fact, such as the ultrafiltration, the glomerular filtration barrier and the urine concentration mechanisms have been elucidated through micro-puncture.

In the 1920s, Wearn and Richards applied micro-puncture for the first time on frog kidneys, demonstrating the presence of free-protein renal ultrafiltrate in Bowman's capsule and suggesting a mechanism of selective filtration (42). In the 1930s Richards, Walker and Hudson focused their studies on renal tubules by using Amphibia (43, 44). In the 1940s, Walker et al. applied micro-puncture in mammals, in particular rats and guinea pigs, confirming the concept of renal ultrafiltration (45, 46).

Since that time, researchers have exploited and improved this technique to better understand renal function in normal and pathological conditions.

For micro-puncture experiments an adequate equipment and careful animal preparation are required, being very cautious during each technical step and in the analysis of data, in order to avoid errors (47). In particular, rats are usually anesthetized with tiobutabarbital (48), while in mice a combination of tiobutabarbital and ketamine is used (49). Then, the artery and vein are cannulated for the monitoring of blood pressure and for the infusion of experimental substances, respectively. The left kidney is then externalized through a flank incision and, after removal of fat and connective tissue, is placed in a Lucite cup for its immobilization (50). If the urine samples are required, also the bladder is cannulated. A wide range of instruments is necessary for in vivo micro-puncture studies, including a high magnification microscope, a micromanipulator for holding glass pipettes and a micro-perfusion pump. A crucial step in these experiments is the preparation of pipettes. Pipettes are made differently according to their function: those for collecting the samples must have thin but enough rigid tips, unlike those for blocking definitively the fluid flow, that have larger diameter (51). The nephron segments directly reached by the micro-puncture pipettes include the proximal convoluted tubule and, in minimal part, distal tubules and collecting ducts. The glomerulus is accessible only in some strains of rats, such as the MWF, known to have many superficial glomeruli under the renal capsule. Nevertheless, it is possible to get information in indirect manner about the loop of Henle by considering the differences in delivery to proximal and distal points.

The first step in micro-puncture studies is mapping the tubules, this is important to know the length of the tubules that have to be punctured. For this purpose, an amount of stained dye is usually injected in the desired tubule in order to see the staining of the downstream segments: the colorant is visible in the proximal tubule, then in the distal tubule since it disappears through the loop of Henle (51). After the tubule is chosen, it can be punctured with the desired pipette that is backfilled with stained oil, generally very viscous. This oil is released in the tubule and move with the fluid flow, preventing the reflux of the liquid and contamination with fluid of the other segments. Thus, the sample can be collected (Figure 4).

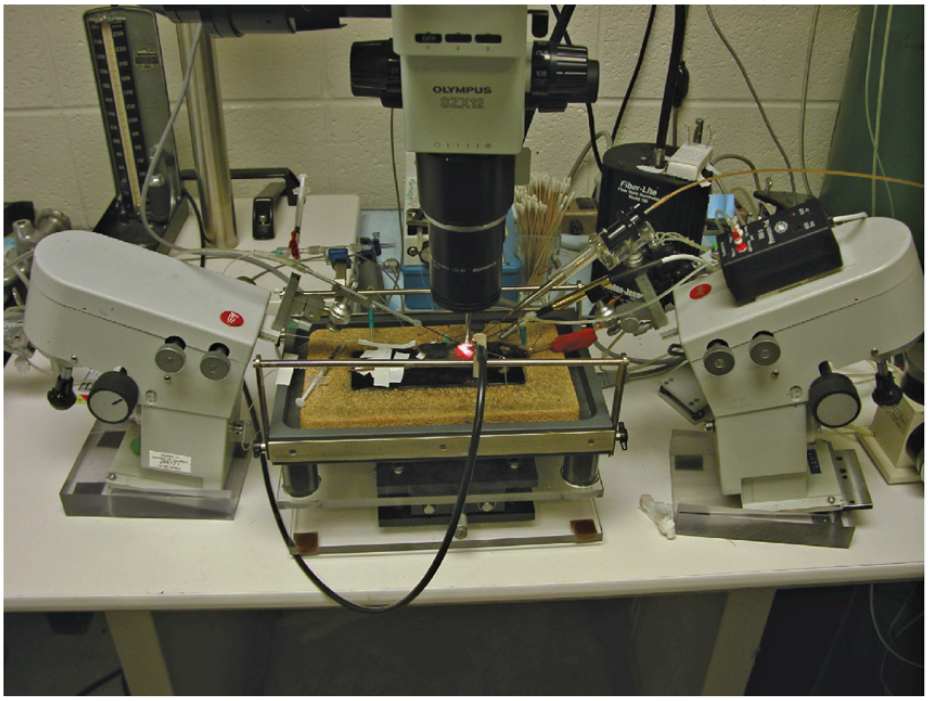

Figure 4. Equipment for micro-puncture experiments. The animal is positioned on the heated table laying on the lateral decubitus to expose the left flank. Externalized left kidney is immobilized in a Lucite cup, and is illuminated with light source from the front. The manipulator on the left is holding the marking pipet, while the manipulator on the right is holding the pressure pipet. Lorenz et al., 2012.

In general, two different approaches for micro-puncture can be used. The first one is the free flow collection, that allows to collect fluid from a tubular segment in free flow conditions, in order to get the amount of a substance filtered through the glomerulus and to study the net tubular reabsorption or secretion (52). The other approach is the micro-perfusion, in which an immobile wax block is inserted just upstream of the segment of interest. The tubule can be perfused with an experimental substance and then the fluid is collected in the distal portion of the tubule. This method has the advantage to manipulate and control the perfusion rate and the composition of the perfusate (53). Some variants of micro-puncture technique have been developed to better understand the solute and water tubular transport. One of this is the microinjection, which requires continuous injection with a micropump of a solution containing inulin and a labeled tracer of interest in some nephron regions. Then, the tracer is compared with inulin, allowing to get the fractional unidirectional reabsorption of the injected substance (54). Another method is the insertion of luminal fluid droplets in the renal tubules, which enable to determinate the alteration in size related to the fluid composition (55).
Micro-puncture has provided high information regarding the SNGFR. According to the standard formula, SNGFR assessment requires the evaluation of inulin in blood and in the fluid sample in ratio with the tubular fluid flow rate (56). As an alternative to inulin, iothalamate can be used (57). In male

rats the SNGFR average value is 35 nL/min, in mice is 12 nL/min (51). It is not recommendable to consider values very far from these, since they could be affected by errors. Lower values than these could mean an incomplete sample collection, instead greater values could represent a fluid collection from juxtamedullary nephrons (29). Errors during SNGFR measurements seem to be caused by sample collection, volume measurements and counting, and they have been evaluated even in particular conditions, such as hydropenia and saline diuresis. It is also possible to recollect fluid from the same tubular site in order to have more powerful and paired statistic results. This method, however, is debated since the oil that has remained in the tubule after the first collection could determinate nephron obstruction, causing hydronephrosis or alteration of fluid flow through macula densa cells, leading in turn to changes in GFR (58).

It is understandable that micro-puncture was the approach of choice for the measurement of SNGFR in rodents, but it is a very laborious technique, which requires complex animal preparation and sophisticated equipment.

2.1.5 Fluorescence microscopy

Fluorescence microscopy represents an extensively used approach in the field of research to evaluate cellular processes *in vitro*. Most of the techniques utilized for this purpose have been commonly applied to cells, isolated tissues, explanted organs or embryos. These approaches, relatively cheap and easy to maintain, provided important information regarding the basic cellular and molecular biological events.

However, the cells tend to modify their phenotype when removed from their original environment and they are not able to reconstruct the complex architecture and the dynamic physiology of living organisms. The *in vivo* systems, indeed, show complex morphological organization and require continuous interactions with other organs, which permit the efficient functioning of the organism. Therefore, the usage of *in vitro* systems is debated since can make the experiments and the following data interpretations limited.

For this reason, the attention of researchers moved to study the biological functions using living organisms. The first experiments were described in 1839 by Wagner, who evaluated the leucocytes movements within the blood vessels in frog feet using bright field microscope (59). In the following decades, researchers used this approach to investigate pathophysiological processes involving especially the vascular physiology and the cell migration (60, 61). In the 1980s a big improvement was made with the advent of epifluorescence microscopy, which permitted to clarify more in detail the cellular physiology in tissues such as vessels (62) and tumors (63). After that, the development of confocal microscopy provided a great advancement in the microscopy field thanks to its ability to get

optical sections from a sample, leading to a huge increase of spatial resolution compared with previous methods. Such technique was used by Villringer et al. in 1989 to study microcirculation on rat brain *in vivo* (64) and by Jester some years later to perform *in vivo* imaging in tissues such as cornea, liver, kidney and thyroid in rabbits and rats (65).

2.1.6 One-photon excitation: confocal microscopy

Upon the absorption of a photon by a fluorophore, an electron existing in the ground state (S0) is raised to the excited state (S1). After a short interval of time in the excited state, the fluorophore relaxes back to its ground state and may emit a low energy photon of light. In order to excite properly the fluorophore, the photon should have the energy matching the energy of the excited state (Es1). Thus, from S1 state the molecules can return back to the ground state without emitting a photon, transferring the electronic energy to produce heat. Alternatively, the electron dropping to the ground state can emit a photon of lower energy than the one originally absorbed, producing a process called "Stoked shift". The efficiency of fluorescence is given by the quantum yield, which can be defined as the ratio between energy emission and energy absorption. The absorption and emission ability of a molecule is characterized by the molar extinction ε and the fluorescence quantum yield ϕ, whose product provides the brightness of a substance (66, 67).

Confocal microscopy is based on single-photon excitation fluorescence and its applications in the field of biomedicine have been widely described. Confocal microscope exhibits a different principle compared to traditional fluorescence microscopy, which produce blurred images when a specific point of the sample is acquired. Instead, confocal microscopy permits to obtain more detailed pictures with higher depth in a small point of the sample thanks to the pinhole that reject all the out of focus. The biological applications of confocal microscopy include the evaluation of cellular organelles and nuclei: using specific fluorophores permits to track the single cell organelles, such as mitochondria and Golgi apparatus, and to image the nuclear chromosomes involved in cell division. Confocal microscopy also helps to make 3D reconstruction of the sample studied because of its ability to section optically the specimen. In addition, combining confocal microscopy and GFP (green fluorescent protein) it is possible to monitor the cellular trafficking and molecular pathway as well as gene expression (68).

Despite the numerous opportunities it offers and its capacity to acquire high resolution 3D images, the utilization of confocal microscopy for deep tissue imaging remains limited due to the strong scattering of light and the consequent photobleaching of the samples, as described elsewhere (69).

2.1.7 Principles of multiphoton microscopy

Intravital imaging of living organs is possible with conventional confocal microscopy, but this method is limited by the relatively low tissue depth and the high photo-toxicity.

Intravital multiphoton microscopy (MPM) is a superior technique that offers 3D images and high-resolution movies of dynamic cellular and subcellular events. Thanks to the deeper laser penetration and less phototoxicity, MPM allowed researchers to address important questions regarding human and animal physiology, becoming the gold standard approach for live imaging.

The concept of MPM was first described in the 1930s by Maria Göppert-Mayer (70), but it started to be used for biological imaging about 50 years later.

Most studies performed so far have used two-photon excitation, therefore the term "two-photon" microscopy rather than "multiphoton" is sometimes preferred.

Unlike the other techniques, such as confocal microscopy, MPM exploits two low-energy photons arriving almost simultaneously on the sample and uses a long wavelength laser exciting in the near infrared range (700-1000 nm). The two photons alone have the half of the energy compared to the single photons used in one-photon excitation, but the resulting fluorescence emission is comparable with that generated in one-photon event. Since the photon energy is inversely proportional to the wavelength, in two-photon excitation the wavelength used should be approximately twice than one photon excitation (71–73). The figure 5 shows a simplified jablonsky diagram for one-photon and two-photon excitation fluorescence.

MPM exhibits several advantages compared to previous microscope methods. First, the laser penetration in the tissue is higher in consequence of less light scattering, allowing to image in the kidney up to 150-200 μm (72). This represents a depth capacity 3-4 times more than confocal microscopy (74). In more optically transparent organs, such as brain, MPM permits the imaging even at higher depth (75, 76).

Second, the phototoxicity is less thanks to the two low-energy photons arriving on the sample. In this way it is possible to image continuously over the time, especially when thick samples are visualized, including brain slices, embryos and living organs (77). Third, the out of focus is reduced, and the fluorescence is high only in the focal plane because the excitation energy drops proportionally to the square of the distance to the focal point. Therefore, the photobleaching is reduced, the necessity of a pinhole is avoided, and more sensitive detectors can be used to collect the fluorophore emission (78, 79)(Figure 6).

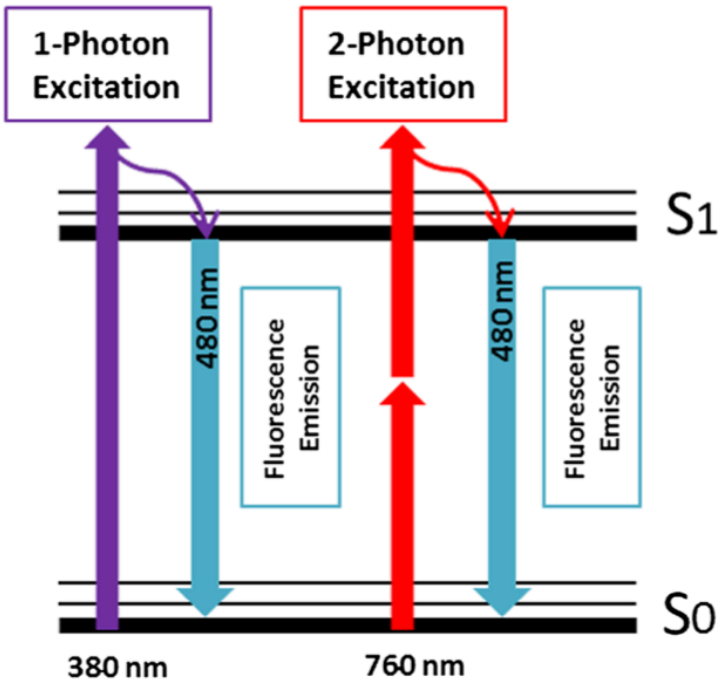

Figure 5. Simplified Jablonsky representation for one-photon and two-photon excitation.
One-photon excitation occurs after the absorption of a single photon which provides sufficient energy to reach the excited state (S1). Two-photon excitation is provided by the simultaneous absorption of two photons of lower energy. The subsequent fluorescent emission of one-photon and two-photon excitation is comparable.
Schiessl at al., 2016.

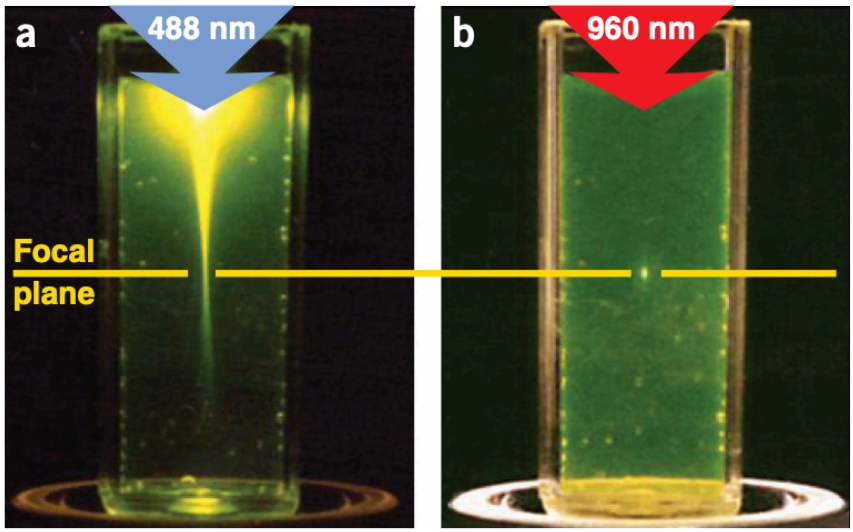

Figure 6. Localization of fluorescence by one-photon and two-photon excitation. In one-photon excitation (a) the fluorescence spreads far from the focal plane, requiring a pinhole to reject all the out of focus. Two photon microscopy(b), instead, emits fluorescence only at the focal plane, reducing photobleaching and avoiding the necessity of a pinhole.
Zipfel et al., 2003.

As consequence of these improvements, MPM permits to capture dynamic events in organs of living animals, still incorporating the complexity of hormonal factors and metabolites with subcellular resolution, becoming the technique of choice for intravital imaging.

As largely shown in literature, the application of MPM gave the opportunity to increase the understanding of many organs, such as brain (80), skin (81), liver (82), heart (83) and kidney (84) as well as investigations in immunology (85) and cancer (86) fields. The kidney, in particular, presents a very intricate structure with different cell types that are difficult to analyze with conventional techniques since they may show changes when removed from the physiological body. For this reason, the imaging of living organs with MPM overcomes the limits shown by confocal microscopy and offers the unique occasion to extend the knowledge of human pathophysiology, with the future perspective to evaluate efficient treatment strategies.

2.1.8 Application of MPM in kidney physiology

One of the advantages offered by MPM is the possibility to study the cellular morphology even without the external labeling. In fact, lysosomal and mitochondrial NADH fluorescence naturally exhibited by cells enables the spontaneous visualization of some tissue structures. Particularly, mitochondrial NADH generates strong autofluorescence during its reduced state. This is particularly true for kidneys, where renal proximal tubules are characterized by a huge number of mitochondria and lysosomes, allowing to recognize them very easily. Other nephron segments such as distal tubules and collecting ducts show less fluorescence intensity and appear as dark empty patches. The glomeruli, instead, lack any fluorescence and are shown as large dark empty spaces close to proximal tubules (87) (Figure 7).

It is understandable that the renal autofluorescence is very helpful to identify and track the tubules of interest during the imaging without exogenous staining. Additionally, the autofluorescence emitted by NADH helps to understand the metabolic state of the organ in real time and to compare physiological processes, such as aging (88), with diseases conditions, including hypoxia and ischemia (89, 90). However, tissue autofluorescence has to be evaluated carefully since it can overlap with the emission of external probes, making sometimes the analysis quite doubtful (91).

Another possibility is to image collagen fibers and skin using second harmonic generation (SHG) technology, which takes advantage not from absorption but from Rayleigh scattering, resulting in frequency-double photon (92, 93). The imaging with SHG provides an advantage in that it is not limited by photobleaching since it does not require fluorescence excitation. SHG can specifically detect structures such as collagen I and III, microtubules and myosin (94, 95). The identification of collagen fibers in kidney results very useful to detect and quantify the renal fibrosis stadium without

external labels, showing high potentiality as pejorative predictor of nephropathies in many renal diseases (96) and in translational cancer research (97).

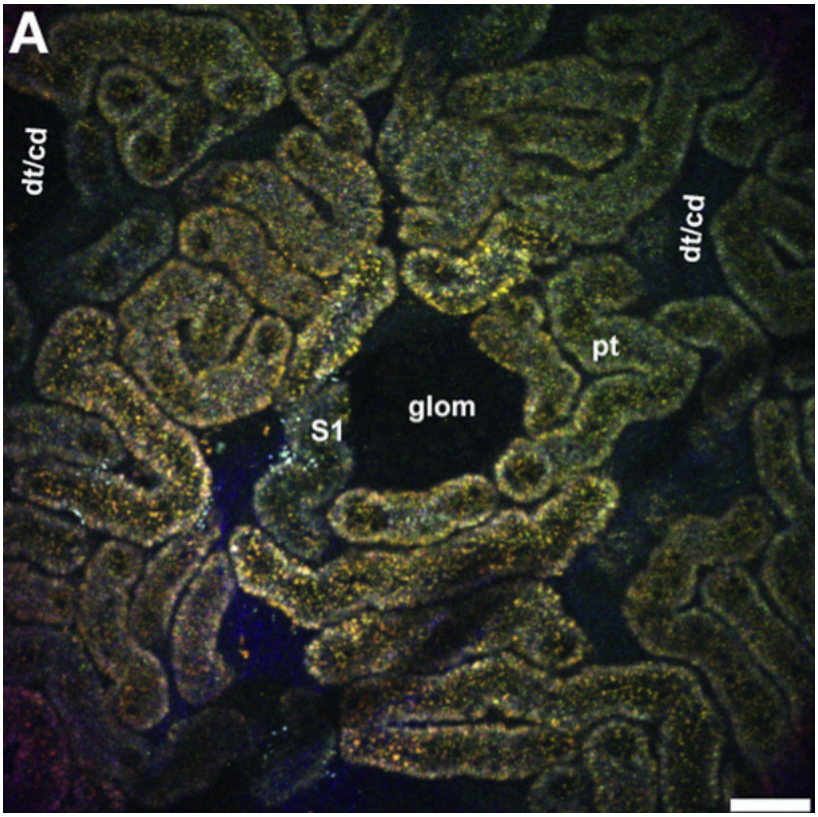

Figure 7. Visualization of outer cortex in rat kidney. Renal autofluorescence in rat kidney helps to recognize the different tubules and other features. The numerous lysosomes and mitochondria present in proximal tubules (pt) show strong autofluorescence (orange vesicles), whereas distal tubules (dt) and collecting ducts (cd) lack any visible fluorescence, appearing as empty patches. Superficial glomeruli (glom) also lack any discernible autofluorescence, so they are represented as circular spaces surrounding proximal tubules.
Sandoval et al., 2017.

The great advantage of MPM is the capacity to label many cellular compartments using concurrently up to 4 different fluorescent dyes, allowing comparation of labeled probes and simultaneous analysis of multiple parameters in different conditions. For example, vessels can be stained with high molecular weight fluorophores that remain in the blood circulation for a relatively long time since their big size, permitting to study any abnormalities in vascular permeability (98) or in red blood cells velocity (99). Indeed, erythrocytes appear as elongated black shadows in normal conditions as they exclude the labeling. The slope of these shadows is inversely correlated to the blood flow, which can be assessed dividing the distance Δx traveled by the erythrocyte by the time Δt spent to cover this

distance. This represents a very powerful tool when a wild type condition is compared to disease models, such as the ischemia-reperfusion injury (100, 101)(Figure 8).

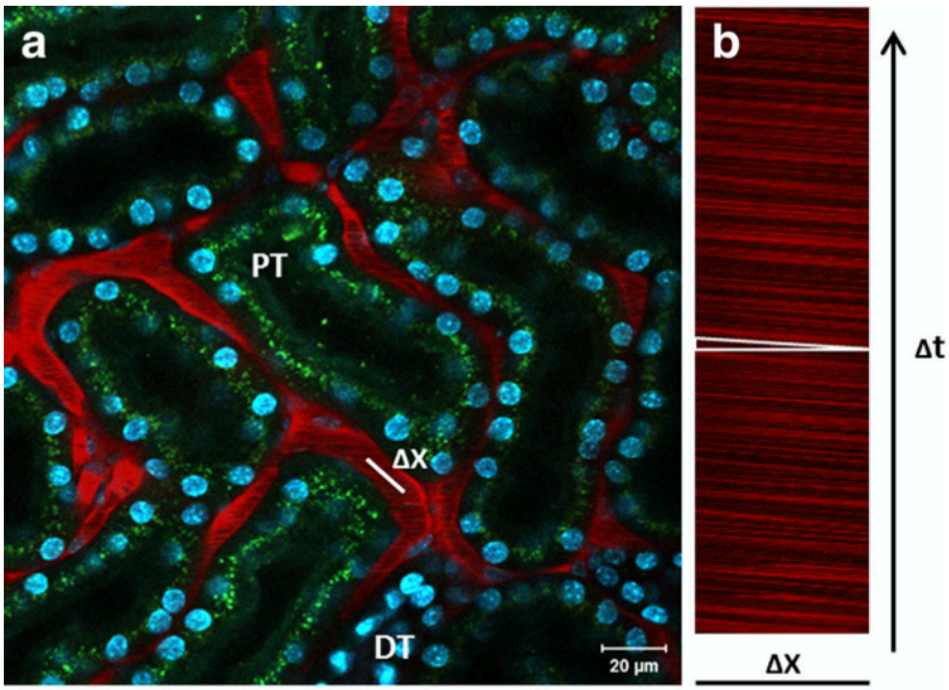

Figure 8. Evaluation of red blood cells velocity using MPM. In the panel a, the renal cortex shows the peritubular vasculature and cell nuclei stained with Texas Red 70 kDa and Hoechst 33342, respectively. The panel b shows that the slopes of dark lines is inversely proportional to the velocity of red blood cells. Schiessl et al., 2016

MPM helped to image in real time the urine concentration mechanism. In 2006, Kang et al. demonstrated that inhibiting the sodium-potassium-chloride cotransporter (NKCC2) with 2 mg/kg furosemide after low molecular weight dextran injection led to a reduction of dye concentration in the distal tubule, as a result of urine dilution and consequently to an enlargement of these tubules (102). Moreover, the enlarged distal tubular segments seemed to compress peritubular capillaries, in line with previous studies (103).

MPM is also used to study the morphology and function of single cells involved in physiological or pathological events, including apoptosis and necrosis. Many fluorescent probes have been designed to this purpose. Blue Hoechst 33342 labels cellular nuclei and emits brighter fluorescent when cells become apoptotic compared to the normal ones. Necrotic cells instead are distinguishable because of loss of membrane integrity, allowing the dye Propidium Iodide (PI) to enter in the damaged cells. These latter cells will appear in red, due to the merge of blue and white color of Hoechst and PI,

respectively. The quantification of the apoptotic and necrotic cells shows a useful approach to assess the efficiency of treatments in preventing or ameliorating renal injuries (104, 105).

In addition, MPM provides the great opportunity to image structures that were inaccessible, such as podocytes (106) and cells of juxtaglomerular apparatus (JGA)(107) in kidney, and that have been studied only *in vitro*. This has considerably increased the knowledge of the mechanisms regulating the glomerular permeability, albumin reabsorption or the glomerulosclerosis. MPM, in fact, has offered stunning images and new details of the glomerular components, opening up the way for new kind of studies with important functional implications both in physiological and pathological conditions.

The new technologies developed higher quantum yield fluorophores, transgenic animal models and new powerful applications that helped investigators to address new biological questions, to improve the experimental techniques and the analysis methods, removing some limits existing for intravital microscopy. In literature many examples of such innovative technologies are shown. As reported by Hackl et al (108), the tracking in vivo of single podocytes during cellular damage, migration or differentiation was possible using transgenic podocin-GFP mice. This approach enabled to visualize the movements of podocytes within the glomerulus from the capillaries to the Bowman's capsule, demonstrating the dynamic activity of the glomerular components. The results obtained with this imaging approach represent an exciting opportunity to investigate the podocytes biology in normal and disease models. Furthermore, intravital microscopy experiments using genetic animals opened the way to elucidate the calcium imaging in kidney, which was prohibitive so far due to the limited delivery of dyes to the interested site. Recent studies on animals expressing calcium indicators have suggested a role of intracellular calcium in podocytes in regulating the functioning and selectivity of glomerular filtration barrier, presumably remodeling the actin fibers in podocytes processes (109).

A challenge in the imaging of kidney physiology was represented by the constrained possibility to visualize superficial glomeruli in rats, limiting the studies of glomerular dynamics. A mutant strain of rats, known as Munich Wistar Frömter (MWF), was then selected from the original Munich Wistar rats by Frömter for their elevated number of superficial glomeruli under the renal capsule. Since then, the MWF rats have been extensively used for kidney physiology *in vivo,* offering a unique approach to investigate the glomerular pathophysiology. These rats show a smaller body weight compared to other strains and present many physiological alterations. They develop proteinuria at 10 weeks and show significant glomerulosclerosis at 35 weeks. The average blood pressure is 140-150 mmHg at 10 weeks and reach approximately 180 mmHg at 9 months of age. The number of nephrons is 50% reduced compared to Wistar rats and the average size of Bowman's capsule is increased: in particular,

the reduced number of nephrons suggest a lowered ability to excrete sodium, which in turn lead to hypertension and glomerular damage (31, 110).

An interesting application of MPM is shown by Schiessl et al, who exploited the surgical implantation of an abdominal window to image the same renal location over several days, allowing to evaluate the mechanisms involved in tubular regeneration. Thanks to this long-term imaging approach, the angiogenesis process, the infiltration of tumor cells and the recruitment of inflammatory cells in kidney was carried out, overcoming the limits shown by previous techniques (111).

In addition, the image processing and correction methods were improved with the advent of new technology. Indeed, some tools and software have been developed in order to reduce the image noises and artifacts caused by the animal breathing and heartbeat, which can make the quantitative analysis very complex. This can be for sure mitigated during the animal preparation with a proper anesthesia and surgery. In addition, taking images with relatively high spatial resolution (512x512 pixels) can help to control some movements (112). Despite these precautions, the artefacts can still remain. To overcome these challenging complications, it is possible to stabilize the images using the "registration" plugin on imaging software Fiji, which realign the x, y and z positions in a region of interest. Moreover, many other image corrections can be performed with the same software. After image acquisition some filters can be applied to enhance the contrast, change the brightness and smooth the image (113). Furthermore, Bölke et al show that some algorithms help to reduce the noise in the pictures acquired with 2PM, preserving the samples from the natural artifacts (114).

The advantages offered by MPM and its capacity to image both proximal and distal nephron segments allowed to investigate *in vivo* the main renal functions, including the glomerular filtration rate, the urine concentration mechanism, the albumin reabsorption, and the functions of juxtaglomerular apparatus. MPM, moreover, can be applied to study the rare genetic disease and the most frequent pathological conditions reproduced in animal models.

2.1.9 Measurements of SNGFR with MPM

New generation microscopy techniques and transgenic murine models as well as improvements in the data analysis have led to overcome the micro-puncture favoring the MPM for the evaluation of renal function.

The assessment of SNGFR represents one of the most fascinating applications of MPM in kidney physiology and can be done observing and quantifying the fluorescent decay time of a low molecular weight dye between two regions of interest drawn within a tubule. This method was first developed by Kang et al. to compare physiological values of SNGFR in Munich Wistar rats with those obtained in Streptozotocin-diabetic rats (102). In particular, a superficial glomerulus connected with early

proximal tubule measuring at least 100 μm was chosen for the measurement. The fluorescent marker Lucifer Yellow was injected as a single bolus in the venous access appearing in the bowman's space within a few seconds. The changes of fluorescent intensity were measured within 2 regions of interest (ROI), of which one was located after the urinary pole and the other at least 100 μm downstream. The length and the diameter of the tubule were calculated to obtain the tubular fluid volume, whereas the passage time of the filtrate represented the ΔT, expressed as the shift of the intensity plots between the 2 ROIs. The absolute value of SNGFR, expressed as nL/min, was finally obtained from the volume/time ratio (Figure 9).

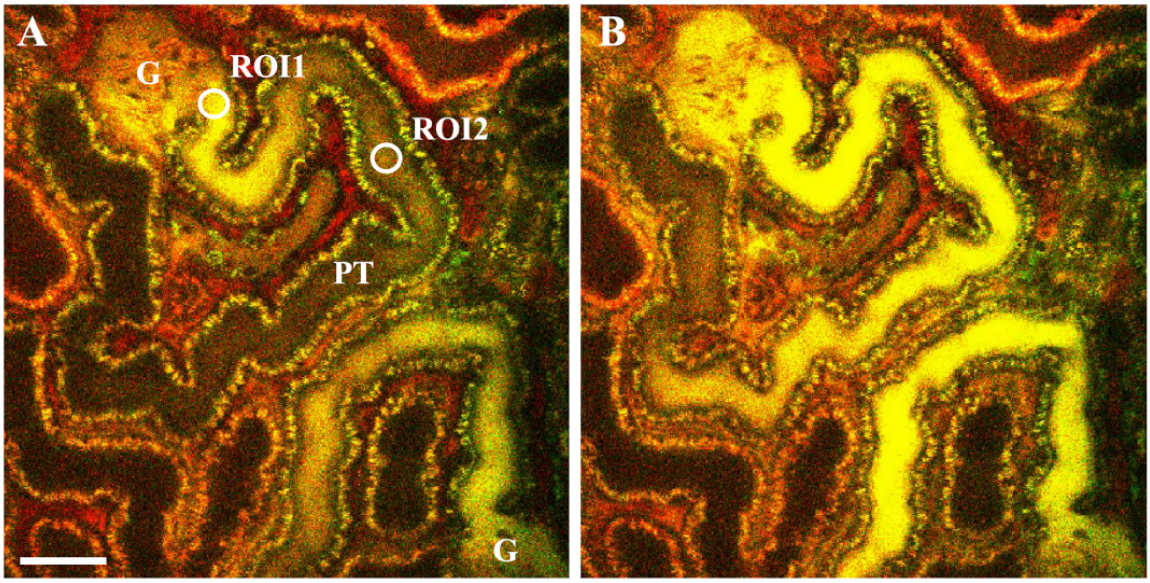

Figure 9. Representation of the assessment of SNGFR using MPM. After the intravenous injection of a low molecular weight dye, the changes in fluorescence intensity are measured within two regions of interest. Kang et al., 2006.

To confirm the feasibility of such approach, Kang et al. measured the SNGFR in hyperfiltering glomeruli shown in diabetic rats treated with Streptozotocin, obtaining results comparable to the micro-puncture technique. This approach, therefore, is quite convenient due to the low molecular weight of the dye used and the possibility to easily calculate the tubular size and transit time, proving to be an accurate and fast method to assess renal function. In addition, this method allowed to accurately measure the Lucifer Yellow transit within the initial 500 μm of early proximal tubule showing a good reproducibility.

However, this technique is limited in terms of temporal resolution when acquiring full frame time-series, reducing the accuracy of SNGFR measurements.

2.1.10 The link between dopamine and SNGFR

As reported by many studies, a normal dopaminergic system is needed to control the renal hemodynamic, electrolyte balance and blood pressure within physiological values. On the contrary, impairment of dopamine production or alterations of dopaminergic receptors lead to different pathological conditions including oxidative stress, hypertension and progression of renal dysfunction. Dopamine exerts complex effects on human body, and it involves many receptors which show different actions. The pharmacological effect of dopamine is dose-dependent, inducing natriuresis and increased renal blood flow at low dose (<5 ug/kg/min), while at higher dose it stimulates the cardiac output (115). In particular, low-dose dopamine is known to increase SNGFR by selective renal vasodilation. Therefore, low-dose dopamine is the treatment of choice in preterm human neonates with respiratory distress and low-urine output, as it leads to a significative increase of GFR (116).

At high dose, dopamine interacts with peripheral α1-adrenoreceptors determining vasoconstriction, whereas the interaction with β1-adrenoreceptors leads to an increase of cardiac output.

That is the reason why dopamine represents a fundamental drug in intensive care units used as vasopressor agent, particularly in hypotensive patients not responding to fluid treatment.

Moreover, dopamine accomplishes its functions through the interaction with two main subgroups of receptors: D1-receptors have been found at least in renal and cerebral arteries, while autonomic ganglia and sympathetic nerves showed the presence of D2-receptors. Particularly, D1-receptors permit locally produced dopamine to inhibit the functioning of main apical and basolateral transporters, such as Na^+K^+ pump and Na^+/H^+ exchange. In addition, D1-receptors activate adenylate cyclase increasing, in turn, the activity of protein kinase A. On the other hand, D2-receptors inhibit adenylate cyclase and regulate ion channels (117).

Despite the great potential of dopamine in raising the renal function in patients with renal injury and increasing the blood pressure in hypotensive patients, its use in clinical practice remain controversial due to the overlapping effects when certain dosages are used.

2.1.11 The acute kidney injury

The acute kidney injury (AKI), previously called acute renal failure (ARF), represents a global health problem characterized by a fast and sometimes reversible decrease in kidney function involving both morphological damages and impaired function (118, 119). Most of patients with AKI show multiple pathophysiology, including sepsis, ischemia and nephrotoxicity, which make difficult the identification and treatment of the disease (120). Conventionally, AKI is classified in three categories: pre-renal AKI, acute post-renal nephropathy and acute kidney disease. This latter is considered to be

the real kidney disease, which is shown only if the pre- and post- renal AKI persist (121). The fast decline of GFR, the acute rise of serum creatinine and the reduction of urinary output in a given time are the main parameters to diagnose the AKI (122). Many factors promote the AKI and they include hypovolemia, vascular surgery, diabetes mellitus, hypoxia, atherosclerosis and sepsis (119).

The mortality of AKI can reach or even exceed the 50% especially in hospitalized patients and patients in ICU that develop severe AKI (123–125). Most cases of AKI recover entirely with right management, particularly if they are diagnosed early. The prognosis, however, strongly depends on the etiology of the disease and the eventual previous renal injuries. Despite the possibility to recover even completely from the disease, repeated events of AKI over the time can determinate a progressive worsening of the renal function leading to chronic kidney disease (CKD) or death. Therefore, it is fundamental to monitor the patients until their renal function is considered back to the normal.

Several clinical conditions represent the etiology of AKI and all them have been extensively reviewed: rhabdomyolysis, ischemia-reperfusion injury, drug toxicity and glomerulonephritis (120).

The Rhabdomyolysis is a medical condition showing necrosis and disruption of damaged muscle cells, with consequent release in the circulation of their contents, such as myoglobin. The filtration of these molecules by the kidney can cause AKI as a consequence of renal tubules obstruction, cellular necrosis, inflammation, and blood constriction (126). Ischemia-reperfusion is also a very common cause of AKI since it causes tubular necrosis and altered glomerular hemodynamic (127). Drug toxicity also represents a huge problem for renal tubular cells, which can be exposed to high concentration of toxins after a continuative use of drugs. Drug-induced nephrotoxicity is the result of direct injury to renal tubules, hemodynamic alterations and blockage of renal excretion. Antibiotics including aminoglycosides are very used in the treatment of serious bacterial infections, however their nephrotoxic activity is well documented. Gentamicin, one of the most used aminoglycosides, accumulates in the proximal tubule cells leading to loss of integrity of brush borders, tubular necrosis and reactive oxygen species formation (128). Besides gentamicin, even other drugs have been reported to induce renal injury, such as cisplatin, indomethacin, amphotericin B, and beta-lactam antibiotics (129). The intravenous administration of contrast agents, widely used for diagnostic and pharmacological approaches, is well known cause of AKI. Several studies on animal models suggest that contrast media-induced kidney injury could be determined by renal ischemia, tubular toxicity and reactive oxygen species production but the pathophysiology is still not well elucidated (130).

Many pharmacological agents have been shown to be effective in the treatment of AKI in animal models, especially in condition of ischemia reperfusion or sepsis, but no one of these was efficient when translated to humans (131). Therefore, a stronger knowledge of the disease at cellular and

subcellular level is needed in order to elucidate the differences between the animal and human conditions and to find efficient drugs compatible to humans.

2.1.12 Renal ischemia reperfusion injury: morphological and functional aspects

Ischemia refers to a mechanism through which the delivery of blood to the body tissues is severely reduced, leading to morphological alterations and impairment of normal functions. Despite reperfusion allows the fast return of oxygenated blood, it contributes to exacerbate the tissue necrosis and cell death in a process called "reperfusion injury".

Renal ischemia-reperfusion injury (IRI) is the main cause of AKI and its cellular and molecular mechanisms are not yet completely elucidated. The lowering of the blood flow is the first feature occurring during renal ischemia and in humans it can be caused by a significant decrease of blood pressure or as a consequence of vascular diseases, such as atherosclerosis and renal artery thrombosis. Surgical procedures involved during renal transplantation, aortic surgery, or clamping of renal artery, are also responsible for renal ischemia, determining in turn AKI (131).

The main renal structure affected during IRI is the proximal tubule, which normally accomplishes the essential function of substances reabsorption. These transport mechanisms, which require huge amount of energy to be efficient, are strongly affected by IRI since the production of ATP required for the transport of molecules is dramatically compromised. The subsequent impairment of basolateral Na^+K^+ pump induces an abnormal accumulation of intracellular sodium, leading in turn to cellular swelling, intracellular abnormalities and necrosis (132). In addition to the tubular damage, also the vascular endothelium is reported to be altered during IRI, causing increase of blood viscosity and loss of fluid from the intravascular space. This would lead, in turn, to defects of renal circulation even during reperfusion phase, as shown by capillary occlusion and lowering of blood flow (133). Moreover, the development of reactive oxygen species (ROS) during reperfusion and the additional renal damage they bring have been widely documented. In particular, ROS have been thought to favor the renal damage not only targeting directly the cells, but especially activating molecular pathway of transcriptional factors, such as NF-kβ (134). Other mechanisms, including alterations of intracellular pH and defects in calcium handling, are involved in the pathogenesis of AKI as confirmed by numerous studies (135).

The decline in GFR observed during IRI is one of the major features of IRI-induced AKI and it could be explained by the tubular obstruction and the reflux of solutes, such as inulin, across the tubular cells caused by tubular damage: the debris and cast formation after tubular occlusion is shown to increase tubular pressure and to lower the filtration pressure. Additionally, the constant reduction of tissue oxygen during the reperfusion could lead to a drop of GFR as a compensatory mechanism to

maintain the oxygen values within normal ranges. However, the massive ROS production further decreases the medullary blood flow, resulting in additional renal injury. As reported by Sutton et al, the increased expression of ICAM and leucocytes recruitment as consequence of ROS-mediated inflammation contribute to the tubular impairment, leading to further GFR decrease (136).

The SNGFR also is reported to be reduced after renal damages in IRI models, as extensively documented (132, 137, 138). However, SNGFR reduction can't be only described as the consequence of mechanical events like tubular damage and morphological changes. Several studies have demonstrated a relationship between TGF and SNGFR reduction in IRI models. The raise of NaCl in tubular fluid after Na^+K^+ pump impairment is a strong stimulus for the activation of TGF, which is able to decrease significantly proximal and distal SNGFR. Moreover, some experiments involving the use of diuretics, such as furosemide and bumetanide, confirm the strong link between TGF and SNGFR (139). From these assumptions it is clear that TGF is the main responsible of SNGFR lowering and the inhibition of macula densa cells, the main actor in TGF mechanism, could prevent the strong SNGFR reduction exhibited in renal injury (140, 141).

2.1.13 Animal models of IRI

The animal models represent a necessary and unique tool to mimic the etiopathogenesis of human diseases, in order to understand the mechanisms underlying the pathology and to develop an efficient treatment.

Different animal species have been used to develop the IRI model, including dog (142), pig (143), mouse (144) and rat (145). IRI-induced AKI is usually obtained in rodents by occluding the renal artery for 30-45 min using a small non traumatic clamp, followed by releasing of the clamp to allow the reperfusion of the kidney (146, 147). Ideally, the ischemia of 45 min with 24 h reperfusion provides a suitable and reliable model to mimic the vascular alteration of human AKI.

The study of Bird et al. shows an example of the morphological and functional abnormalities exhibited in IRI-treated rats, after 1 hour of ischemia and 24 hours of reperfusion. Macroscopically, the ischemic kidneys appear spotted and with a sponge consistency compared to normal kidneys. At the histological level, the renal tubules show significant and variable necrosis accompanied by intraluminal cast and debris formation. The vessels result to be congested, with a deposit of pigments derived from lysed erythrocytes in peritubular capillaries (Figure 10).

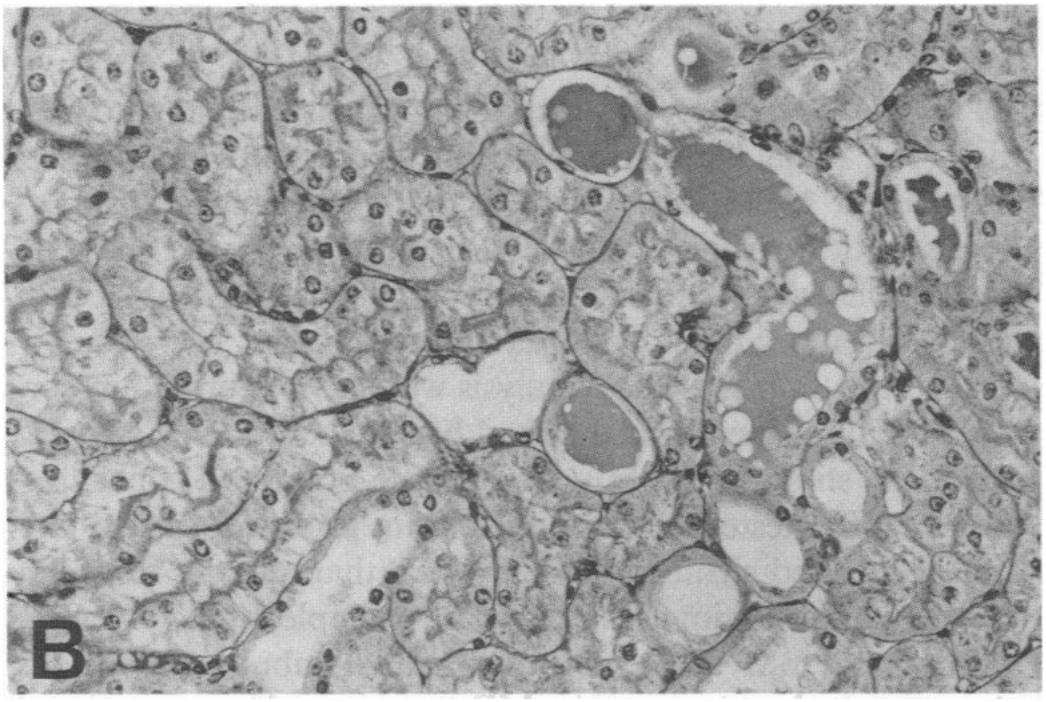

Figure 10. The histological changes in ischemic rats. The cells of superficial cortex show a great degree of tubular necrosis with consequent loss of nuclear detail. The formation of intraluminal cast and cellular debris as well as vessels congestion are evident. Bird et al., 1988.

The tubules exhibit slower flow rate when some dyes are injected. Regarding functional aspects, the 24 hours reperfusion cause a significant reduction in whole GFR and in SNGFR, as shown by micro-puncture experiments. The renal injury is also confirmed by a significant reduction in plasma creatinine over 24 hours (148).

IRI-induced AKI was extensively studied over the last decades using different approaches. As shown by Hall et al., multiphoton microscopy was used to image the mitochondrial structure and function during IRI. Particularly, they demonstrated that clamping the renal artery induced a fast and strong rise of tubular NADH fluorescence as a consequence of hypoxia caused by a decreased activity of respiratory chain, which force the NADH to remain in the reduced state. In addition, the authors show that during ischemia the potential difference across the mitochondrial membrane is dramatically dissipated in the proximal tubule within a few minutes, whereas the distal tubules better maintain the mitochondrial structure. Moreover, thanks to the advantages offered by in vivo imaging the investigators were able to detect the morphological changes of tubules at great resolution, such as membrane blebbing and shedding of cellular components into the lumen (73).

Another example of IRI study using intravital microscopy is shown in the work of Schiessl et al., who injected in anesthetized rats the fluorescent dye dihydroethidium (DHE) to image the ROS production in vivo. When enters in contact with superoxide, DHE moves to the nucleus where it binds nucleic

acids emitting a bright red fluorescence. According to their results, the investigators demonstrated the strong increase of DHE fluorescent in proximal tubules cells right after the onset of ischemia, which persisted even during the reperfusion. These results showing the development of ROS during ischemia were in line with previous studies (149).

The positron emission tomography (PET) is another tool used to investigate IRI since it can produce images at higher resolution and quantification of dynamic processes. It provides great reliability especially when it is combined with computerized tomography. Moreover, the qualitative and quantitative assessment of processes such as hypoxia, apoptosis and endothelial disfunctions can be achieved thanks to new PET tracers (150).

Other advanced technologies, including Infra-Red and magnetic resonance imaging, have been shown to offer great potentiality as clinical diagnostic tool to investigate AKI in murine models and patients (151).

2.2 RESULTS

2.2.1 SNGFR measurements with innovative Linescan method

A superficial glomerulus connected to an early proximal tubule extending at least 100 μm downstream from the exit of the Bowman's space was chosen for the measurement. From the Praire view software a linescan path starting from the urinary pole and crossing many times the tubular lumen orthogonally to the cellular wall was hand drawn (Figure 11). In the linescan window the number of acquired lines was raised until the total acquisition lasted approximately 10 seconds (from 2000 to 13000 lines). This gives enough time for the FITC to be filtered through the glomerulus. The linescan was acquired while performing the iv bolus infusion of the FITC marker. Laser power and PMT gain of green channel were adjusted during dye bolus to avoid saturation of the fluorescence signal. The analysis of the linescan was performed with Fiji software. The resulting output of the linescan is a path of fluorescent lines, each representing a tubular crossing. The x axis of this path corresponds to the length of the drawn line, while the y axis to the duration of the linescan. The bolus arriving is characterized by an increase of fluorescence intensity in the first vertical tracing. Two lines of interest, one right after the urinary pole and the other at least 100 μm downstream, were selected for the further analysis (Figure 12).

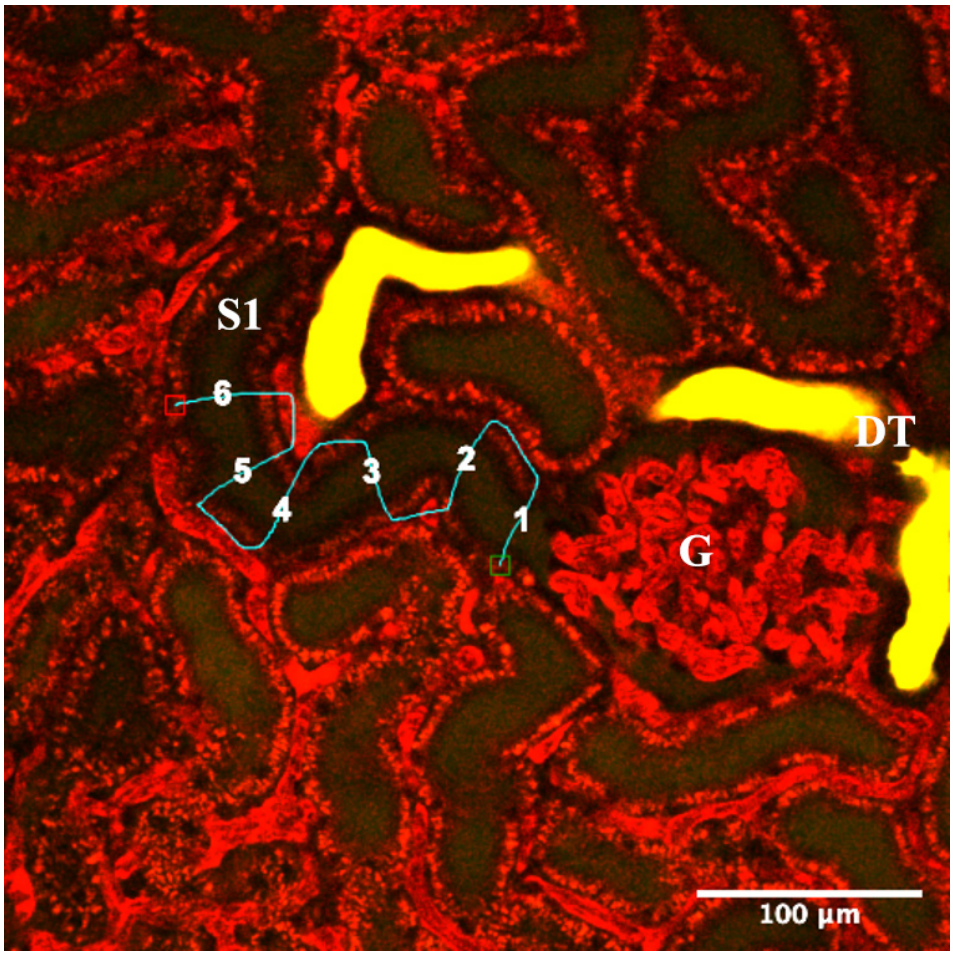

Figure 11. Representation of linescan tool for the assessment of SNGFR. A superficial glomerulus (G) with connected S1 proximal tubule on the same optical plane is chosen for the measurement. A line starting from the urinary pole and ending at least 100 µm downstream is hand drawn. For this evaluation 6 crossing lines were designed along the tubule (1-6). Glomerular and peritubular vessels were labeled with TRITC 500 kDa. DT (distal tubule) shows concentrated dye.

The fluorescence intensity profile of the two lines over time was plotted after background removal. The resulting curves were smoothed using a Gamma Variate function in Fiji. The time expressed in seconds that takes to the fluorescent dye to cross the two lines of interest (Delta T) is expressed by the distance between the maxima of each fitted line multiplied by the scanline period (Figure 13). The tubular length and mean diameter were measured and used for calculation of tubular volume as shown previously (102). Finally, the SNGFR value expressed as nL/min was given by the formula SNGFR= Volume (nL) *60/Delta t.

In order to make the results more robust, the SNGFR value for each tubule was measured at least 3 times changing the position of ROI2.

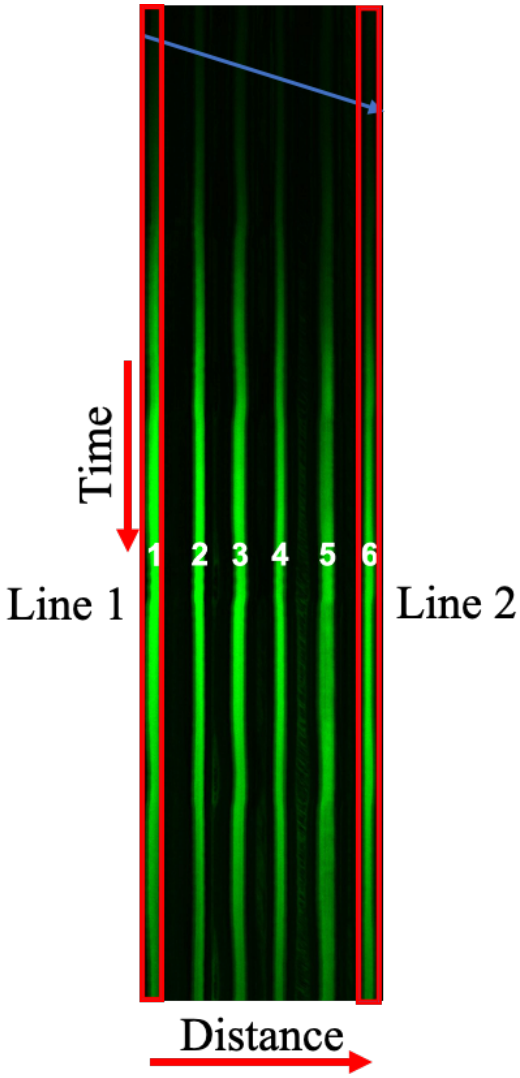

Figure 12. Analysis of the linescan technique. The output of linescan is a path of fluorescent vertical lines, each representing a different tubular crossing, where the x axis corresponds to the distance of the linescan and the y axis represents the time spent for the acquisition. The fluorescence intensity first occurs at line1, which represents the arrival of the FITC bolus in the tubular lumen, then it gradually appears in the other lines.

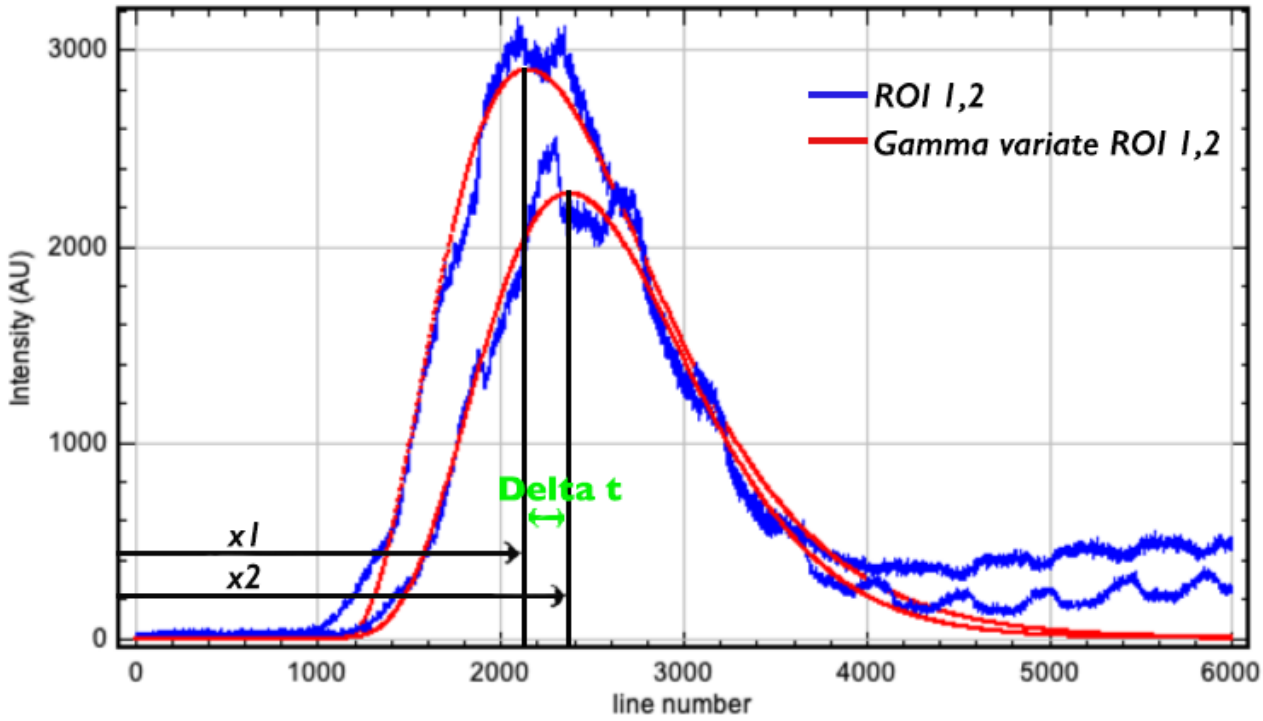

Figure 13. Representation of the fluorescence intensity profile of the two selected lines over time. On x axis is reported the number of acquired lines, which is further converted in time (sec), whereas the y axis represents the fluorescence intensity expresses as arbitrary unit. In the panel the original curves and the smoothed curves using gamma variate function are shown. The Delta t is calculated as the difference in seconds between the maxima points of the two smoothed curves.

2.2.2 Validation of linescan method

We first aimed to assess SNGFR measurements using the innovative linescan approach in control MWF rats. SNGFR in control rats averaged 19.6 ± 1.22 nl/min (46 early proximal tubules from 5 different animals), as shown in figure 14. These values were comparable with those obtained previously with renal micro-puncture (152). In order to demonstrate the efficiency of this technique, SNGFR was also measured in low-dose dopamine-treated and ischemic rats. Significantly higher values were obtained in 3 μg/kg/min dopamine-treated rats (25.5 ± 2 nl/min, 34 early proximal tubules from 3 different animals, P=0,0117), reflecting the hyperfiltration mechanism caused by vasodilation following low-dose dopamine treatment (Figure 14).

SNGFR was then measured in rats underwent 30 minutes of unilateral ischemia-reperfusion injury. The ischemic condition was confirmed by the necrotic tubules, the intraluminal cast and debris formation, and the vessels congestion shown in the animal kidneys, consistent with previous data (Figure 15). Ischemic rats exhibited significantly lower levels of SNGFR compared to the controls

(13.2 ± 1.07 nl/min, 32 early proximal tubules from 3 different animals, P=0,0067), confirming the acute kidney injury process as described before (148) (Figure 14).

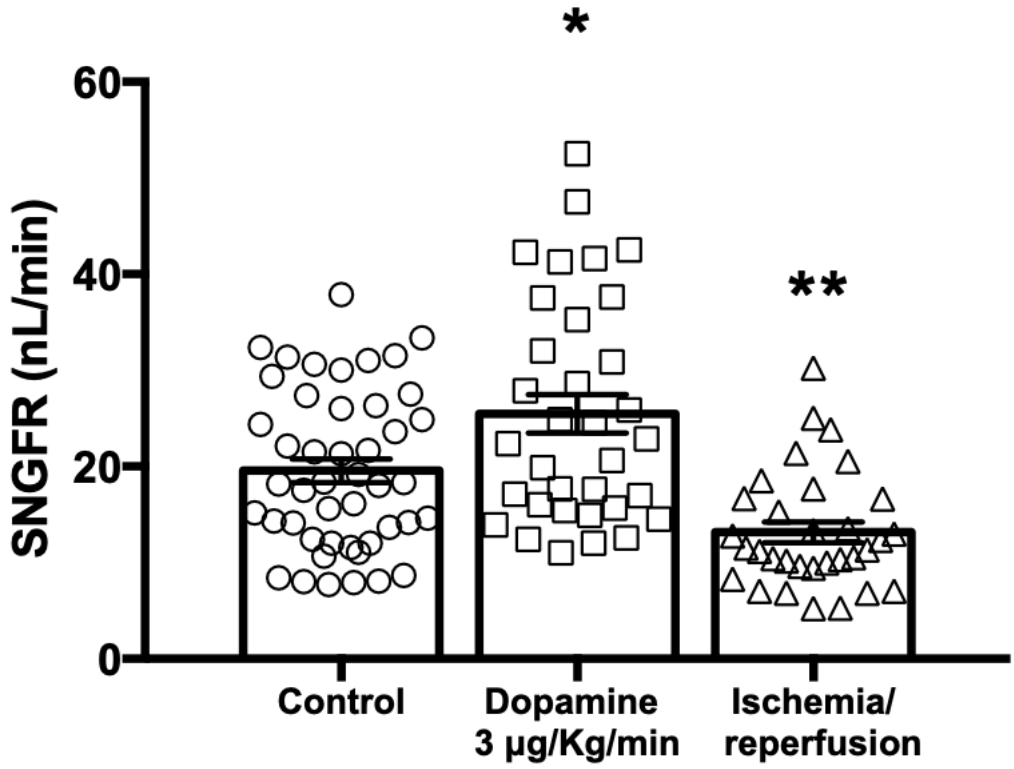

Figure 14. SNGFR measurements in control, 3 µg/kg/min dopamine and ischemia/reperfusion rats. Low-dose dopamine treated animals show significantly higher SNGFR than control group, whereas ischemic rats exhibit significantly lower SNGFR compared to control group. Each point for all groups represents a single value of SNGFR measured.

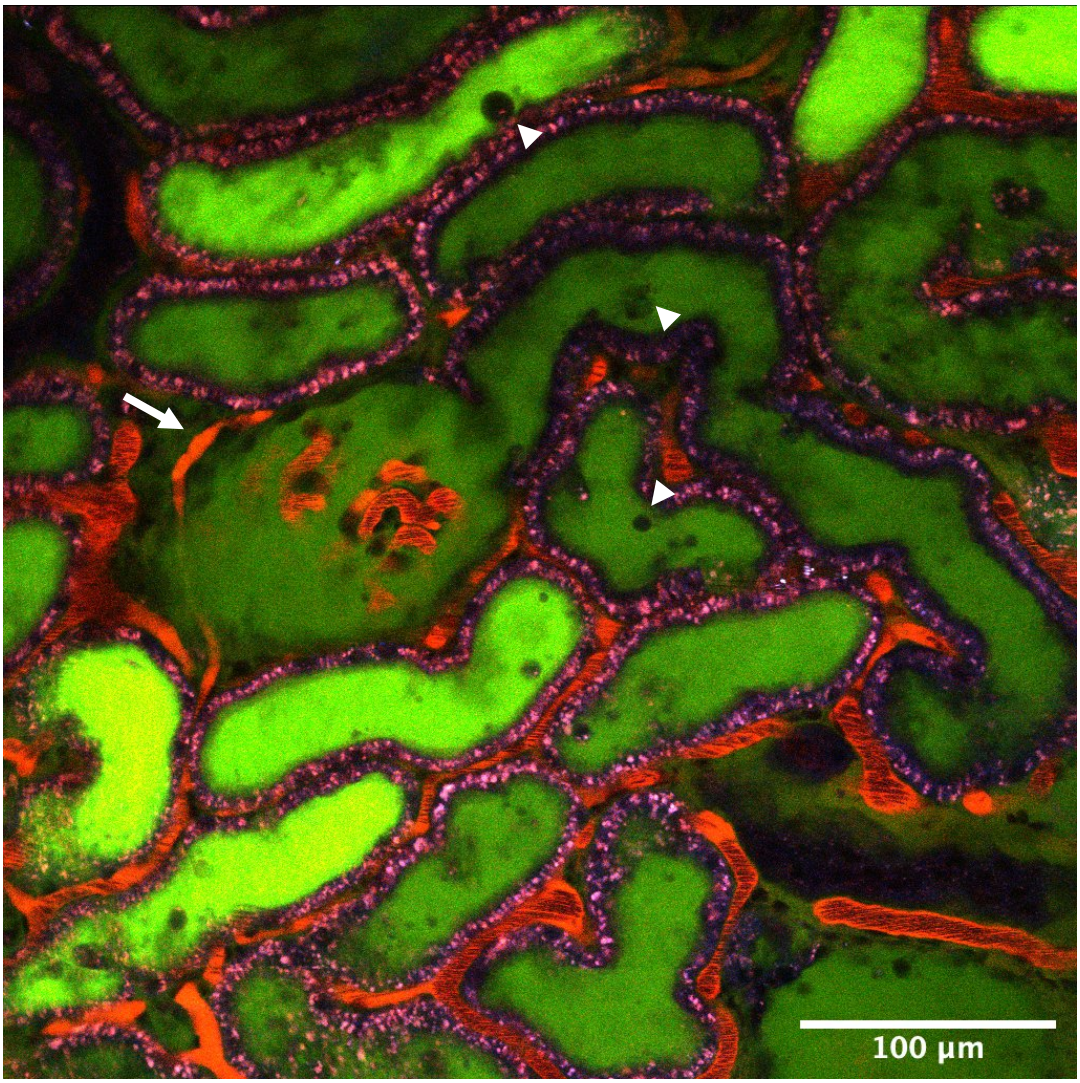

Figure 15. Effects of ischemia/reperfusion injury on rat renal cortex. The ischemic renal tubules show variable and widespread necrosis, as confirmed by the intraluminal debris and cellular cast formation (arrowhead). The peritubular capillaries congestion as a consequence of vascular endothelium impairment is also visible (arrow). Blood vessels and tubular lumen are stained with TRITC 500 kDa and FITC 3-5 kDa, respectively.

3. ASSESSING TUBULAR FUNCTION OF PROXIMAL TUBULE

3.1 INTRODUCTION

3.1.1 Glucose handling by the kidney: tubular reabsorption

The renal glucose handling is crucial to understand the kidney function. The kidneys play a pivotal role in glucose homeostasis, releasing glucose into the circulation (gluconeogenesis), taking up the glucose from the blood to allow tissues utilization, and, most importantly, reabsorbing glucose from ultrafiltrate. The plasma glucose concentration is 70-100 mg/dL in fasting conditions, and his mobilization to the tissues and to the blood is regulated by insulin, glucagon and other hormones.

Since it is not protein-bound or complexed with macromolecules, the plasma glucose is freely filtered by the kidneys, then it is nearly all reabsorbed by the proximal tubules so that only traces normally appear in the urine (153). After filtration, glucose concentration in the lumen matches glucose concentration in plasma, whereas it dramatically drops when proximal tubules start absorbing glucose. Consequently, glucose reabsorption is an active transport mechanism since it moves against a concentration gradient. The S1 proximal tubules reabsorb the majority of filtered glucose, while the remaining glucose reaching the S3 proximal tubules is readily reabsorbed, as shown by experiments on isolated rabbit nephrons (154). The glucose reabsorption requires the apical uptake mediated by a member of Na/glucose cotransporter family (SGLT) which couple the movements of glucose and Na^+, while the exit from the cells is guaranteed by a member of GLUT transporter family, located on the basolateral membrane (153). Six members of SGLT family have been identified and included in a bigger family of transporters, known as SLC5: SGLT1 and SGLT2 are the best characterized, and they differ for their localization in the nephron, affinity for the glucose and glucose transport capacity (155). Regarding the GLUT family, five transporters called GLUT1, GLUT2, GLUT3, GLUT4 and GLUT5 have been identified in human tissues and they are widely distributed in most organs, including kidney, liver, brain, intestine and placenta (156).

Figure 16 shows in detail the glucose reabsorption by SGLT and GLUT in renal tubules. The high-capacity/low-affinity SGLT2 transporter mediates the apical glucose transport in the S1 proximal tubule with a Na^+/glucose stoichiometry 1:1, and it is responsible for the 90% of glucose uptake (157). On the other hand, the S3 proximal tubule accomplishes this function using high-affinity/low-capacity SGLT1 transporter with a Na^+/glucose stoichiometry 2:1 (158). Once entered in the cell, glucose is reabsorbed in the blood circulation through the basolateral GLUT2 transporter in S1 and GLUT1 transporter in S3 proximal tubules (159).

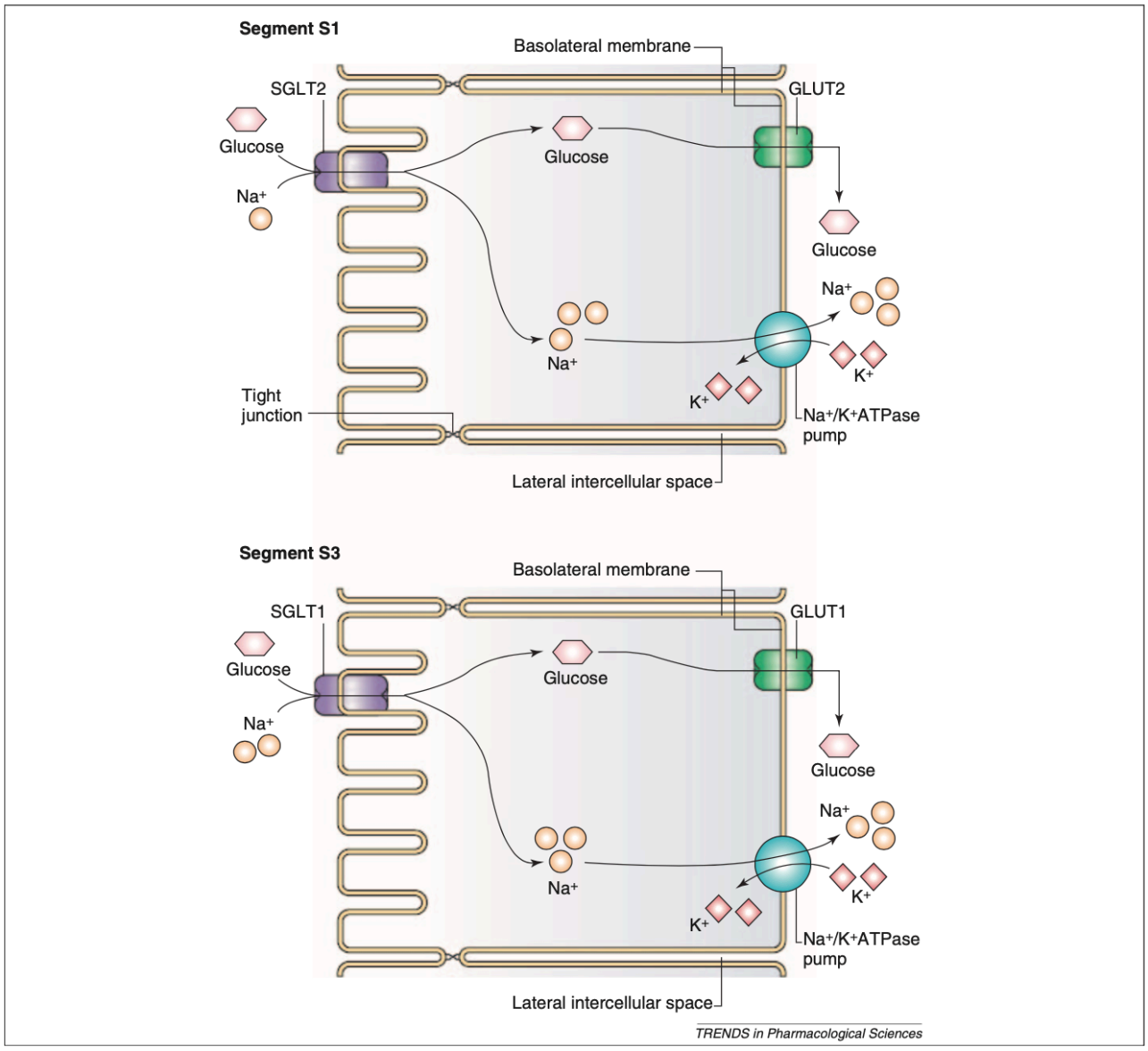

Figure 16. Glucose reabsorption by SGLT and GLUT in renal proximal tubules. Nearly all the glucose filtered by the kidney is reabsorbed along the renal proximal tubules. More than 90% of glucose is reabsorbed by SGLT2 located on the apical membrane of early proximal tubules. Remaining glucose is further reabsorbed in late proximal tubules by SGLT1. Once in the cell, glucose returns to the bloodstream by facilitated diffusion and this mechanism is mediated by GLUT2 and GLUT1 transporters located on the basolateral membrane of early and late proximal tubules, respectively. Bailey et al., 2011.

Unlike GLUT1 which may be saturated even at normal glucose concentration, GLUT2 is distributed in tissues presenting high glucose fluxes where it is difficult to become saturated (160). Compared to the SGLT family, the GLUT transporters are Na^+ independent, moving glucose by facilitated diffusion. The basolateral Na^+K^+ pump maintains the Na^+ concentration relatively low, forcing the

Na^+ to exit from the cell. Thus, this mechanism ensures an electrochemical Na^+ gradient driving the glucose movement to the cell (161).

Physiologically, glucose does not appear in the urine even after a meal when the plasma glucose concentration is about 180 mg/dL. If this threshold value is exceeded patients experience glycosuria. When the plasma glucose concentration reaches 400 mg/dL the glucose transporters SGLT1 and SGLT2 are fully saturated, therefore they can't reabsorb further glucose filtered, raising dramatically the glucose excretion. This imbalance between the filtration of glucose and the capacity of renal tubules to reabsorb it can occur when the plasma glucose levels are high, as during the diabetes mellitus, or when tubular reabsorption is compromised, as in the Fanconi-Bickel syndrome (162).

3.1.2 Glucose metabolism in Fanconi Bickel syndrome

Fanconi Bickel syndrome (FBS) is a rare autosomal recessive disease characterized by hepatic and renal glucose accumulation, leading to an altered glucose and galactose utilization, and disfunctions of proximal tubule (163). Patients affected by FBS suffers from electrolyte and pH imbalances, and they exhibit features such as rickets, polyuria, hepatomegaly, and osteoporosis (164, 165). It is known that the biochemical aspects of FBS include fasting hypoglycemia, post prandial hyperglycemia and glucose intolerance but the molecular mechanisms underlying the dysglycemia are not well elucidated (166). The pathology of FBS is caused by heterozygous and homozygous mutations in GLUT2 gene, which is mostly expressed in hepatocytes (167) , renal proximal tubules (168) , pancreatic cells (169) and neuronal cells (170). GLUT2 has a pivotal role in maintaining the physiological glucose homeostasis by glucose reabsorption through renal proximal tubules, glucose release from hepatic cells and insulin secretion from pancreatic cells. In FBS patients the lack of GLUT2, which normally permits the reuptake of glucose in bloodstream, results in glycogen accumulation in liver and kidney and can lead to glomerular hyperfiltration and micro-albuminuria (171). Moreover, impairment of GLUT2 is known to cause glycosuria, metabolic acidosis, phosphaturia, hypercalciuria and hypophosphatemia as well as nephropathy (172, 173). As stated above, the dysglycemia shown in FBS leads to different pathological patterns such as the fasting hypoglycemia, which is aggravated by renal glycosuria, and the post prandial hyperglycemia, due to a defect of insulin production from pancreatic β-cells. Other conditions related to the dysglycemia are neonatal diabetes and frank diabetes mellitus. Despite the dysglycemia caused by FBS, patients show normal values of glycated haemoglobin-A1c. Moreover, GLUT2 is thought to work properly in enterocytes of patients affected by FBS, as evidenced by the normal glucose transport in intestinal cells (174). The role of GLUT2 in pancreatic cells is not yet well investigated, but the high number of cases of neonatal diabetes suggests that it could be involved in insulin production during the fetal phase (175) (Figure 17).

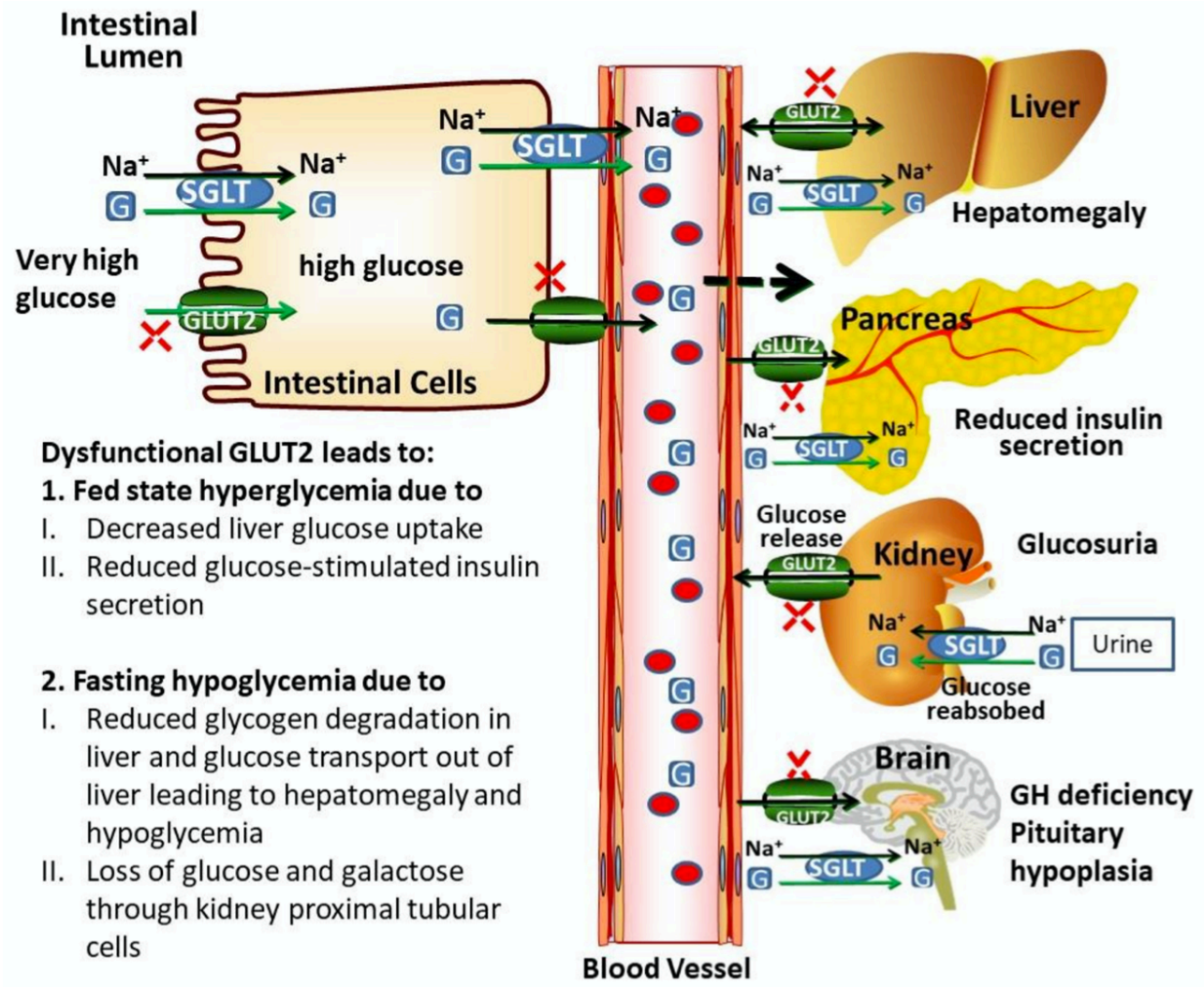

Figure 17. Summary of pathophysiology of GLUT2 disfunction in FBS. GLUT2 maintains the physiological glucose homeostasis in liver, pancreas, kidney and brain. Overall, GLUT2 disfunctions cause fasting hypoglycemia, postprandial hyperglycemia, glucose and galactose intolerance, hepatomegaly, glucosuria, reduced GSIS (glucose-stimulated insulin secretion) and GH (growth hormone) deficiency. The postprandial hyperglycemia is due to decreased glucose uptake by liver and reduced insulin secretion by pancreatic cells, while fasting hypoglycemia is caused by the lack of glucose reabsorption by the kidney and lowered glycogen degradation in liver. The reduced GH production in brain is a consequence of parasympathetic and sympathetic systems alterations. Sharari et al., 2020

At present there is not a specific treatment in clinical practice for FBS but the integration of phosphate, vitamin D, potassium and bicarbonate is the only therapy compensating the disease (176, 177). Further investigations are needed to better understand the mechanisms regulating the pathological

patterns of the disease especially in kidney, liver and pancreas, and to develop a therapy that specifically triggers the molecular defect.

3.1.3 Limitations of *in vitro* approaches and advantages of *in vivo* imaging to assess the glucose metabolism

The intricated structure of the kidney allows it to have many specialized functions. This complexity, however, has limited the full understanding of metabolic and transport processes in renal tubules. Efforts to elucidate the renal metabolism were made in the last century using *in vitro* methods, such as isolated cells or tubules, and ex vivo kidney slices (178, 179). Despite these approaches resulted fundamental to raise the understanding of the basic mechanisms underlying the renal metabolism, such limited techniques are constrained in that the cells are removed from their original contest which physiologically influence the cell metabolism. Experiments on isolated tubules provided insights within the context of the organ, but the results obtained did lack spatial and temporal resolution to link the function with the metabolism in a specific tubular segment. As stated above, the cells and freshly isolated tissues can't accurately reproduce the complex interactions occurring in living systems.

In the last decades the imaging tools are improving our capacity to understand the dynamic cell processes, becoming powerful methods to be used for clinical and preclinical assessment of metabolic functions maintaining the context of whole organ. In this scenario, MPM represents an ideal tool to investigate the tubular transport of metabolites and proteins thanks to its ability to resolve tubular mechanisms at cellular resolution. As shown by Hato et al., the glucose tubular uptake can be evaluated in murine living kidney to assess the functionality of glucose receptors and the metabolic state. In particular, the authors coupled the MPM with positron emission tomography (PET) to assess cortical and proximal tubule glucose tracer uptake, following experimental perturbations of renal metabolism. The continuous infusion of glucose analogue in animals allowed to image over the time and analyze the cellular reabsorption, quantifying the kinetics of glucose transport in the living kidney. The results obtained by the authors revealed an innovative application of intravital microscopy to evaluate the glucose uptake in vivo, overcoming the limits exhibited by previous methods (180).

3.1.4 Physiological role of beta-lactoglobulin

Beta-lactoglobulin (BLG) is one of the most abundant whey proteins in milk of many species, including bovines, baboons and rhesus monkeys, but it is absent from human milk (181). In ruminant milk, BLG exists as dimer at normal pH with a molecular weight of 36 kDa. BLG has been widely studied in the last decades especially in the field of chemical food because of its molecular

characteristics. Indeed, it provides an important nutritional value given by its copious aminoacidic composition. BLG is thought to be involved in many biological processes. Since it has many ligand bindings sites, BLG can bind vitamins A and D, palmitic acid as well as other hydrophobic compounds (182). In addition, LBG seems to have great binding affinity with fatty acid, phospholipids and aromatic compounds (181). Besides its ligand binding ability, BLG may contributes to protect body against diseases. According to recent studies, BLG exhibits antimicrobial and antioxidant activities, which could be used to treat sepsis and infections (183). As shown by Li et al, BLC could be associated with curcumin to improve its bioactivity and antioxidant activity (184). Furthermore, Tai et al demonstrated that BLG plays a key role in promoting the immune response, enhancing the cell proliferation through a receptor-mediated mechanism (185). The whey proteins in fact are known to stimulate the mucosal immunity and to improve the migration of immune cells to the secondary lymphoid organs (186). As shown by Belford et al, BLG stimulates the growth activity in many cell types, including human skin, human embryonic lungs fibroblast and rat myoblast (187). BLG was also exploited to ameliorate the encapsulating systems in nutraceuticals thanks to its high solubility, binding ability and resistance against peptide digestion (188).

3.1.5 Proteins tubular uptake

The glomerular filtration barrier selectively filters molecules to limit the filtration of beneficial substances and the waste in the urine of the majority of proteins. However, albumin, lysozyme, hormones, light chains of immunoglobulins and other proteins can be filtered in certain amount. Therefore, the kidney needs to retrieve most of them to prevent proteinuria and albuminuria. Indeed, human kidneys filter more the 3 g of albumin per day and the renal tubules reabsorb 96%-99% of filtered albumin so that only traces appear in the urine, consistent with micro-puncture experiments on rats (189). More than 70% of filtered albumin is reabsorbed by proximal tubules, whereas another 26% is taken up by more distal nephron segments (190). Similarly, about 10 g of low molecular weight proteins are filtered by the kidney and a similar amount is then reabsorbed. Moreover, the protein uptake by renal tubules is essential to recovery vitamins, hormones and enzymes. Figure 18 shows the fraction of the filtered load that the proximal tubule reabsorbs.

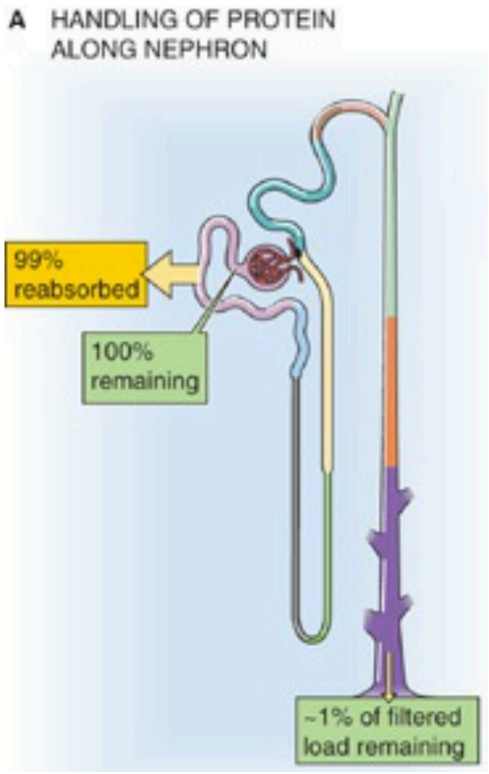

Figure 18. Protein handling by the kidney. The kidneys reabsorb 96-99% of filtered albumin as well as other proteins, such as lysozyme, β2-microglobulin and light chains of immunoglobulins. The green boxes show the percentage of the protein load that remains in the tubular lumen in the different nephron segments. Adapted from Boron et al., 2012

Protein and peptide reabsorption is carried out through a mechanism of receptor-mediated endocytosis and this function takes place mostly in the early proximal tubule cells. First part of the process is the binding of the proteins to the receptors at the apical membrane, including megalin and cubilin. Then, the internalization into clathrin-coated endocytic vesicles occurs, followed by the fusion of the vesicles with endosomes. Subsequently, the vesicle membranes are recycled to the apical surface and their content is targeted for lysosomes for storage or degradation. The proteins avoiding the lysosomes are moved to the basolateral membrane, mostly by transcytosis, then they are released in the blood circulation (191) (Figure 19). Damages to the proximal tubules can lead to proteinuria even when the glomerular filtration barrier is not compromised. This explains how the kidney play a fundamental role in the metabolism of peptides and proteins.

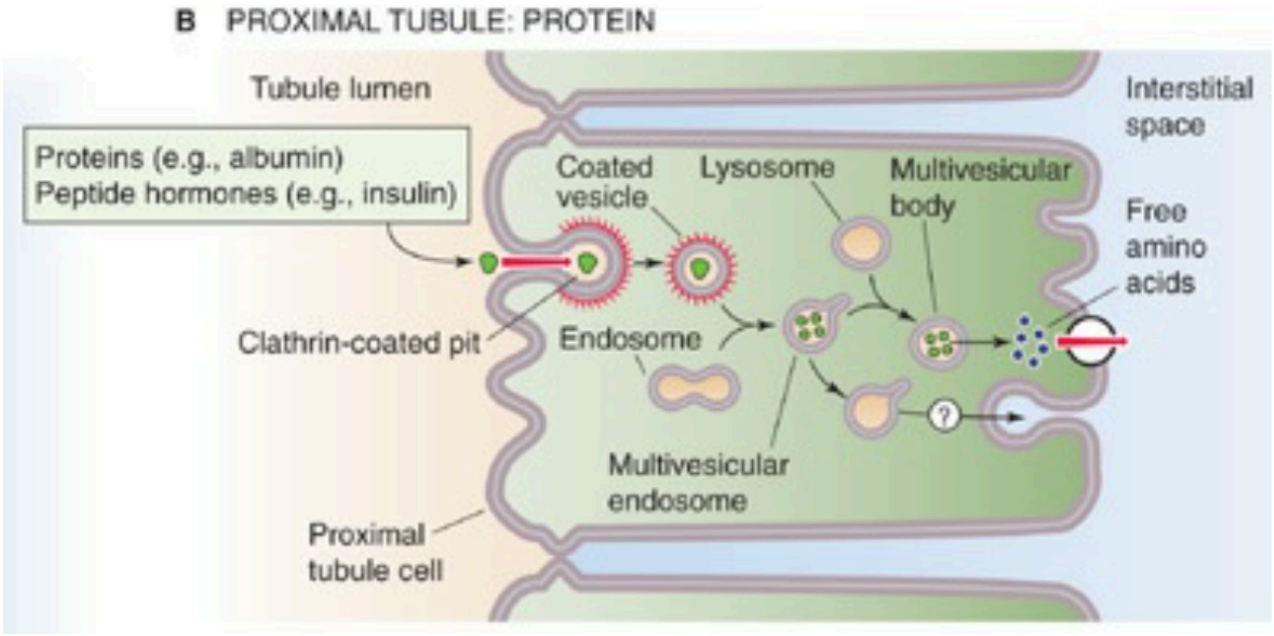

Figure 19. Protein reabsorption in kidney by receptor-mediated endocytosis. See text for details. Adapted from Boron et., 2012

3.1.6 *In vivo* assessment of tubular protein uptake

As largely discussed above, the *in vitro* systems are too simple to investigate complex cell processes, such as the tubular uptake of proteins, which involve several receptors and is regulated by hormones. In literature several examples regarding the *in vivo* protein uptake in kidney using MPM are described. Russo et al, for instance, demonstrated the use of intravital microscopy to investigate the causes leading to albuminuria in diabetic nephropathy. Indeed, the infusion of albumin-labeled dye in rats allowed to analyze the albumin endocytosis and distribution along the proximal tubule in control and diabetic rats, offering new insights in understanding the albuminuria process useful to develop new diagnostic tools and treatments efficient in therapy of diabetic nephropathy (192).

The group of Molitoris et al. instead, investigated the process of glomerular filtration and tubular uptake of albumin to clarify the role of proximal tubules cells in regulating these processes. Using a rat model exhibiting an albumin overload, the authors quantified the glomerular sieving coefficients (GSC) and the tubular uptake of Texas red-labeled albumin using MPM. Indeed, they demonstrated a significant lowering in albumin uptake across the proximal tubules. In addition, they identified potential proteins and pathways influenced by albumin overload, suggesting an important role of tubular cells in responding quickly to alterations of physiological conditions to keep the albumin values within regular levels (193).

Another example showing the investigation of protein reabsorption using MPM is given by the work of Endres et al., who evaluated the mechanisms leading to albuminuria in Dahl salt-sensitive rats, an

animal model of hypertension. The investigators confirmed that both glomerulus structure and proximal tubule cells affect the albuminuria, suggesting that triggering these two renal compartments may provide an efficient treatment against hypertension (194).

3.2 RESULTS

3.2.1 Imaging and analysis methods of *in vivo* glucose tubular uptake

Tubular auto-fluorescence was used to identify the area of interest rich in proximal tubules before fluorescent dye injection. Then, a total of 100 µl fluorescent glucose analog 2-NBDG was injected in mice for 10 minutes and the intravital imaging of the kidney was performed over 30 minutes. Images acquisition was timed every 3 seconds to avoid laser damages. Laser power and PMT gain were adjusted during imaging to avoid clipping or saturation of the fluorescence signal.

Image processing was performed using Fiji software. Indeed, time series were first denoised with Fiji PureDenoise plugin using automated global estimation. Then, a CLAHE filter was applied to each frame with a block size of 32 and a standardization to a Zscore by subtracting the mean fluorescence and dividing by the standard deviation of the mean was carried out.

In order to quantify the fluorescence in tubular cells (TCs) and tubular lumen, Tseries were segmented with Ilastik, a semiautomated machine learning-based segmentation software. A parallel random forest classifier was trained in Ilastik by using at least three frames for each processed Tseries. Images were segmented in two classes (TCs and tubular lumen/ peritubular interstitium), therefore producing segmentation masks where each pixel was assigned two possible values depending on their assignment by the algorithm.

In order to minimize the sample drift due to breathing and hearth beat during the imaging experiments, the segmentation masks were then added as a third channel to the denoised-shading corrected Tseries and used as target of choice for the Fiji plugin Descriptor based series registration (2d/3d+t).

After the Tseries stabilization, ROIs were positioned over each S1 proximal tubule recognized by their strong autofluorescence and significant increase of 2-NBDG marker over the time of the infusion. For each ROI, to obtain the fluorescent glucose signal shown in the cells the previously processed segmentation mask was multiplied in order to set to zero the areas covered by the lumen and the interstitium. Subsequently, the Tseries were converted to 32bit and a NaN (Not a Number) value was assigned to zero pixels. The ROIs were then measured. The quantification of the lumen was carried out in a similar way, giving a zero value to the pixels corresponding to the cell class in the segmentation mask (Figure 20).

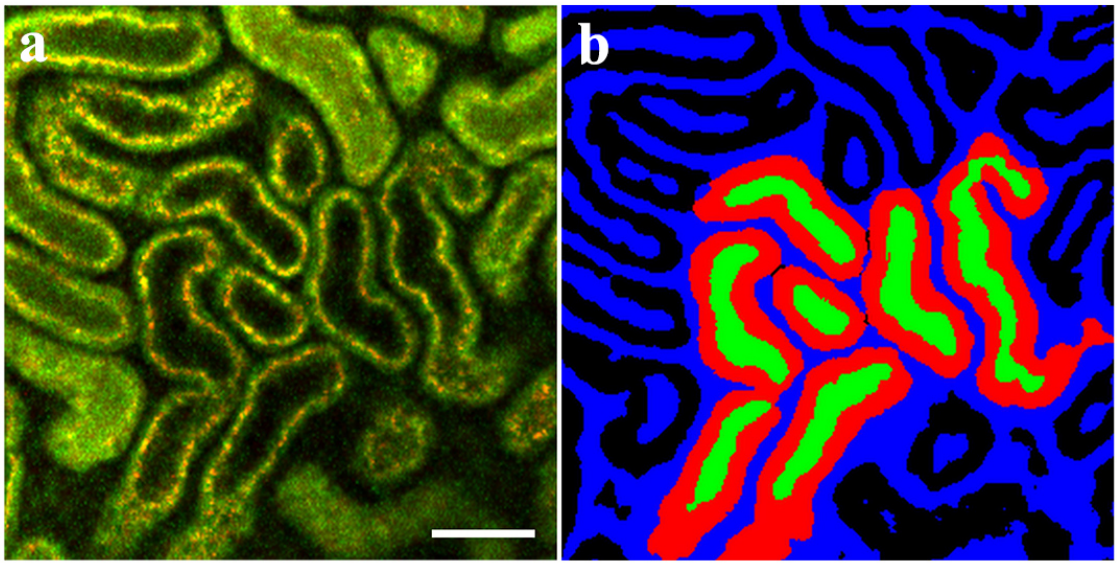

Figure 20. Image processing of glucose infusion in mice kidney using Ilastik software. Panel a shows the autofluorescence of the proximal tubules before the glucose infusion. Early proximal tubules exhibit marked autofluorescence at apical membrane, whereas late proximal tubules show stronger fluorescence in cellular compartments. Panel b shows the tubular segmentation of S1 proximal tubules after Ilastik processing. In particular, two classes of segmentation were developed: red color was assigned to tubular cells, while green color represented lumen. Scale bar measures 50 μm.

3.2.2 GLUT2 mice show an altered glucose utilization in renal tubules

To measure and quantify the glucose uptake in control and cKO mice, we evaluated the reabsorption of fluorescent glucose analogue 2-NBDG across the renal proximal tubules using multi-photon microscopy. The glucose infusion lasted 10 minutes and the imaging was carried out over 30 minutes. The typical autofluorescence of proximal tubules was visible in all animals, however the tubular morphology in cKO mice was altered with an apical and intraluminal widely distributed fluorescent spotting, as a consequence of renal damage. After 4 minutes from the glucose administration, 2-NBDG was more noticeable in the lumen of S1 proximal tubules of control mice than in cKO mice, where fluorescence was instead appreciable in the distal tubules. The Control mice showed further increase of fluorescence over the time, and after 15 minutes 2-NBDG was evident in the cellular compartment of early proximal tubules as a physiological mechanism of reabsorption. At 15 minutes, the fluorescence in cKO mice was very appreciable in late proximal tubules, showing an altered mechanism of reabsorption in the early proximal tubules (Figure 21).

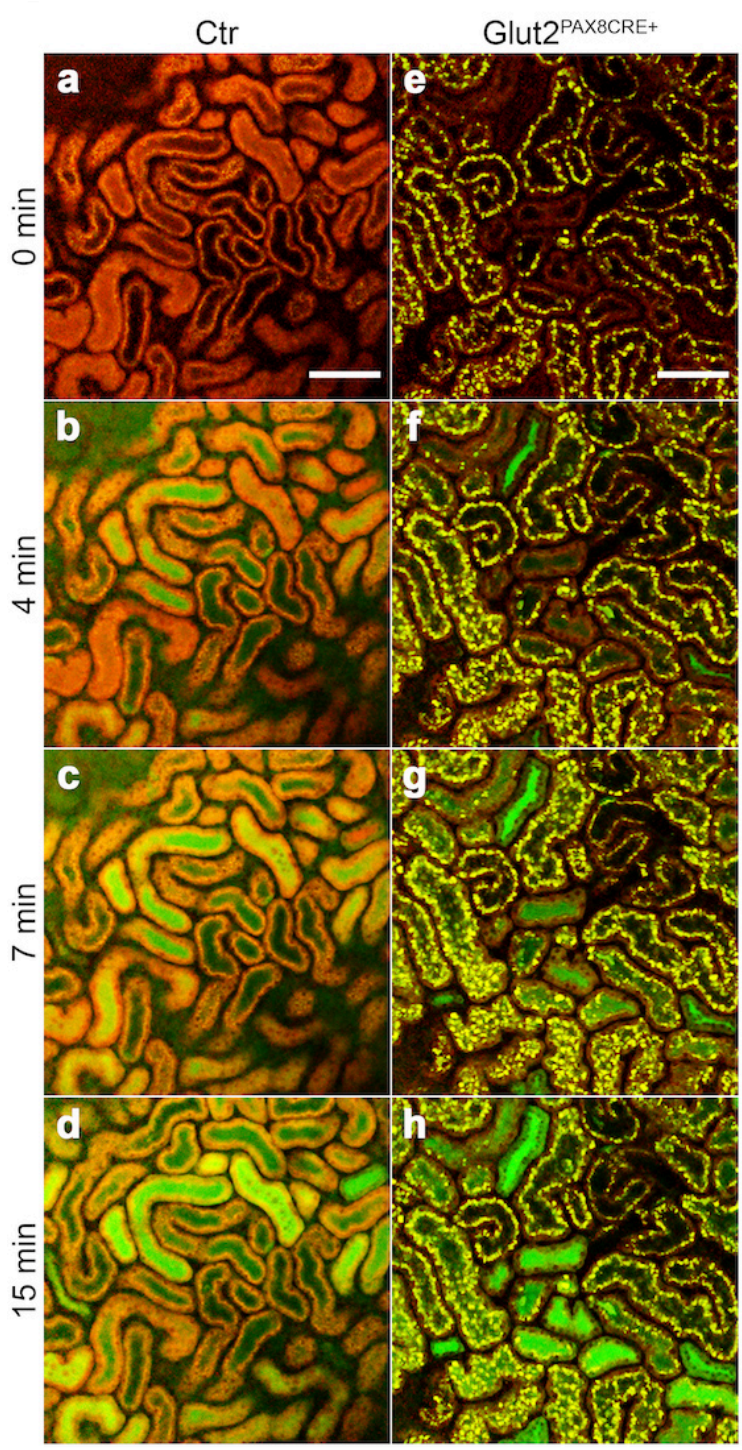

Figure 21. Glucose uptake in renal tubules of control and GLUT2 cKO mice. The tubular autofluorescence visible in renal cortex is well preserved in control mice (a), while cKO mice show significant altered tubular morphology, suggesting renal damage (e). After the infusion of 2-NBDG, control animals show a gradual increase of fluorescence first in lumen (b and c), then in cell compartments of early proximal tubules (d) showing physiological uptake mechanism. On the contrary, cKO animals exhibit less fluorescence in early proximal tubules (f and g), whereas the 2-NBDG signal is very appreciable in late proximal tubules (h), suggesting an impaired mechanism of tubular reabsorption. Scale bar measures 100 μm.

After the imaging of the renal tubules, the t-series of glucose infusion were analyzed as stated above. In particular, only the early proximal tubules were chosen for the analysis in order to evaluate the functionality of GLUT2 transporter.

The fluorescence intensity of intracellular glucose was normalized with the filtered glucose fluorescence in early proximal tubules. Analysis of time-fluorescence intensity curves, shown as cells/lumen ratio, revealed a faster process of tubular glucose reabsorption in control mice, becoming then comparable within the 2 groups after 7 minutes (Figure 22).

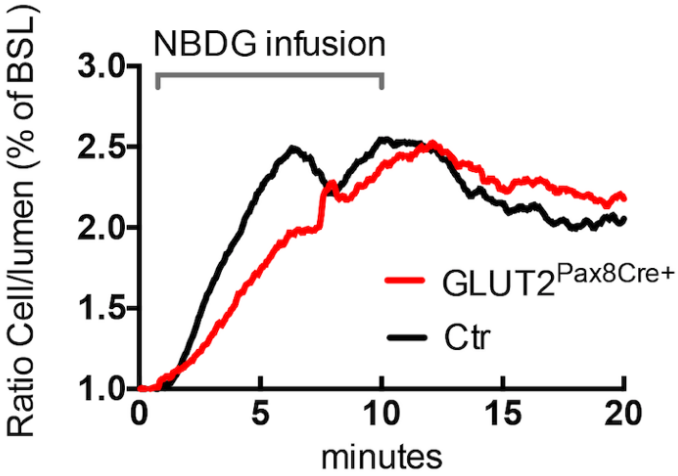

Figure 22. Analysis of time fluorescence intensity curves of glucose uptake. The curves are expressed as the ratio between the fluorescence of 2-NBDG in cells and lumen for control and cKO groups. As indicated in the figure, the control animals exhibit a faster process of glucose reabsorption across the early proximal tubules than cKO group, suggesting that impairment of GLUT2 cause an alteration of the renal glucose uptake.

3.2.3 Imaging of *in vivo* beta-lactoglobulin tubular uptake

Before fluorescent marker administration, autofluorescence of the renal cortex was used to focus the proximal tubules of interest. Then, 25 µl of fluorescent Alexa 568-conjugated beta-lactoglobulin were injected in mice as bolus and the intravital imaging of the globulin uptake across the proximal tubules was performed for 5 minutes in order to image the apical uptake. The t-series was acquired every 1 second. Five minutes later the end of t-series, the imaging of the same zoomed region was carried out over 25 minutes in order to evaluate the clearance time of beta-lactoglobulin from the tubules. For beta-lactoglobulin clearance the t-series was acquired every 3 second to avoid tissues damages.

Laser power and PMT gain were adjusted during imaging to avoid clipping or saturation of the fluorescence signal.

Image processing was performed using Fiji software. In particular, for each frame of the t-series the fiji plugin Descriptor based series registration (2d/3d+t) was applied in order to reduce the drift and the artifacts caused by breathing and heart beats of the animals. Then, the channels were split and only the channel of interest (red) corresponding to the beta-lactoglobulin signal was used for the analysis. The ROIs were positioned within the apical membrane of each S1 proximal tubules and the mean fluorescence intensity was plotted over the time. At least 4 tubules were analyzed, and the final result was reported as mean value. The resulting curves were smoothed with a linear regression (Figure 23).

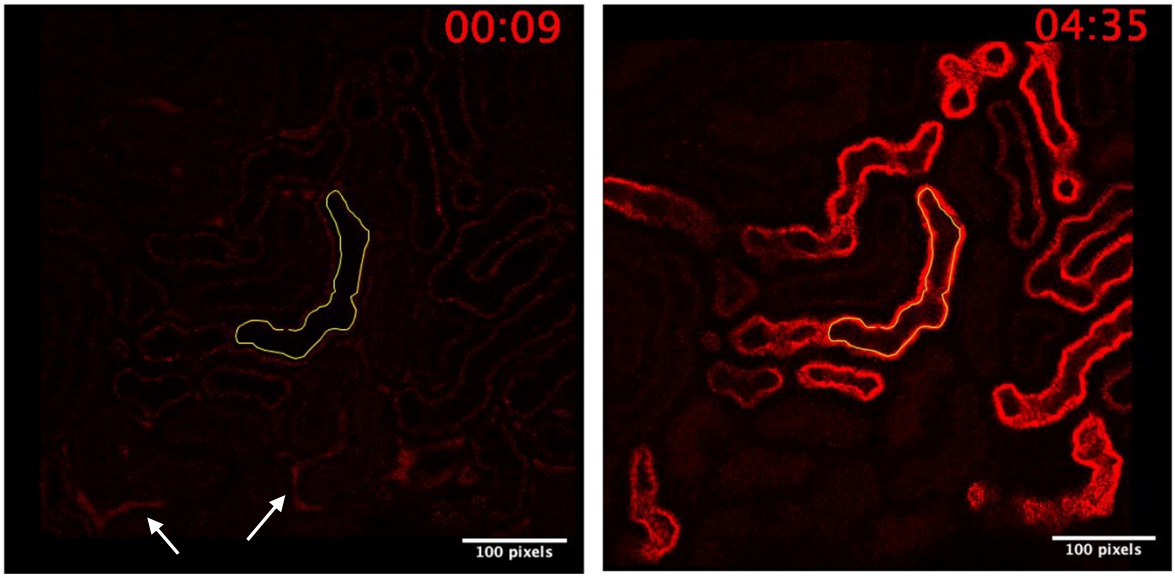

Figure 23. Analysis method of beta-lactoglobulin tubular uptake. The panel on the left shows the renal cortex of mice at the beginning of beta-lactoglobulin infusion. It is possible to observe the red autofluorescence of proximal tubular cells, while the red colored vessels (arrows) demonstrate the lactoglobulin arrival to the kidney vasculature. Additionally, an example of ROI selected to analyze the mean fluorescence in early proximal tubules is shown in yellow. The panel on the right shows the same region during the beta-lactoglobulin uptake across the apical membrane of proximal tubules. The time on the upper part of pictures is expresses in seconds.

3.2.4 MPM is an efficient tool to image the protein uptake across the proximal tubules

The evaluation of beta-lactoglobulin uptake by the proximal tubules of control mice was carried out by using intravital multiphoton microscopy. Fluorescent beta-lactoglobulin was injected in the animals as single bolus, then the imaging was performed over 30 minutes (5 minutes for the uptake study and 25 minutes to investigate the clearance of the uptake). The strong apical autofluorescence of early proximal tubules was very helpful to distinguish them from more distal segments and to focus

the right tubules. Right after the beta-lactoglobulin infusion, a red fluorescence was visible in the peritubular capillaries demonstrating a prompt arrival of the dye into the renal vasculature. After about 30 seconds the beta-lactoglobulin fluorescence was already visible across the brush borders of early proximal tubules, as expected. This fluorescence signal, clearly distinguishable from the autofluorescence of proximal tubules, become much stronger over the time and the maximum value was reached about 5 minutes later. We didn't notice any fluorescence across late proximal or distal tubules, confirming that protein uptake occurred only in early nephron segments (Figure 24).

We subsequently carried out the imaging of the same zoomed area for other 25 minutes, in order to investigate the clearance of the beta-lactoglobulin uptake. After 15 minutes from the beta-lactoglobulin administration (min 10:00) the fluorescence in the apical membrane is still very bright but it started to decrease progressively over the time. After about 25 minutes (30 minutes later the dye infusion) the red signal around brush borders is much weaker and some fluorescence is visible in the cellular compartments, as predictable in a physiological protein reabsorption process (Figure 25).

The analysis of the time-fluorescence intensity curves shows the intensity of the beta-lactoglobulin signal in brush border of early proximal tubules over the time, expressed as fluorescence arbitrary unit. In particular the curve represents the average of 6 tubules analyzed coming from one mouse, after the smoothing with a mathematical non-linear regression. As displayed in the graph (Figure 26), the signal increases progressively over the seconds to reach a plateau at around 5 minutes. The graph regarding the clearance time of the beta-lactoglobulin was obtained in similar way, measuring the average of the same tubules used for first analysis, and also in this case the curve was analyzed with a mathematical non-linear regression. As shown from the graph, the mean apical fluorescence was nearly stable for 10 minutes, then it started slowly to decrease.

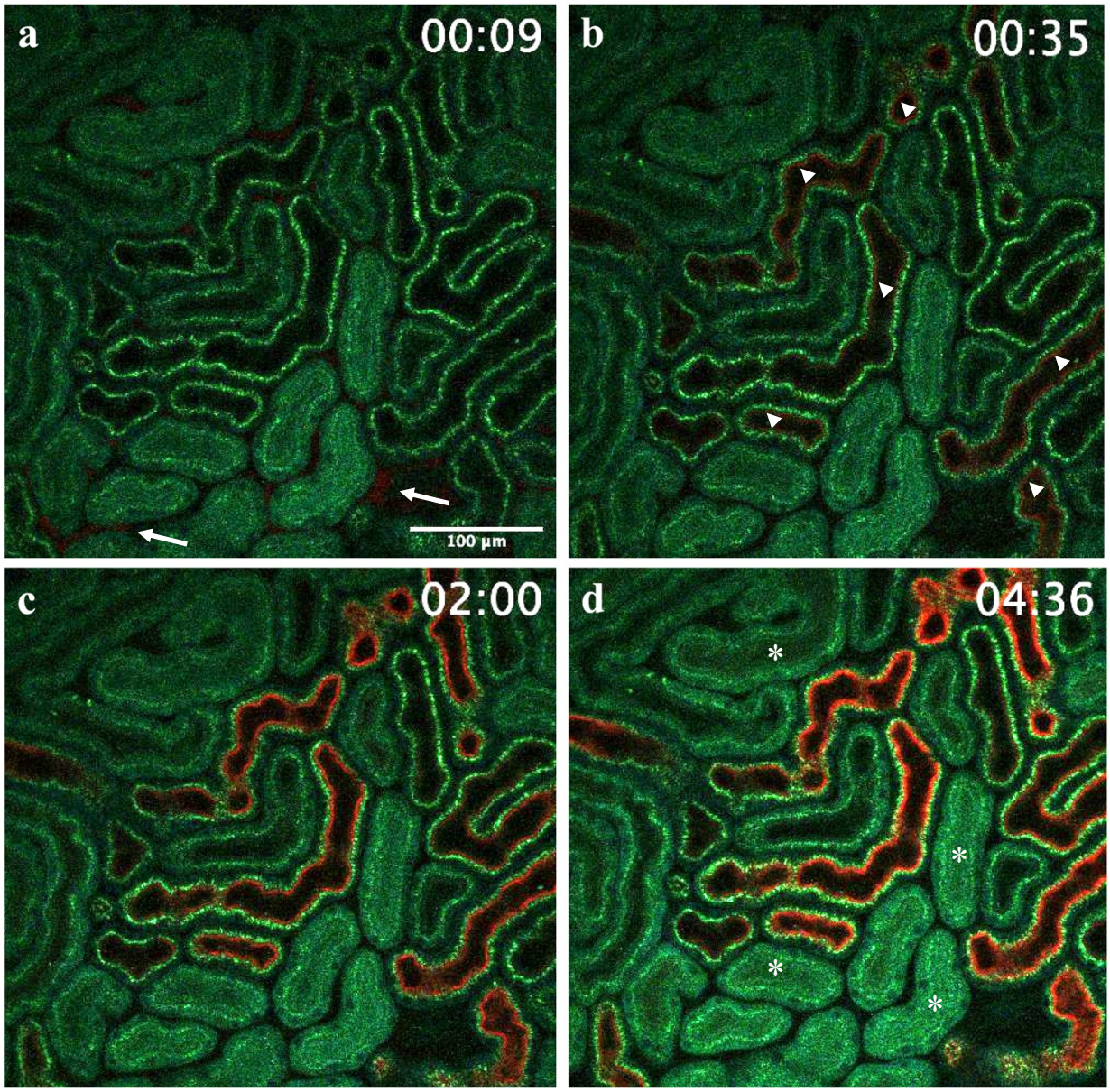

Figure 24. Beta-lactoglobulin uptake in mouse renal proximal tubules. The autofluorescence of proximal tubules in mouse renal cortex is well visible in green and beta-lactoglobulin signal is barely noticeable in peritubular capillaries (arrows) shown on red (a). The fluorescence of beta-lactoglobulin across the brush border of early proximal tubules is already visible after 30 seconds (b, arrowheads), it increases over the time (c) and reach the maximum intensity at about 5 minutes (d). Fluorescence of beta-lactoglobulin was not detectable in late proximal tubules (*), showing a physiological protein uptake mechanism.

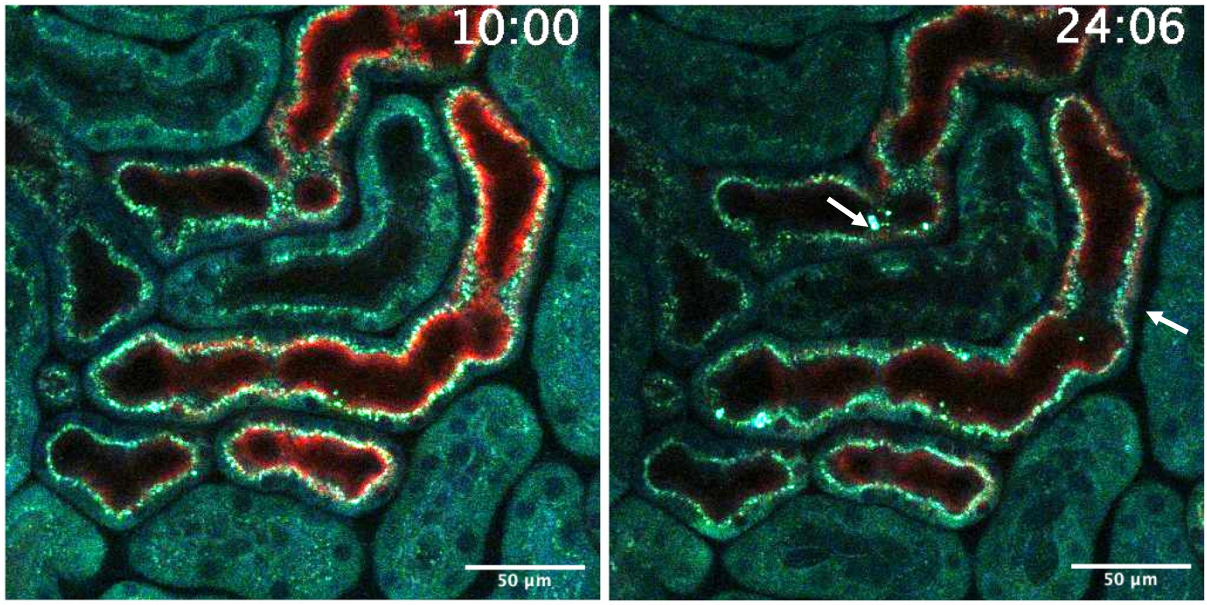

Figure 25. Image showing the clearance of beta-lactoglobulin uptake. The images show some of the same zoomed tubules seen in Figure 24 to see more in detail the fluorescence of beta-lactoglobulin. At 10 minutes (15 minutes from the injection) the red fluorescence is still bright across the brush border of early proximal tubules (left panel), whereas after 30 minutes from the dye administration (24 minutes) the apical signal of beta-lactoglobulin became very weak and some fluorescence is noticeable in the cellular compartments (arrows, right panel).

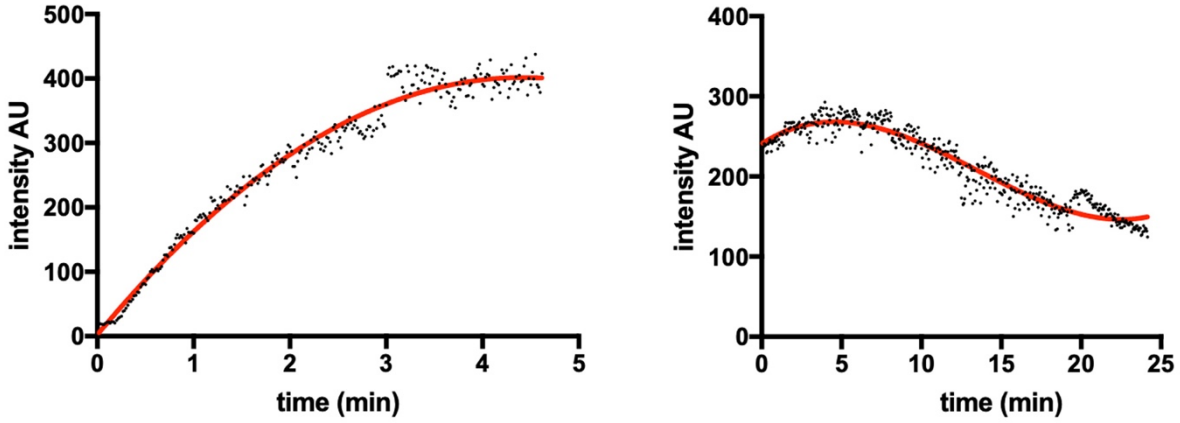

Figure 26. Analysis of time-fluorescence intensity curves of beta-lactoglobulin uptake. The graph on the left shows the initial uptake of beta-lactoglobulin, whose fluorescence in the apical membrane of proximal tubules increases gradually to became maximum at 5 minutes. The panel on the right describe the clearance of beta-lactoglobulin uptake in the same tubules after other subsequent 25 minutes of imaging. Particularly, the initial apical signal is already lower compared to maximum value observed in the first graph and it remains quite stable at 10 minutes. After that, it starts decreasing over time with consequent disappearing of apical fluorescence.

4. DETECTION AND QUANTIFICATION OF RENAL FIBROSIS

4.1 INTRODUCTION

4.1.1 Evaluation of tubulo-interstitial renal fibrosis with histological techniques

Tubulo-interstitial renal fibrosis can be described as the reduction of number of normal renal cells, replaced by extracellular matrix (ECM) components, including types I and III collagen. Physiologically, very little collagen fibers are visible in the glomeruli and interstitial space, while abundant ECM surrounds renal vessels. On the contrary, fibrotic samples exhibit strong deposit of collagen fibers in the tubular interstitium (195). Therefore, renal fibrosis constitutes an important landmark of progression in many diseases, including diabetic nephropathy and cancer.

Renal fibrosis is generally quantified using histological staining. Masson's trichrome and picrosirius red are the most used approaches, but they are limited in terms of variability of the staining and the data interpretation by the pathologist. Moreover, the signal obtained with histological techniques is not very specific, unless polarized microscope is used. Additionally, these methods lack 3D resolution so that they are strongly dependent from the thickness of the slice samples (95). Considering all these aspects, it is understandable that the reproducibility and reliability of these analyses can be controversial (Figure 27).

SHG is a MPM tool that uses a laser source inducing a second-order nonlinear polarization in the sample and emits at double harmonic frequency. SHG was first used in 1980s to image rat tail tendon, then it started to be exploited to detect the morphology of thick samples (196). SHG presents several advantages compared with histological approaches. First, since it is associated only at types I and III collagen fibers, it offers great specificity of the signal detected. Indeed, no SHG signal is detectable in non-fibrillar type IV collagen as shown by Strupler et al (96). Second, SHG has an endogenous 3D resolution that is proper of MPM, permitting 3D reconstructions useful for the analysis and avoiding variations due to variable thickness of the samples. Third, SHG only requires fresh unlabeled samples and no particular preparation is needed. Moreover, quantification of fibrosis using SHG can benefit the MPM advantages, like higher tissue penetration especially in thick samples and less light dispersion (95, 197).

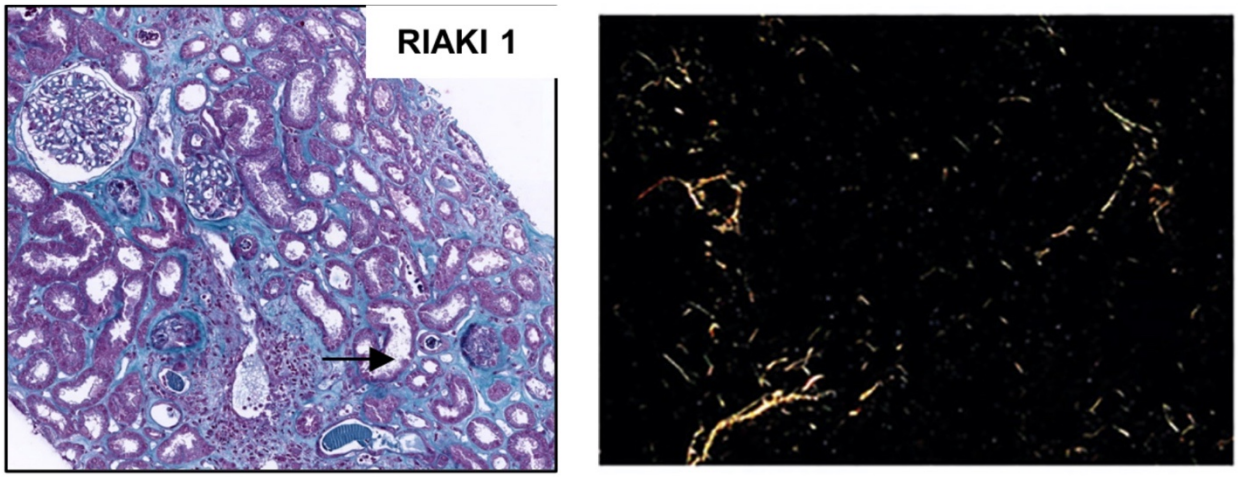

Figure 27. Detection of renal fibrosis using histological methods. The panel on the left illustrates Masson's trichrome staining of a kidney section showing intraluminal cast and tubular necrosis consequent to rhabdomyolysis injury. The panel on the right represents picrosirius-red stained kidney under polarized light microscopy. Boudhabhay et al., 2020 and Ranjit et al., 2016.

4.2 RESULTS

4.2.1 *Ex vivo* fibrosis quantification using MPM

For detection of fibrosis, kidney samples collected from dicer/aqp2 mice were used. Unstained paraffin-embedded 4 µm thick sections were used for *ex vivo* imaging with 2 photon microscopy. The fibrillar collagen was detectable from SHG signal. SHG and 2-photon excitation fluorescence (2PEF) were simultaneously excited by tuning the laser to 900 nm. For each group (control, cKO 1 month and cKO 2 months) at least 3 images were acquired in cortex, outer medulla and papilla. Images were collected at 1024x1024 resolution (0.58 µm per pixel) with a dwell time of 2.4 µs.

In order to quantify fibrosis in mice kidney slices, images were segmented with Ilastik. A parallel random forest classifier with a variable importance table was trained in Ilastik by using at least three images. Images were segmented in three classes (renal autofluorescence, fibrosis, lumen and peritubular interstitium) thus creating segmentation masks where each pixel was assigned three possible values depending on their assignment by the algorithm. For images classification, ROIs as short brushers were placed in all three compartments, then a simple segmentation was created (Figure 28).

For the quantification of the signal, the autofluorescence, the fibrosis and the total areas were measured as number of pixel particles in Fiji software. Then, the final result was given by the fibrosis/autofluorescence ratio.

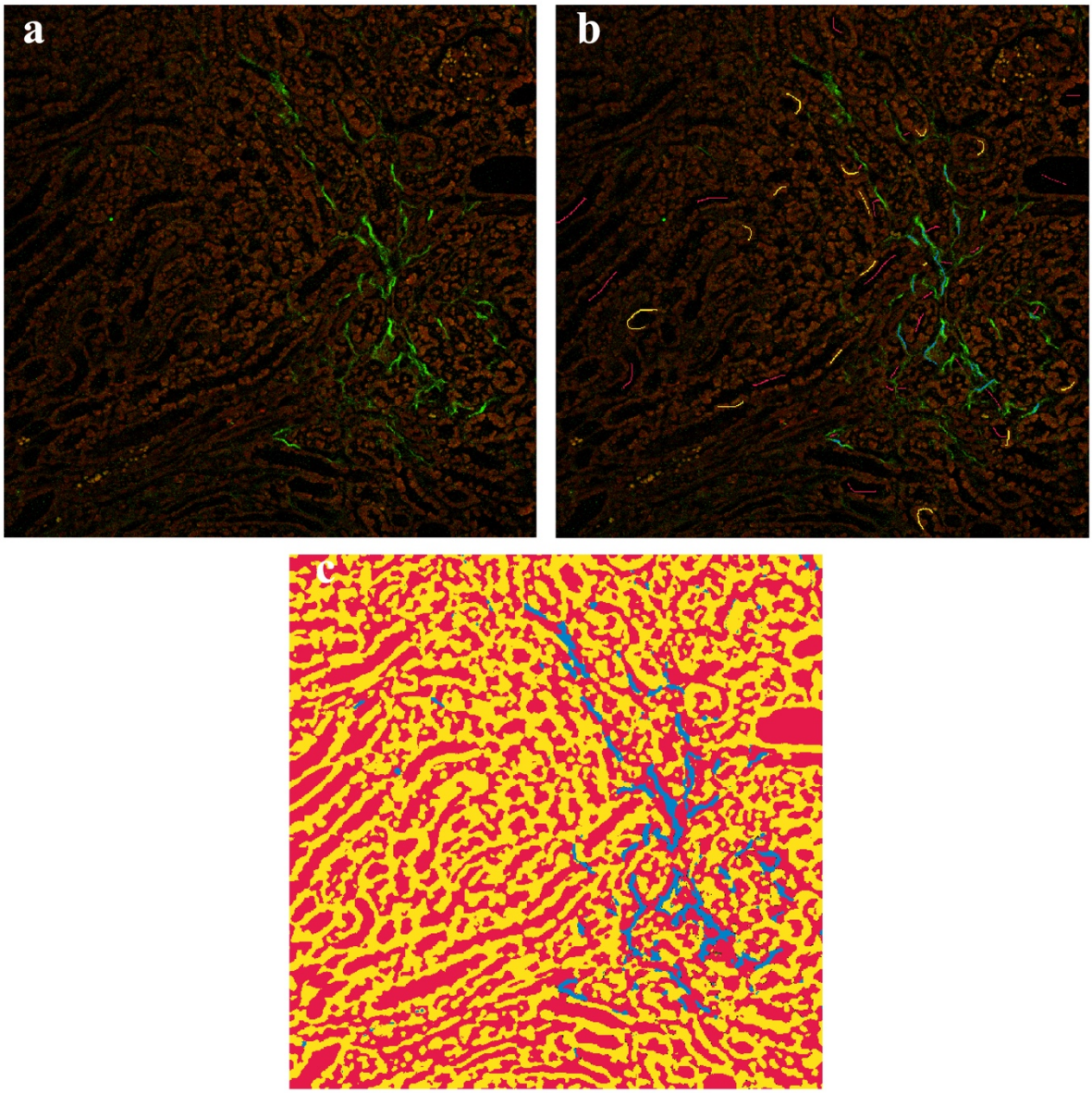

Figure 28. Quantification of renal fibrosis in kidney slices using Ilastik algoritm. The panel a shows the renal OSOM in mice kidney slices. The autofluorescence was detected with 2PEF (visible in brown), whereas SHG signal is shown in green. For image classification, several ROIs drawn as short brushers of different color were placed in three compartments: red for lumen/interstitium, yellow for autofluorescence, blue for collagen fibers (panel b). Panel c shows the simple segmentation made by Ilastik after the images training. Segmentation masks were created and for each pixel three possible values were assigned depending on their assignment by the algorithm.

4.2.2 Imaging and quantification of renal fibrosis in mice with nephrogenic diabetes insipidus

To evaluate the progression of fibrosis in kidney slices, we used a mouse model of nephrogenic diabetes insipidus (NDI) developed in our laboratories. CKO dicer/aqp2 mice showed indeed reduction of AQP2 levels and defects of urine concentration mechanism, typical of NDI.

In order to develop a protocol for visualization and quantification of renal fibrosis in kidney slices, the animals were sacrificed, the kidneys embedded in paraffin and unstained 4 μm thick sections used for imaging with MPM. Images detection was carried out in cortex, outer medulla and inner medulla of control, cKO 1 month old and cKO 2 months old animals. SHG and 2PEF signals were simultaneously acquired and showed merged in blue and green, respectively. 2PEF showed well conserved glomeruli, tubules and arterioles in control and 1 month cKO animals, while 2 months cKO mice exhibit some morphological alterations, such as tubular dilatation. The SHG signal was evident mostly in peritubular interstitium of cKO mice, while no distinct collagen fibers were detected in controls. In diabetic mice, fibrosis was found in outer medulla already at one month, whereas a robust SHG signal in cortex was visible only at two months. Appreciable renal fibrosis was instead absent in inner medulla in all groups (Figure 29).

The quantification of the fibrosis signals in kidney slices was carried out with Ilastik. In the images used for algorithm training, we manually put ROIs as short signs at level of autofluorescence, collagen fibers, and peritubular interstitium/lumen. Then, segmentation masks produced were analyzed in Fiji and the number of particles in all 3 classes were measured. The fibrosis/autofluorescence ratios shown in figure 30 confirmed the results displayed by the images. Multiphoton microscopy coupled with machine learning algorithms revealed to be a useful tool to visualize and quantify the renal fibrosis stadium in disease models.

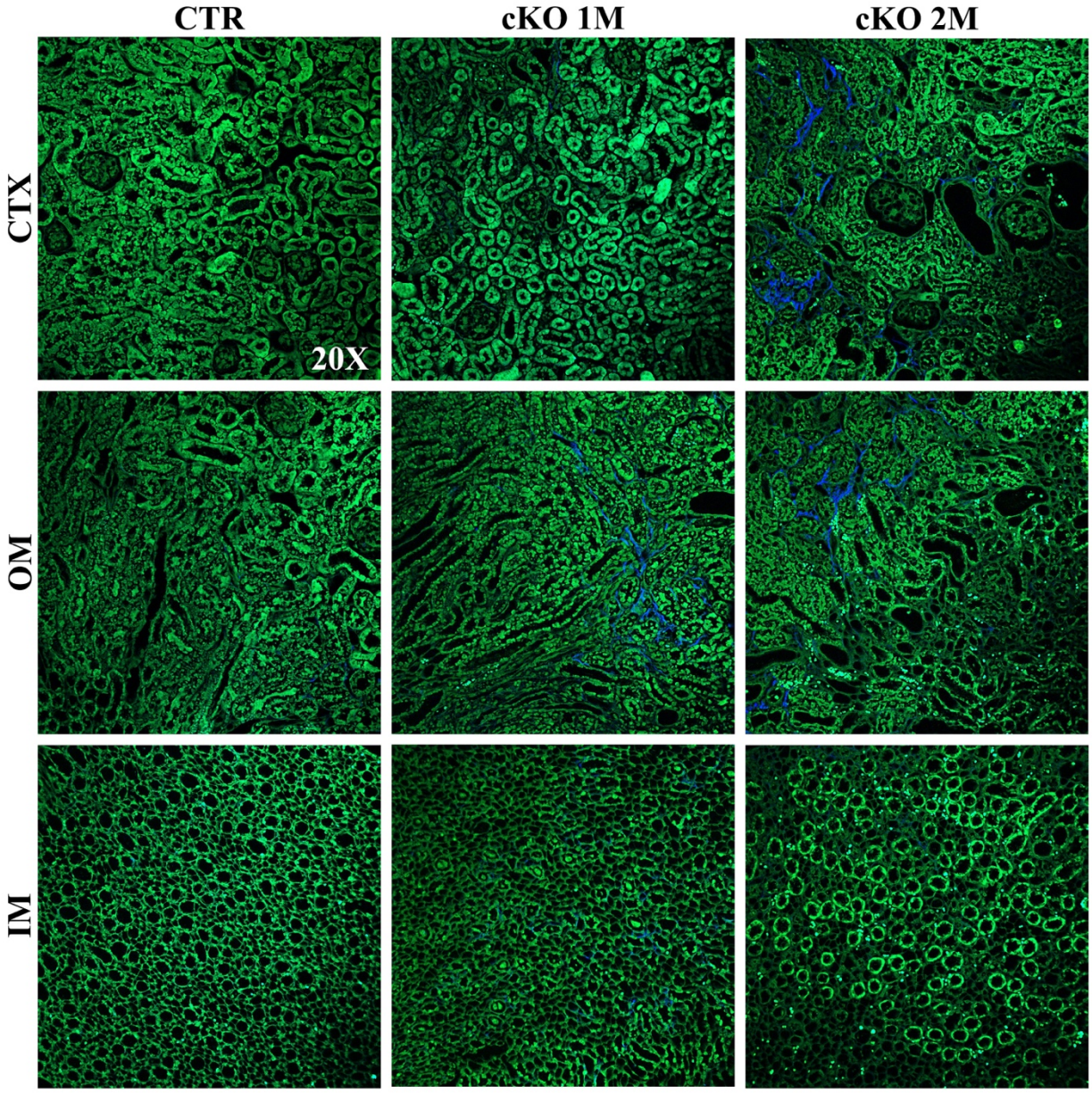

Figure 29. Renal fibrosis evaluation using SHG in mice renal slices. 2PEF is well represented in green, while SHG signal is shown in blue. No fibrotic signal was detected in controls mice (CTR), whereas cKO 1 month old mice (cKO 1M) showed strong fibrosis in outer medulla (OM). On the other hand, cKO 2 months old mice (cKO 2M) exhibited robust SHG signal both in cortex (CTX) and in outer medulla. No appreciable fibrosis was noted in inner medulla (IM) in all groups. Magnification was 20X.

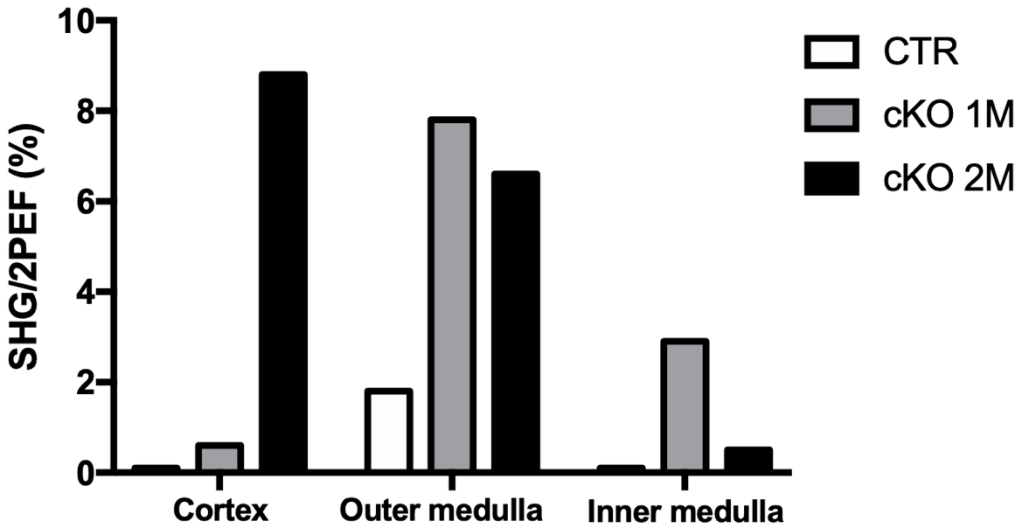

Figure 30. Analysis of fibrosis quantification in mice renal slices. The fibrosis signal is reported as SHG/2PEF ratio. As shown from the graph, in the renal cortex the fibrosis is present only in cKO 2M mice showing the highest SHG value obtained. In outer medulla both cKO 1 M and cKO 2 M mice exhibit a strong fibrosis, while only a modest signal is detected in control group. Almost no SHG signal is revealed in inner medulla, except some fibers found in cKO 1M mice. These results are in line with upper panel.

5. MATERIALS AND METHODS

5.1 Multiphoton microscopy

Two-photon microscopy (2PM) was performed using an upright Ultima Investigator 2-photon microscope (Bruker, MS, USA) equipped with a 20X objective XLUMPlanFL20XW NA 1.0 (Olympus, Japan) and supplemented by a converter arm (Inverterscope, LSM TECH, USA) to allow inverted imaging. The microscope was controlled by Prairie View software. Ti-Sapphire laser (Mai Tai® DeepSee™, Spectra-Physics, USA) was tuned for an excitation wavelength of 800nm for *in vivo* experiments. For the detection of green channel, emitted light between 500 and 550nm was recorded using Hamamatsu model H10770PB-40 GaAsP-detector. For the detection of red channel and blue channel light between 570 and 620 and between 435 and 485nm, respectively, were recorded using Hamamatsu model R3896 multi-alkali detectors. The images were collected at 512x512 resolution and the pixel dwell time was 2.8 µs (Figure 31).

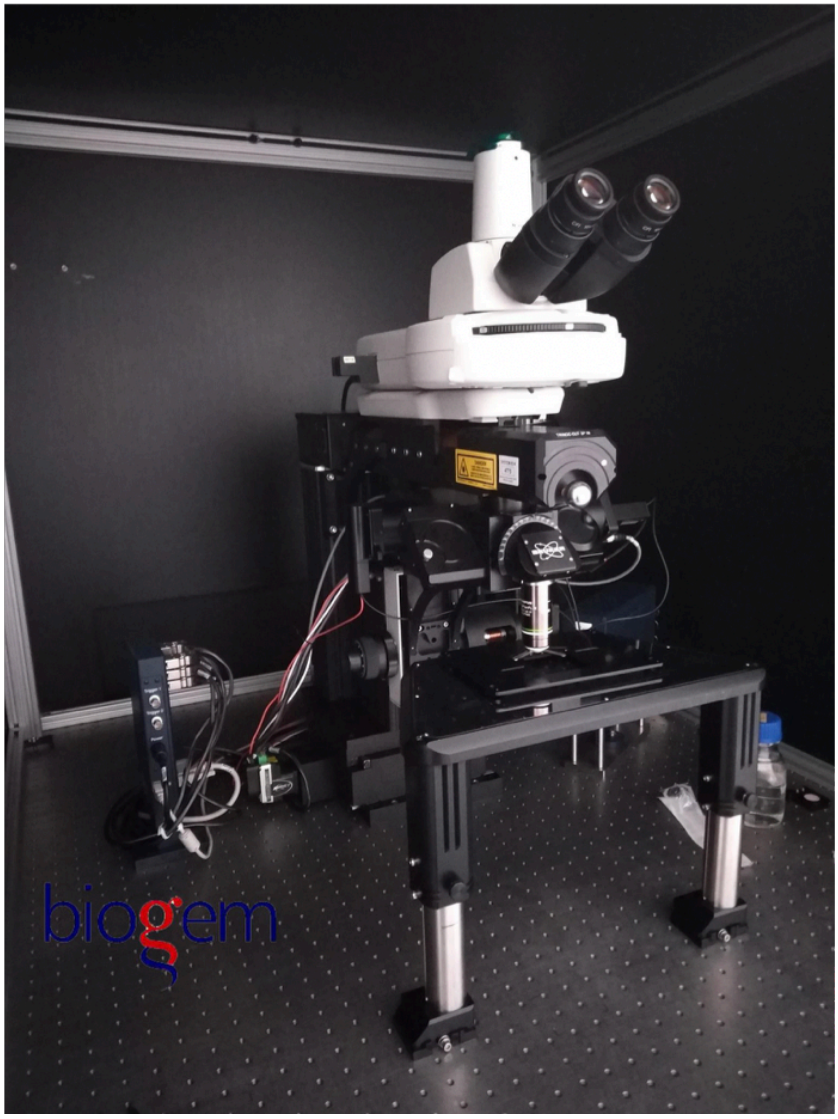

Figure 31. Two-photon microscopy of the intravital microscopy facility at Biogem Scarl

5.2 Fluorescent dyes and drugs

For SNGFR experiments the 500 kDa Tetramethylrhodamine isothiocyanate–dextran (TRITC, 52194-1G, sigma) and the freely filtered 3-5 kDa Fluorescein isothiocyanate–dextran (FITC, FD4-1G, sigma) were used to label peritubular and glomerular capillaries (150µl of a 10 mg/ml stock iv bolus) and tubular lumen (30 µl of a 10 mg/ml stock iv bolus), respectively.

For glucose uptake experiments the fluorescent glucose analog 2-[N-(7-nitrobenz-2-oxa-1,3-diazol-4-yl) amino]-2-deoxyglucose (2-NBDG, N13195, Invitrogen) was injected at 25 µg/min for 10 min at a flow rate of 10 µl/min.

For beta-lactoglobulin uptake experiments the fluorescent Alexa 568-conjugated beta-lactoglobulin (A20184, Invitrogen) at 1 µg/g body weight from a stock of 1,25 mg/mL was used.

Dopamine hydrochloride (S.A.L.F. Spa) was diluted in normal saline and given iv at low dosage of 3 µg/kg/min in continuous infusion (20 µl/min). The infusion of dopamine started two minutes after the beginning of the imaging and lasted until the end of the experiment. For control animals a continuous infusion (20 µl/min) of normal saline was given for all the experiments. The injection of fluorescent probes and drug was carried out using an automatic infusion pump (KD Scientific).

5.3 Animals and surgical preparation

For SNGFR experiments 10 Munich-Wistar Frömter (MWF) female rats (170-220 g) at 10-12 weeks were used. For glucose uptake study a total of 9 mice were used at 5-27 weeks, of which 5 male GLUT2 $^{lox/lox}$ PAX8 $^{wt/wt}$ mice (26-28 g) for control experiments, and 2 male (12-31 g) and 2 females (14-24 g) GLUT2 $^{lox/lox}$ PAX8 $^{Cre/\ wt}$ mice for cKO experiments. For beta-lactoglobulin uptake experiments 1 C57BL/6 control mouse was used for the experiments.

The animals were anesthetized with an intraperitoneal injection of thiobutabarbital (Inactin, 120 mg/Kg body weight) for rats and with tiletamine hydrochloride and zolazepam hydrochloride (40 mg/Kg, Zoletil) and xylazine hydrochloride (4 mg/kg, Rompun) for mice, then they were shaved and placed on a thermic pad (kent) to maintain the body temperature at 37°C. In rats the trachea was cannulated with polyethylene catheter (PE210, 2Biological instruments) to facilitate the breathing, then the right jugular vein and the left carotid artery were cannulated with polyethylene catheter (PE50, 2Biological instruments) for dyes and drug infusion and for blood pressure measurements, respectively. A double cannulation for the jugular vein was designed in order to ensure a simultaneous injection of the drug and the fluorescent dye. In mice the right jugular vein was cannulated with polyethylene catheter (PE10, 2Biological instruments) for dyes infusion. After that, the left kidney was exteriorized through a 10-15 mm flank incision, being careful to avoid organ damages and bleeding. The animals thus were placed on the stage of an inverted microscope with the exteriorized

kidney placed in a 50-mm-diameter coverslip-bottomed cell culture dish bathed in warm saline solution. This inverted approach, which requires the positioning of the microscope objective below the kidney, is generally preferred since it provides more stable conditions and minimize the movements due to breathing and heartbeat (84)(Figure 32).

All animal protocols were approved by animal license (ID n 747/2019-PR, 11/11/2019) and by the Animal Ethics Committee (CESA) of Biogem (Italy).

For imaging and quantification of renal fibrosis, 3 mice were used for the conduction of the experiments, of which 1 control at 1 month, 1 cKO dicer/aqp2 at 1 month and 1 cKO dicer/aqp2 at 2 months. The animals were sacrificed, then the kidneys were embedded in paraffin and unstained 4 μm thick sections were cut and further used for imaging with multiphoton microscopy.

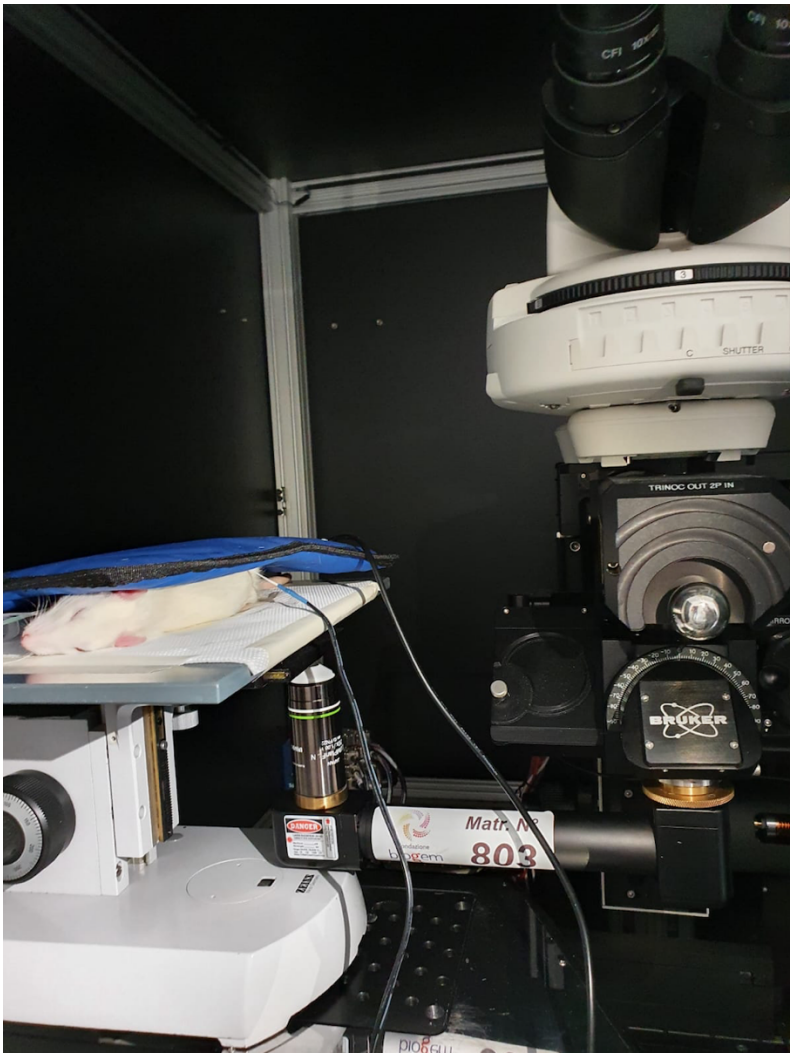

Figure 32. Representation of the inverted approach for kidney imaging. The converter arm is connected to the microscope from a side and holds the objective facing up from the other side. The animal covered by a heating pad is placed on apposite stage and has the exteriorized kidney immersed in warm saline solution. The imaging of the kidney was performed from below to reduce the animal movements.

For the experiments concerning the ischemia-reperfusion injury in rats, after kidney externalization the renal pedicle was clamped for 30 minutes to obtain the ischemia, then the clamp was removed to allow the reperfusion of the kidney and the assessment of SNGFR.

During *in vivo* imaging, the arterial blood pressure and the heart rate were continuously monitored by means of a pressure transducer (BP-1, 2Biological instruments), connected to a power lab system (ADinstruments), in order to guarantee the animal wellness and to keep the normal kidney function. The pressure transducer was previously calibrated using a pharmaceutical pressure manometer. The mean blood gas values were measured using Epoc blood system analysis (Siemens) at the end of surgery and during the imaging experiment.

At the end of the experiments the animals were euthanized according to the national guidelines.

5.4 Data analysis

Data were analyzed using Graph Pad Prism 7 software. Statistical analysis was performed by ANOVA for SNGFR measurements considering single values of SNGFR for each of three groups and by paired t-test for glucose uptake experiments considering the average values from each animal in the two groups.

6. DISCUSSION

MPM is a powerful consolidated tool to study the kidney physiology in health and disease. Taking advantage from deep optical sections of living tissues, it provides stunning images and high-resolution movies of pathophysiological renal processes. Because of its great potential, MPM represents a superior technique compared to confocal microscopy, allowing to investigate *in vivo* tissues and cellular compartments that were studied only *in vitro*. Since the kidney has a huge connection with blood vessels, it permits an easy labeling of renal structures by injecting specific fluorescent tracers in the bloodstream. In addition, the kidney can be exteriorized from the body of animal models without compromising the renal function: therefore, the investigation of many renal parameters can be carried out in non-invasive way.

In this study we offer an overview of the main MPM applications used to elucidate the renal function in control and disease models. In particular, we used existing MPM approaches shown by other researchers and, in the same time we developed an innovative method for the assessment of renal filtration.

Most of the results shown in literature regarding the assessment of SNGFR came from pioneering technique of renal micro-puncture. Micro-puncture permitted to elucidate the main renal functions, including the ultrafiltration, the glomerular filtration barrier and the urine concentration mechanism. Despite the great reliability of this method, it is a very laborious technique that requires sophisticated equipment, such as micromanipulators and glass pipettes, and very complex animal preparation. With the advent of new technologies, MPM replaced renal micro-puncture and started to be used for the evaluation of kidney function. The estimation of SNGFR using MPM can be assessed by observing and quantifying the fluorescent decay time of a low molecular weight marker between two regions of interest selected within a tubule. This method developed by Kang et al. represents an efficient and fast approach to assess renal function, but it requires the full frame acquisition during the bolus injection, thus reducing the velocity and accuracy of measurements. The new method to measure SNGFR we propose in this work is based on the previous study of Kang et al. but it relies on another approach, called Linescan. Linescan tool allows to acquire repetitive scans with very high temporal resolution within a region of interest and it is generally used in multiphoton microscopy experiments to assess the blood flow in tissues. According to our experience, Linescan is a better approach to assess SNGFR *in vivo* compared to the full frame acquisition: indeed, it offers very fast acquisition of the drawn ROIs and permits to have precise and reliable results, comparable with previous methods. The values of SNGFR measured in this study are in the same range as obtained by micro-puncture technique on the same rat model (152). Moreover, a great reproducibility of the SNGFR values was

shown when a different length of the same tubule was used for the measurement changing the second crossing.

To validate this original application, SNGFR was measured in low-dose dopamine treated rats. Dopamine is the first vasopressor agent used in intensive care units especially for hypotensive patients and it is the drug of choice to increase GFR in preterm human neonates with low-urine output. Dopamine is known to cause two main effects in humans, according to the dosage used: in particular, at low dosage (<5 μg/kg/min) it raises SNGFR values by specifically vasodilating the renal artery, representing a good treatment option in patients with lower kidney function, such as during the AKI. For this reason, we decided to treat the rats with low-dose dopamine (3 μg/kg/min) in order to confirm the earlier results shown in literature with our approach. Our results corroborate the effect of low-dose dopamine in raising the SNGFR in line with previous experiments (115), showing the reliability of the measurements.

Moreover, we also aimed to assess SNGFR during ischemia-reperfusion injury. The IRI is a very common cause AKI, a global health problem that still need to be elucidated. Many pharmacological drugs tested in animal models for the treatment of AKI showed effectiveness, but no appreciable results were seen when translated to human condition. Therefore, a deeper knowledge of the disease is needed to better understand the differences between the animal and human AKI and to find new therapeutical drugs matching with human condition. For this purpose, we induced ischemia by clamping the left renal peduncle for 30 minutes, then we allowed the reperfusion of the kidney by removing the clamp. This approach provides the best option to mimic the human acute renal injury in rodents. From the morphological point of view, the ischemic kidney showed variable tubular necrosis, characterized by loss of the proximal tubules structure and shedding of the cellular components in the tubular lumen, leading to intraluminal cast and cellular debris formation. In addition, we also observed a constriction of blood vessels and consequent reduction in renal blood flow resulting from damages to the vascular endothelium. The IRI-induced AKI also causes a significant reduction at the SNGFR level, leading in turn to the fall of total glomerular filtration rate. This renal injury seems to be due to tubular obstruction presumably accompanied by tubular reflux of the solutes across the damaged cells. Additionally, also the TGF mechanism shows a pivotal role in regulating the SNGFR since lower values of filtration were observed after a constant activation of TGF due to increased sodium load, while the control of macula densa activity at TAL level permitted to stabilize the SNGFR, as shown previously by Mason et al. (141). After 30 minutes of IRI, we used the linescan tool to measure SNGFR in the ischemic rats, demonstrating a significant reduction of the SNGFR values, as previously highlighted (148).

This assessment offers a unique opportunity to better understand the pathophysiology of AKI induced by IRI. Indeed, multiphoton microscopy and the linescan method are very powerful tools to evaluate in real time and at high temporal resolution the dynamic events of the renal function in a way that was not possible before.

Kidney is a very complex organ enrolled to perform specialized tubular functions, such as the retrieval of vitamins and proteins, and the secretion of unnecessary substances. Efforts to elucidate the tubular mechanisms in health and disease were carried out using isolated cells or tissues slices. The information obtained with these approaches provided insights to researchers, but the organ needed to be removed from the original physiological context, limiting the reliability of the results.

In vivo MPM imaging, instead, allows to study in real time the dynamic physiological processes, including the protein and glucose reabsorption. This can be performed thanks to the low phototoxicity offered by MPM, which permits to image over the time without damaging the structures. In addition, the high spatial and temporal resolution obtainable from MPM help to monitor continuously these active events even at subcellular level.

In this study we used the fluorescent glucose analog 2-NBDG to investigate the tubular uptake of glucose in control and in GLUT2 $^{lox/lox}$ PAX8 $^{Cre/wt}$ mice. The glucose reabsorption in S1 proximal tubules requires the glucose uptake inside the cell mediated by apical SGLT2, followed by glucose exit through basolateral GLUT2. GLUT2 cKO mice we generated in our institute mimic the human FBS, developing glycosuria and glycogen accumulation in proximal tubules cells. Indeed, the ablation of GLUT2 in our model limited the cellular glucose exit and forced it to accumulate in cells. Presumably, the proximal tubules respond to cellular glycogen accumulation by limiting the expression of apical SGLT2, thus explaining the glycosuria. This compensatory mechanism would reduce the influx of cellular glucose and the progression of cells injury.

To elucidate the ability of GLUT2 cKO mice to reabsorb glucose, we performed intravital imaging of proximal tubules during the administration of fluorescent glucose. According to previous findings, 2-NBDG represents a good fluorescent dye that shows many applications in optical microscopy especially for clinical studies in the field of cancer (198, 199). From the autofluorescence physiologically exhibited by renal tubules we observed an altered proximal tubules morphology in GLUT2 cKO mice, showing multiple apical and intraluminal granules, compared to the controls. This demonstrates a proximal tubular damage caused by glucose intracellular accumulation. After the continuous infusion of 2-NBDG, GLUT2 cKO mice showed a slower rate of glucose reabsorption, as can be noticed from the difference of time-fluorescence slopes in figure 22. This difference in glucose handling is confirmed by the presence in GLUT2 cKO mice of accumulated glucose also in late proximal and distal tubules, suggesting an altered and reduced glucose uptake in early proximal

tubules. From these results we can assert that GLUT2 cKO animals show a defect of glucose reabsorption along the early proximal tubules, leading to glycosuria, and that this can represent an adaptative mechanism of proximal tubule cells to stop the progression of cell damage. These experiments demonstrate the feasibility of intravital MPM and 2-NBDG to monitor the glucose metabolism over the time in living animals, overcoming the limitations showed by previous techniques. Future attempts will be aimed to address new pharmacological drugs able to rescue the metabolic dysfunctions in disease models.

The protein reabsorption is one of the key renal functions and it usually requires a receptor-mediated endocytosis process at the apical membrane of proximal tubules. This mechanism results compromised if components of glomerular filtration barrier, including podocytes, and proximal tubules receptors are damaged, with consequent development of proteinuria and waste of useful substances. MPM represents a valid tool for tracking the protein uptake process with a cellular resolution in living animals. Here, we used MPM to investigate in real time the uptake of Alexa 568-conjugated beta-lactoglobulin infused in C57BL6 control mice. This fluorescent tracer was rapidly filtered by the glomerulus since its relatively low molecular weight and it appeared in less than 1 minute along the apical membrane of early proximal tubules, confirming the fast process of apical endocytosis. The beta-lactoglobulin signal increased gradually over the time and reached a plateau after 5 minutes from the iv injection. No fluorescence was detected in late proximal or distal tubules, confirming a normal protein uptake process. We exploited the high spatial resolution and the lower phototoxicity of MPM to monitor the clearance of beta-lactoglobulin uptake over 25 minutes. The apical fluorescence of beta-lactoglobulin remained nearly stable at 15 minutes after the dye infusion, after that it started decreasing, and some fluorescence was visible in cellular compartments as consequence of the reabsorption mechanism. These experimental results demonstrate the efficiency and the great potentiality of intravital microscopy to follow such dynamic events and to compare disease with control conditions. Our future aim indeed is to use this approach to evaluate protein uptake in models with disfunctions of glomerular filtration barrier or proximal tubules receptors, such as diabetes and FBS.

Tubulo-interstitial fibrosis represents an important prognostic parameter of many diseases, such as diabetic nephropathy and cancer. Fibrotic biopsies are usually analyzed and quantified with histological staining, such as Masson's trichrome and picrosirius red. However, these techniques represent a reductional approach due to the variability of the staining procedure and the analysis by the pathologist as well as the absence of great specificity of the signal. In addition, histological procedures are constrained in that they lack 3D resolution making them greatly dependent from the thickness of the specimen visualized. SHG instead represents a promising tool for the analysis of

renal fibrosis since it does not require any particular preparation of the sample and it constitute a versatile technique as it can be applied to fresh, frozen and fixed slices. SHG offers great specificity of the fibrotic signal, indeed it is specifically associated to types I and III collagen fibers, excluding non-fibrillar type IV collagen. Moreover, it can exploit the intrinsic advantages of the MPM, including less photobleaching, increased depth in the sample and high resolution.

In this study we coupled the MPM and SHG tool to identify and quantify renal fibrosis in mice kidney slices. In order to conveniently set up this approach, we used a mouse model with diabetes insipidus phenotype we developed in our institute. As expected, we successfully managed to simultaneously image renal parenchyma using 2PEF and collagen fibers with SHG. In line with previous studies, we didn't detect fibrosis signal in control group except very few random fibers or around the vessels. The diabetic mice, instead, showed a significant increase of fibrosis localized mostly in the tubulo-interstitial space. The analysis of the SHG pixel covered shows a time-dependent rise in collagen accumulation in these animals: indeed, cKO mice at 2 months present comparable collagen fibers deposit as mice at 1 months in outer medulla, but they additionally exhibited a robust fibrosis in cortex. This result confirms the specificity and reliability of the SHG technique to detect fibrosis in tissue slices. We subsequently quantified fibrosis using Ilastik, an open-source software that is able to make image classifications thanks to an assisted machine learning program. The concept behind Ilastik is that its predictions are based on the input drawn by the users as short brush. It uses a random forest classifier that calculate the image features (color, shape, texture) to segment the image of choice in well-established classes. After a training phase of the program that requires to give inputs to a small set of representative images, the program is capable to classify other images with similar features never seen before, ensuring reproducibility and reliability (200).

Therefore, the combined SHG-machine learning approach proved to be a valid and efficient approach to image and quantify the renal tubule-interstitial fibrosis in kidney slices, ensuring specificity of the signal and great reproducibility of the results unlike the manual quantification systems such as ImageJ. Since the renal tubulo-interstitial fibrosis is a common feature in many renal disorders, SHG assisted by machine learning algorithms could be used as diagnostic and prognostic tool in clinical routine for human diseases.

Taken together, these results show that intravital imaging with MPM is a great tool to investigate *in vivo* the renal physiology at cellular and subcellular resolution. By using specific fluorescent probes and animal models, it is allowed to elucidate in real time the most important renal processes in health and disease, such as SNGFR and substances tubular reabsorption. MPM, indeed, offers the possibility to study both global diseases, such as diabetes, and genetic rare diseases, including the FBS.

Moreover, given the ability of MPM to detect specifically renal fibrosis in tissue slices, it may provide an innovative tool for clinical application.

7. REFERENCES

1. Levey AS, Inker LA. Assessment of Glomerular Filtration Rate in Health and Disease: A State of the Art Review. *Clin. Pharmacol. Ther.* [published online ahead of print: 2017]; doi:10.1002/cpt.729

2. Satchell SC, Braet F. Glomerular endothelial cell fenestrations: An integral component of the glomerular filtration barrier. *Am. J. Physiol. - Ren. Physiol.* 2009; doi:10.1152/ajprenal.90601.2008

3. Singh A et al. Glomerular endothelial glycocalyx constitutes a barrier to protein permeability. *J. Am. Soc. Nephrol.* [published online ahead of print: 2007]; doi:10.1681/ASN.2007010119

4. Jeansson M, Haraldsson B. Morphological and functional evidence for an important role of the endothelial cell glycocalyx in the glomerular barrier. *Am. J. Physiol. - Ren. Physiol.* [published online ahead of print: 2006]; doi:10.1152/ajprenal.00173.2005

5. Arif E, Nihalani D. Glomerular Filtration Barrier Assembly: An insight. *Postdoc J.* [published online ahead of print: 2013]; doi:10.14304/surya.jpr.v1n4.4

6. Miner JH. The glomerular basement membrane. *Exp. Cell Res.* 2012; doi:10.1016/j.yexcr.2012.02.031

7. Jarad G, Cunningham J, Shaw AS, Miner JH. Proteinuria precedes podocyte abnormalities in Lamb2-/- mice, implicating the glomerular basement membrane as an albumin barrier. *J. Clin. Invest.* [published online ahead of print: 2006]; doi:10.1172/JCI28414

8. Marshall S. The Podocyte: a Potential Therapeutic Target in Diabetic Nephropathy?. *Curr. Pharm. Des.* [published online ahead of print: 2007]; doi:10.2174/138161207781662957

9. Tryggvason K, Patrakka J, Wartiovaara J. Hereditary Proteinuria Syndromes and Mechanisms of Proteinuria. *N. Engl. J. Med.* [published online ahead of print: 2006]; doi:10.1056/nejmra052131

10. Schurer W, Fleuren GJ, Hoedemaeker PJ, Molenaar I. A model for the glomerular filter. *Kidney Blood Press. Res.* [published online ahead of print: 1980]; doi:10.1159/000172766

11. Huang TW, Langlois JC. Podoendin: A new cell surface protein of the podocyte and endothelium. *J. Exp. Med.* [published online ahead of print: 1985]; doi:10.1084/jem.162.1.245

12. Maack T, Johnson V, Kau ST, Figueiredo J, Sigulem D. Renal filtration, transport, and metabolism of low-molecular-weight proteins: A review. *Kidney Int.* [published online ahead of print: 1979]; doi:10.1038/ki.1979.128

13. Kaufman DP, Knohl SJ. *Physiology, Glomerular Filtration Rate (GFR)*. 2018:

14. Dalal R, Sehdev JS. *Physiology, Renal, Blood Flow and Filtration*. 2018:

15. Davis MJ. Perspective: Physiological Role(s) of the Vascular Myogenic Response. *Microcirculation* 2012; doi:10.1111/j.1549-8719.2011.00131.x

16. SCHUBERT R, MULVANY MJ. The myogenic response: established facts and attractive hypotheses. *Clin. Sci.* [published online ahead of print: 1999]; doi:10.1042/cs19980403
17. Vallon V. Tubuloglomerular feedback and the control of glomerular filtration rate. *News Physiol. Sci.* [published online ahead of print: 2003]; doi:10.1152/nips.01442.2003
18. Kurokawa K. Tubuloglomerular feedback: Its physiological and pathophysiological significance. In: *Kidney International, Supplement*. 1998:
19. Jin R, Grunkemeier GL, Brown JR, Furnary AP. Estimated Glomerular Filtration Rate and Renal Function. *Ann. Thorac. Surg.* [published online ahead of print: 2008]; doi:10.1016/j.athoracsur.2008.05.007
20. Shannon JA, Smith HW. THE EXCRETION OF INULIN, XYLOSE AND UREA BY NORMAL AND PHLORIZINIZED MAN 1. *J. Clin. Invest.* [published online ahead of print: 1935]; doi:10.1172/jci100690
21. Rahn KH, Heidenreich S, Brückner D. How to assess glomerular function and damage in humans. *J. Hypertens.* 1999; doi:10.1097/00004872-199917030-00002
22. Lamb EJ, Tomson CRV, Roderick PJ. Estimating kidney function in adults using formulae. In: *Annals of Clinical Biochemistry*. 2005:
23. Soveri I et al. Measuring GFR: A systematic review. *Am. J. Kidney Dis.* [published online ahead of print: 2014]; doi:10.1053/j.ajkd.2014.04.010
24. Schwartz GJ, Furth SL. Glomerular filtration rate measurement and estimation in chronic kidney disease. *Pediatr. Nephrol.* [published online ahead of print: 2007]; doi:10.1007/s00467-006-0358-1
25. Levey AS. Measurement of renal function in chronic renal disease. *Kidney Int.* [published online ahead of print: 1990]; doi:10.1038/ki.1990.182
26. Caterino M et al. Urine proteomics revealed a significant correlation between urine-Fibronectin abundance and estimated-GFR decline in patients with bardet-Biedl syndrome. *Kidney Blood Press. Res.* [published online ahead of print: 2018]; doi:10.1159/000488096
27. Jerums G, Panagiotopoulos S, Premaratne E, MacIsaac RJ. Integrating albuminuria and GFR in the assessment of diabetic nephropathy. *Nat. Rev. Nephrol.* 2009; doi:10.1038/nrneph.2009.91
28. Levey AS et al. K/DOQI clinical practice guidelines for chronic kidney disease: Evaluation, classification, and stratification. *Am. J. Kidney Dis.* 2002;
29. Wright FS, Giebisch G. Glomerular filtration in single nephrons.. *Kidney Int.* 1972; doi:10.1038/ki.1972.30
30. Jamison RL, Lacy FB. Effect of saline infusion on superficial and juxtamedullary nephrons in the rat.. *Am. J. Physiol.* [published online ahead of print: 1971];

doi:10.1152/ajplegacy.1971.221.3.690
31. Remuzzi A, Puntorieri S, Mazzoleni A, Remuzzi G. Sex related differences in glomerular ultrafiltration and proteinuria in Munich-Wistar rats. *Kidney Int.* [published online ahead of print: 1988]; doi:10.1038/ki.1988.206
32. Hayslett JP, Kashgarian M, Epstein FH. Functional correlates of compensatory renal hypertrophy.. *J. Clin. Invest.* [published online ahead of print: 1968]; doi:10.1172/jci105772
33. Brenner BM, Daugharty TM. The measurement of glomerular filtration rate in single nephrons of the rat kidney.. *Yale J. Biol. Med.* 1972;
34. Denic A et al. Single-Nephron Glomerular Filtration Rate in Healthy Adults. *N. Engl. J. Med.* [published online ahead of print: 2017]; doi:10.1056/nejmoa1614329
35. Tonneijck L et al. Glomerular hyperfiltration in diabetes: Mechanisms, clinical significance, and treatment. *J. Am. Soc. Nephrol.* 2017; doi:10.1681/ASN.2016060666
36. Hanssen OE. THE RELATIONSHIP BETWEEN GLOMERULAR FILTRATION AND LENGTH OF THE PROXIMAL CONVOLUTED TUBULES IN MICE. *Acta Pathol. Microbiol. Scand.* [published online ahead of print: 1961]; doi:10.1111/j.1699-0463.1961.tb00409.x
37. Brenner BM, Daugharty TM, Ueki IF, Troy JL. Quantitative assessment of proximal tubule function in single nephrons of the rat kidney.. *Am. J. Physiol.* [published online ahead of print: 1971]; doi:10.1152/ajplegacy.1971.220.6.2058
38. Lindheimer MD, Lalone RC, Levinsky NG. Evidence that an acute increase in glomerular filtration has little effect on sodium excretion in the dog unless extracellular volume is expanded.. *J. Clin. Invest.* [published online ahead of print: 1967]; doi:10.1172/JCI105528
39. Moore LC. Tubuloglomerular feedback and SNGFR autoregulation in the rat. *Am. J. Physiol. - Ren. Fluid Electrolyte Physiol.* [published online ahead of print: 1984]; doi:10.1152/ajprenal.1984.247.2.f267
40. Denic A et al. Detection and Clinical Patterns of Nephron Hypertrophy and Nephrosclerosis among Apparently Healthy Adults. *Am. J. Kidney Dis.* [published online ahead of print: 2016]; doi:10.1053/j.ajkd.2015.12.029
41. Steiner RW. Increased Single-Nephron GFR in Normal Adults: Too Much of a Good Thing… or Maybe Not?. *Am. J. Kidney Dis.* 2018; doi:10.1053/j.ajkd.2017.11.005
42. Wearn JT, Richards AN. OBSERVATIONS ON THE COMPOSITION OF GLOMERULAR URINE, WITH PARTICULAR REFERENCE TO THE PROBLEM OF REABSORPTION IN THE RENAL TUBULES. *Am. J. Physiol. Content* [published online ahead of print: 1924]; doi:10.1152/ajplegacy.1924.71.1.209
43. Walker AM, Hudson CL. THE REABSORPTION OF GLUCOSE FROM THE RENAL

TUBULE IN AMPHIBIA AND THE ACTION OF PHLORHIZIN UPON IT. *Am. J. Physiol. Content* [published online ahead of print: 1936]; doi:10.1152/ajplegacy.1936.118.1.130
44. Richards AN, Walker AM. METHODS OF COLLECTING FLUID FROM KNOWN REGIONS OF THE RENAL TUBULES OF AMPHIBIA AND OF PERFUSING THE LUMEN OF A SINGLE TUBULE. *Am. J. Physiol. Content* [published online ahead of print: 1936]; doi:10.1152/ajplegacy.1936.118.1.111
45. Walker AM, Bott PA, Oliver J, MacDowell MC. THE COLLECTION AND ANALYSIS OF FLUID FROM SINGLE NEPHRONS OF THE MAMMALIAN KIDNEY. *Am. J. Physiol. Content* [published online ahead of print: 1941]; doi:10.1152/ajplegacy.1941.134.3.580
46. Sands JM. Micropuncture: Unlocking the secrets of renal function. *Am. J. Physiol. - Ren. Physiol.* 2004; doi:10.1152/classicessays.00019.2004
47. Shirley DG, Zewde T, Walter SJ. Renal function in normal and potassium-depleted rats before and after preparation for micropuncture experimentation. *Pflügers Arch. Eur. J. Physiol.* [published online ahead of print: 1990]; doi:10.1007/BF00370225
48. Walter SJ, Sampson B, Shirley DG. A micropuncture study of renal tubular lithium reabsorption in sodium-depleted rats.. *J. Physiol.* [published online ahead of print: 1995]; doi:10.1113/jphysiol.1995.sp020598
49. Goligorsky MS. Renal disease. Techniques and protocols. Preface.. *Methods Mol. Med.* 2003;
50. Armstrong WM et al. Micropuncture and Microanalysis in Kidney Physiology. In: *Laboratory Techniques in Membrane Biophysics*. 1969:
51. Lorenz JN. Micropuncture of the Kidney: A primer on techniques. *Compr. Physiol.* [published online ahead of print: 2012]; doi:10.1002/cphy.c110035
52. Frohnert PP, Höhmann B, Zwiebel R, Baumann K. Free flow micropuncture studies of glucose transport in the rat nephron. *Pflügers Arch. Eur. J. Physiol.* [published online ahead of print: 1970]; doi:10.1007/BF00587238
53. Shafik IM, Quamme GA. Micropuncture techniques in renal research. *Methods Enzymol.* [published online ahead of print: 1990]; doi:10.1016/0076-6879(90)91008-T
54. Lang F, Greger R, Lechene C, Knox FG. Micropuncture Techniques. In: *Renal Pharmacology*. 1978:
55. Harris PJ, Cullinan M, Thomas D, Morgan TO. Digital image capture and analysis for split-drop micropuncture. *Pflügers Arch. Eur. J. Physiol.* [published online ahead of print: 1987]; doi:10.1007/BF00581164
56. Leser KH, Osswald H. Maleate induced fall of glomerular filtration rate - A micropuncture study in the rat. *Naunyn. Schmiedebergs. Arch. Pharmacol.* [published online ahead of print: 1985];

doi:10.1007/BF00634246
57. Capasso G, Unwin RJ, Pica A, Quagliuolo L, Giovane A. Iothalamate measured by capillary electrophoresis is a suitable alternative to radiolabeled inulin in renal micropuncture. *Kidney Int.* [published online ahead of print: 2002]; doi:10.1046/j.1523-1755.2002.00510.x
58. Romano G, Favret G, Federico E, Bartoli E. The validity of the recollection technique in micropuncture experiments on the rat kidney. *Exp. Physiol.* [published online ahead of print: 1997]; doi:10.1113/expphysiol.1997.sp004005
59. Wagner R. Erlauterungstaflen zur Physiologie und Entwicklungsgeschichte. In: Voss L ed. Leipzig, germany: 1839:
60. Wood A, Thorogood P. An analysis of in vivo cell migration during teleost fin morphogenesis.. *J. Cell Sci.* 1984;
61. Irwin JW, MacDonald J. Microscopic observations of the intrahepatic circulation of living guinea pigs. *Anat. Rec.* [published online ahead of print: 1953]; doi:10.1002/ar.1091170102
62. Nuttall AL. Velocity of red blood cell flow in capillaries of the guinea pig cochlea. *Hear. Res.* [published online ahead of print: 1987]; doi:10.1016/0378-5955(87)90013-X
63. MacDonald IC, Schmidt EE, Morris VL, Chambers AF, Groom AC. Intravital videomicroscopy of the chorioallantoic microcirculation: A model system for studying metastasis. *Microvasc. Res.* [published online ahead of print: 1992]; doi:10.1016/0026-2862(92)90079-5
64. Villringer A et al. Confocal laser microscopy to study microcirculation on the rat brain surface in vivo. *Brain Res.* [published online ahead of print: 1989]; doi:10.1016/0006-8993(89)91616-8
65. Jester J V., Andrews PM, Matthew Petroll W, Lemp MA, Dwight Cavanagh H. In vivo, realtime confocal imaging. *J. Electron Microsc. Tech.* [published online ahead of print: 1991]; doi:10.1002/jemt.1060180108
66. Lakowicz JR. *Principles of fluorescence spectroscopy*. 2006:
67. Oheim M, Michael DJ, Geisbauer M, Madsen D, Chow RH. Principles of two-photon excitation fluorescence microscopy and other nonlinear imaging approaches. *Adv. Drug Deliv. Rev.* 2006; doi:10.1016/j.addr.2006.07.005
68. Dey P, Dey P. Fluorescence and Confocal Microscope: Basic Principles and Applications in Pathology. In: *Basic and Advanced Laboratory Techniques in Histopathology and Cytology*. 2018:
69. Pawley JB. Fundamental limits in confocal microscopy. In: *Handbook of Biological Confocal Microscopy: Third Edition*. 2006:
70. Göppert-Mayer M. Elementary processes with two quantum transitions. *Ann. der Phys.* [published online ahead of print: 2009]; doi:10.1002/andp.200910358
71. Schießl IM, Castrop H. Deep insights: intravital imaging with two-photon microscopy. *Pflugers*

Arch. Eur. J. Physiol. 2016; doi:10.1007/s00424-016-1832-7
72. Helmchen F, Denk W. Deep tissue two-photon microscopy. *Nat. Methods* 2005; doi:10.1038/nmeth818
73. Hall AM, Molitoris BA. Dynamic multiphoton microscopy: Focusing light on acute kidney injury. *Physiology* 2014; doi:10.1152/physiol.00010.2014
74. Molitoris BA, Sandoval RM. Intravital multiphoton microscopy of dynamic renal processes. *Am. J. Physiol. - Ren. Physiol.* 2005; doi:10.1152/ajprenal.00473.2004
75. Levene MJ, Dombeck DA, Kasischke KA, Molloy RP, Webb WW. In Vivo Multiphoton Microscopy of Deep Brain Tissue. *J. Neurophysiol.* [published online ahead of print: 2004]; doi:10.1152/jn.01007.2003
76. Kobat D, Horton NG, Xu C. In vivo two-photon microscopy to 1.6-mm depth in mouse cortex. *J. Biomed. Opt.* [published online ahead of print: 2011]; doi:10.1117/1.3646209
77. Rocheleau J V., Piston DW. Two-Photon Excitation Microscopy for the Study of Living Cells and Tissues. *Curr. Protoc. Cell Biol.* [published online ahead of print: 2003]; doi:10.1002/0471143030.cb0411s20
78. Svoboda K, Yasuda R. Principles of Two-Photon Excitation Microscopy and Its Applications to Neuroscience. *Neuron* 2006; doi:10.1016/j.neuron.2006.05.019
79. Zipfel WR, Williams RM, Webb WW. Nonlinear magic: Multiphoton microscopy in the biosciences. *Nat. Biotechnol.* 2003; doi:10.1038/nbt899
80. Helmchen F, Denk W. New developments in multiphoton microscopy. *Curr. Opin. Neurobiol.* 2002; doi:10.1016/S0959-4388(02)00362-8
81. Laiho LH, Pelet S, Hancewicz TM, Kaplan PD, So PTC. Two-photon 3-D mapping of ex vivo human skin endogenous fluorescence species based on fluorescence emission spectra. *J. Biomed. Opt.* [published online ahead of print: 2005]; doi:10.1117/1.1891370
82. Thorling CA et al. Multiphoton microscopy in defining liver function. *J. Biomed. Opt.* [published online ahead of print: 2014]; doi:10.1117/1.jbo.19.9.090901
83. Rubart M. Two-photon microscopy of cells and tissue. *Circ. Res.* 2004; doi:10.1161/01.RES.0000150593.30324.42
84. Dunn KW et al. Functional studies of the kidney of living animals using multicolor two-photon microscopy. *Am. J. Physiol. - Cell Physiol.* [published online ahead of print: 2002]; doi:10.1152/ajpcell.00159.2002
85. Cahalan MD, Parker I, Wei SH, Miller MJ. Two-photon tissue imaging: Seeing the immune system in a fresh light. *Nat. Rev. Immunol.* 2002; doi:10.1038/nri935
86. Perrin L, Bayarmagnai B, Gligorijevic B. Frontiers in intravital multiphoton microscopy of

cancer. *Cancer Rep.* 2020; doi:10.1002/cnr2.1192
87. Sandoval RM, Molitoris BA. Intravital multiphoton microscopy as a tool for studying renal physiology and pathophysiology. *Methods* [published online ahead of print: 2017]; doi:10.1016/j.ymeth.2017.07.014
88. Lin AL, Rothman DL. What have novel imaging techniques revealed about metabolism in the aging brain?. *Future Neurol.* 2014; doi:10.2217/fnl.14.13
89. Lu HH et al. Molecular imaging of ischemia and reperfusion in vivo with mitochondrial autofluorescence. *Anal. Chem.* [published online ahead of print: 2014]; doi:10.1021/ac5006469
90. Hall AM, Rhodes GJ, Sandoval RM, Corridon PR, Molitoris BA. In vivo multiphoton imaging of mitochondrial structure and function during acute kidney injury. *Kidney Int.* [published online ahead of print: 2013]; doi:10.1038/ki.2012.328
91. Hato T, Winfree S, Dagher PC. Intravital imaging of the kidney. *Methods* 2017; doi:10.1016/j.ymeth.2017.03.024
92. Reeve JE, Anderson HL, Clays K. Dyes for biological second harmonic generation imaging. *Phys. Chem. Chem. Phys.* [published online ahead of print: 2010]; doi:10.1039/c003720f
93. Zipfel WR et al. Live tissue intrinsic emission microscopy using multiphoton-excited native fluorescence and second harmonic generation. *Proc. Natl. Acad. Sci. U. S. A.* [published online ahead of print: 2003]; doi:10.1073/pnas.0832308100
94. Nucciotti V et al. Probing myosin structural conformation in vivo by second-harmonic generation microscopy. *Proc. Natl. Acad. Sci. U. S. A.* [published online ahead of print: 2010]; doi:10.1073/pnas.0914782107
95. Ranjit S et al. Label-free fluorescence lifetime and second harmonic generation imaging microscopy improves quantification of experimental renal fibrosis. *Kidney Int.* [published online ahead of print: 2016]; doi:10.1016/j.kint.2016.06.030
96. Strupler M et al. Second harmonic microscopy to quantify renal interstitial fibrosis and arterial remodeling. *J. Biomed. Opt.* [published online ahead of print: 2008]; doi:10.1117/1.2981830
97. Perry SW, Burke RM, Brown EB. Two-photon and second harmonic microscopy in clinical and translational cancer research. *Ann. Biomed. Eng.* [published online ahead of print: 2012]; doi:10.1007/s10439-012-0512-9
98. Sandoval RM, Molitoris BA. Quantifying glomerular permeability of fluorescent macromolecules using 2-photon microscopy in Munich Wistar rats. *J. Vis. Exp.* [published online ahead of print: 2013]; doi:10.3791/50052
99. Ferrell N et al. Shear stress is normalized in glomerular capillaries following 5⁄6 nephrectomy. *Am. J. Physiol. - Ren. Physiol.* [published online ahead of print: 2015];

doi:10.1152/ajprenal.00290.2014
100. McCurley A et al. Inhibition of avb5 integrin attenuates vascular permeability and protects against renal ischemia-reperfusion injury. *J. Am. Soc. Nephrol.* [published online ahead of print: 2017]; doi:10.1681/ASN.2016020200
101. Sharfuddin AA et al. Soluble thrombomodulin protects ischemic kidneys. *J. Am. Soc. Nephrol.* [published online ahead of print: 2009]; doi:10.1681/ASN.2008060593
102. Jung JK, Toma I, Sipos A, McCulloch F, Peti-Peterdi J. Quantitative imaging of basic functions in renal (patho)physiology. *Am. J. Physiol. - Ren. Physiol.* [published online ahead of print: 2006]; doi:10.1152/ajprenal.00521.2005
103. Aravindan N, Shaw A. Effect of furosemide infusion on renal hemodynamics and angiogenesis gene expression in acute renal ischemia/reperfusion. *Ren. Fail.* [published online ahead of print: 2006]; doi:10.1080/08860220500461229
104. Ashworth SL, Sandoval RM, Tanner GA, Molitoris BA. Two-photon microscopy: Visualization of kidney dynamics. *Kidney Int.* 2007; doi:10.1038/sj.ki.5002315
105. Kelly KJ, Sandoval RM, Dunn KW, Molitoris BA, Dagher PC. A novel method to determine specificity and sensitivity of the TUNEL reaction in the quantitation of apoptosis. *Am. J. Physiol. - Cell Physiol.* [published online ahead of print: 2003]; doi:10.1152/ajpcell.00353.2002
106. Peti-Peterdi J, Sipos A. A high-powered view of the filtration barrier. *J. Am. Soc. Nephrol.* 2010; doi:10.1681/ASN.2010040378
107. Peti-Peterdi J, Morishima S, Darwin Bell P, Okada Y. Two-photon excitation fluorescence imaging of the living juxtaglomerular apparatus. *Am. J. Physiol. - Ren. Physiol.* [published online ahead of print: 2002]; doi:10.1152/ajprenal.00356.2001
108. Hackl M et al. Tracking the fate of glomerular epithelial cells in vivo using serial multiphoton imaging in novel mouse models with fluorescent lineage tags. *Nat Med* 2013;
109. Burford JL et al. Intravital imaging of podocyte calcium in glomerular injury and disease. *J. Clin. Invest.* [published online ahead of print: 2014]; doi:10.1172/JCI71702
110. Rovira-Halbach G et al. Single nephron hyperfiltration and proteinuria in a newly selected rat strain with superficial glomeruli1. *Kidney Blood Press. Res.* [published online ahead of print: 1986]; doi:10.1159/000173097
111. Schiessl IM et al. Renal interstitial platelet-derived growth factor receptor-β cells support proximal tubular regeneration. *J. Am. Soc. Nephrol.* [published online ahead of print: 2018]; doi:10.1681/ASN.2017101069
112. Dunn KW, Sutton TA, Sandoval RM. Live-animal imaging of renal function by multiphoton microscopy.. *Curr. Protoc. Cytom.* [published online ahead of print: 2007];

doi:10.1002/0471142956.cy1209s41
113. Ritsma L et al. Surgical implantation of an abdominal imaging window for intravital microscopy. *Nat. Protoc.* [published online ahead of print: 2013]; doi:10.1038/nprot.2013.026
114. Bölke T et al. Data-adaptive image-denoising for detecting and quantifying nanoparticle entry in mucosal tissues through intravital 2-photon microscopy. *Beilstein J. Nanotechnol.* [published online ahead of print: 2014]; doi:10.3762/bjnano.5.210
115. Seri I, Aperia A. Contribution of dopamine2 receptors to dopamine-induced increase in glomerular filtration rate. *Am. J. Physiol. - Ren. Fluid Electrolyte Physiol.* [published online ahead of print: 1988]; doi:10.1152/ajprenal.1988.254.2.f196
116. Tulassay T et al. Effects of dopamine on renal functions in premature neonates with respiratory distress syndrome. *Int. J. Pediatr. Nephrol.* 1983;
117. Choi MR. Renal dopaminergic system: Pathophysiological implications and clinical perspectives. *World J. Nephrol.* [published online ahead of print: 2015]; doi:10.5527/wjn.v4.i2.196
118. Bellomo R, Kellum JA, Ronco C. Acute kidney injury. *Lancet* 2012; doi:10.1016/S0140-6736(11)61454-2
119. Lameire NH et al. Acute kidney injury: An increasing global concern. *Lancet* 2013; doi:10.1016/S0140-6736(13)60647-9
120. Makris K, Spanou L. Acute Kidney Injury: Definition, Pathophysiology and Clinical Phenotypes.. *Clin. Biochem. Rev.* 2016;
121. Thadhani R, Pascual M, Bonventre J. Acute Renal Failure. *N. Engl. J. Med.* [published online ahead of print: 1996]; doi:10.1056/NEJM199605303342207
122. Bellomo R, Ronco C, Kellum JA, Mehta RL, Palevsky P. Acute renal failure - definition, outcome measures, animal models, fluid therapy and information technology needs: the Second International Consensus Conference of the Acute Dialysis Quality Initiative (ADQI) Group. In: *Critical care (London, England)*. 2004:
123. Uchino S et al. Acute renal failure in critically ill patients: A multinational, multicenter study. *J. Am. Med. Assoc.* [published online ahead of print: 2005]; doi:10.1001/jama.294.7.813
124. Levy EM, Viscoli CM, Horwitz RI. The effect of acute renal failure on mortality: A cohort analysis. *J. Am. Med. Assoc.* [published online ahead of print: 1996]; doi:10.1001/jama.275.19.1489
125. Metnitz PGH et al. Effect of acute renal failure requiring renal replacement therapy on outcome in critically ill patients. *Crit. Care Med.* [published online ahead of print: 2002]; doi:10.1097/00003246-200209000-00016
126. Warren JD, Blumbergs PC, Thompson PD. Rhabdomyolysis: A review. *Muscle and Nerve* 2002; doi:10.1002/mus.10053

127. Grace PA. Ischaemia-reperfusion injury. *Br. J. Surg.* 1994; doi:10.1002/bjs.1800810504
128. Balakumar P, Rohilla A, Thangathirupathi A. Gentamicin-induced nephrotoxicity: Do we have a promising therapeutic approach to blunt it?. *Pharmacol. Res.* 2010; doi:10.1016/j.phrs.2010.04.004
129. Mendoza SA. Nephrotoxic drugs. *Pediatr. Nephrol.* 1988; doi:10.1007/BF00853443
130. Persson PB, Tepel M. Contrast medium-induced nephropathy: The pathophysiology. *Kidney Int.* [published online ahead of print: 2006]; doi:10.1038/sj.ki.5000367
131. Chatterjee PK. Novel pharmacological approaches to the treatment of renal ischemia-reperfusion injury: A comprehensive review. *Naunyn. Schmiedebergs. Arch. Pharmacol.* 2007; doi:10.1007/s00210-007-0183-5
132. Venkatachalam MA, Bernard DB, Donohoe JF, Levinsky NG. Ischemic damage and repair in the rat proximal tubule: Differences among the S1, S2, and S3 segments. *Kidney Int.* [published online ahead of print: 1978]; doi:10.1038/ki.1978.87
133. Frega NS, DiBona DR, Guertler B, Leaf A. Ischemic renal injury. *Kidney Int.* 1976;
134. Muller DN et al. NF-κB inhibition ameliorates angiotensin II-induced inflammatory damage in rats. In: *Hypertension*. 2000:
135. Weight SC, Bell PRF, Nicholson ML. Renal ischaemia-reperfusion injury. *Br. J. Surg.* 1996; doi:10.1002/bjs.1800830206
136. Sutton TA. Alteration of microvascular permeability in acute kidney injury. *Microvasc. Res.* [published online ahead of print: 2009]; doi:10.1016/j.mvr.2008.09.004
137. Singh P et al. Aberrant tubuloglomerular feedback and HIF-1α confer resistance to ischemia after subtotal nephrectomy. *J. Am. Soc. Nephrol.* [published online ahead of print: 2012]; doi:10.1681/ASN.2011020130
138. Hellberg POA, Kallskog TOK. Neutrophil-mediated post-ischemic tubular leakage in the rat kidney. *Kidney Int.* [published online ahead of print: 1989]; doi:10.1038/ki.1989.230
139. Tucker BJ, Blantz RC. Effect of furosemide administration on glomerular and tubular dynamics in the rat. *Kidney Int.* [published online ahead of print: 1984]; doi:10.1038/ki.1984.144
140. Peterson OW, Gabbai FB, Myers RR, Mizisin AP, Blantz RC. A single nephron model of acute tubular injury: Role of tubuloglomerular feedback. *Kidney Int.* [published online ahead of print: 1989]; doi:10.1038/ki.1989.298
141. Mason J, Takabatake T, Olbricht C, Thurau K, Pätz S. The early phase of experimental acute renal failure. III. Tubuloglomerular feedback. *Pflügers Arch. Eur. J. Physiol.* [published online ahead of print: 1978]; doi:10.1007/BF00581151
142. Yatsu T et al. Effect of YM435, a dopamine DA1 receptor agonist, in a canine model of

ischemic acute renal failure. *Gen. Pharmacol.* [published online ahead of print: 1998]; doi:10.1016/S0306-3623(98)00085-8
143. Baker RC et al. Methylprednisolone increases urinary nitrate concentrations and reduces subclinical renal injury during infrarenal aortic ischemia reperfusion. *Ann. Surg.* [published online ahead of print: 2006]; doi:10.1097/01.sla.0000225094.59283.b4
144. Matthijsen RA et al. Myeloperoxidase is critically involved in the induction of organ damage after renal ischemia reperfusion. *Am. J. Pathol.* [published online ahead of print: 2007]; doi:10.2353/ajpath.2007.070184
145. Bhalodia Y et al. Renoprotective activity of Benincasa cerifera fruit extract on ischemia/reperfusion-induced renal damage in rat. *Iran. J. Kidney Dis.* 2009;
146. Damianovich M et al. ApoSense: A novel technology for functional molecular imaging of cell death in models of acute renal tubular necrosis. *Eur. J. Nucl. Med. Mol. Imaging* [published online ahead of print: 2006]; doi:10.1007/s00259-005-1905-x
147. Sanz AB, Santamaría B, Ruiz-Ortega M, Egido J, Ortiz A. Mechanisms of renal apoptosis in health and disease. *J. Am. Soc. Nephrol.* 2008; doi:10.1681/ASN.2007121336
148. Bird JE et al. Ischemic acute renal failure and antioxidant therapy in the rat. The relation between glomerular and tubular dysfunction. *J. Clin. Invest.* [published online ahead of print: 1988]; doi:10.1172/JCI113498
149. Schießl IM, Hammer A, Riquier-Brison A, Peti-Peterdi J. Just Look! Intravital Microscopy as the Best Means to Study Kidney Cell Death Dynamics. *Semin. Nephrol.* 2016; doi:10.1016/j.semnephrol.2016.03.009
150. Haufe SE, Riedmüller K, Haberkorn U. Nuclear medicine procedures for the diagnosis of acute and chronic renal failure. *Nephron - Clin. Pract.* 2006; doi:10.1159/000091576
151. Sharfuddin AA, Sandoval RM, Molitoris BA. Imaging techniques in acute kidney injury. *Nephron - Clin. Pract.* 2008; doi:10.1159/000142929
152. Munger K, Baylis C. Sex differences in renal hemodynamics in rats. *Am. J. Physiol. - Ren. Fluid Electrolyte Physiol.* [published online ahead of print: 1988]; doi:10.1152/ajprenal.1988.254.2.f223
153. Mather A, Pollock C. Glucose handling by the kidney.. *Kidney Int. Suppl.* 2011; doi:10.1038/ki.2010.509
154. Barfuss DW, Schafer JA. Differences in active and passive glucose transport along the proximal nephron. *Am. J. Physiol. - Ren. Fluid Electrolyte Physiol.* [published online ahead of print: 1981]; doi:10.1152/ajprenal.1981.241.3.f322
155. Wright EM, Turk E. The sodium/glucose cotransport family SLC5. *Pflugers Arch. Eur. J.*

Physiol. 2004; doi:10.1007/s00424-003-1063-6
156. Bell GI et al. Molecular biology of mammalian glucose transporters. *Diabetes Care* [published online ahead of print: 1990]; doi:10.2337/diacare.13.3.198
157. Lee YJ, Lee YJ, Han HJ. Regulatory mechanisms of Na+/glucose cotransporters in renal proximal tubule cells. In: *Kidney International*. 2007:
158. Quamme GA, Freeman HJ. Evidence of a high-affinity sodium-dependent D-glucose transport system in the kidney. *Am. J. Physiol. - Ren. Fluid Electrolyte Physiol.* [published online ahead of print: 1987]; doi:10.1152/ajprenal.1987.253.1.f151
159. Thorens B, Lodish HF, Brown D. Differential localization of two glucose transporter isoforms in rat kidney. *Am. J. Physiol. - Cell Physiol.* [published online ahead of print: 1990]; doi:10.1152/ajpcell.1990.259.2.c286
160. Dominguez JH, Song B, Maianu L, Garvey WT, Qulali M. Gene expression of epithelial glucose transporters: The role of diabetes mellitus. *J. Am. Soc. Nephrol.* 1994;
161. Sacktor B. Sodium-coupled hexose transport. *Kidney Int.* [published online ahead of print: 1989]; doi:10.1038/ki.1989.202
162. Liang Y et al. Effect of canagliflozin on renal threshold for glucose, glycemia, and body weight in normal and diabetic animal models. *PLoS One* [published online ahead of print: 2012]; doi:10.1371/journal.pone.0030555
163. Manz F et al. Fanconi-Bickel syndrome. *Pediatr. Nephrol.* [published online ahead of print: 1987]; doi:10.1007/BF00849262
164. Mohandas Nair K, Sakamoto O, Jagadeesh S, Nampoothiri S. Fanconi-bickel syndrome. In: *Indian Journal of Pediatrics*. 2012:
165. Batool H, Zubaida B, Hashmi MA, Naeem M. Genetic testing of two Pakistani patients affected with rare autosomal recessive Fanconi-Bickel syndrome and identification of a novel SLC2A2 splice site variant. *J. Pediatr. Endocrinol. Metab.* [published online ahead of print: 2019]; doi:10.1515/jpem-2019-0235
166. Sharari S, Abou-Alloul M, Hussain K, Khan FA. Fanconi–bickel syndrome: A review of the mechanisms that lead to dysglycaemia. *Int. J. Mol. Sci.* 2020; doi:10.3390/ijms21176286
167. Karim S, Adams DH, Lalor PF. Hepatic expression and cellular distribution of the glucose transporter family. *World J. Gastroenterol.* [published online ahead of print: 2012]; doi:10.3748/wjg.v18.i46.6771
168. Freitas HS, D'Agord Schaan B, Seraphim PM, Nunes MT, Machado UF. Acute and short-term insulin-induced molecular adaptations of GLUT2 gene expression in the renal cortex of diabetic rats. *Mol. Cell. Endocrinol.* [published online ahead of print: 2005]; doi:10.1016/j.mce.2005.03.005

169. McCulloch LJ et al. GLUT2 (SLC2A2) is not the principal glucose transporter in human pancreatic beta cells: Implications for understanding genetic association signals at this locus. *Mol. Genet. Metab.* [published online ahead of print: 2011]; doi:10.1016/j.ymgme.2011.08.026
170. Mounien L et al. Glut2-dependent glucose-sensing controls thermoregulation by enhancing the leptin sensitivity of NPY and POMC neurons. *FASEB J.* [published online ahead of print: 2010]; doi:10.1096/fj.09-144923
171. Berry GT, Baker L, Kaplan FS, Witzleben CL. Diabetes-like renal glomerular disease in Fanconi-Bickel syndrome. *Pediatr. Nephrol.* [published online ahead of print: 1995]; doi:10.1007/BF02254185
172. Santer R et al. Fanconi-Bickel syndrome - A congenital defect of the liver-type facilitative glucose transporter. In: *Journal of Inherited Metabolic Disease*. 1998:
173. Mannstadt M et al. Fanconi-Bickel syndrome and autosomal recessive proximal tubulopathy with hypercalciuria (ARPTH) are allelic variants caused by GLUT2 mutations. *J. Clin. Endocrinol. Metab.* [published online ahead of print: 2012]; doi:10.1210/jc.2012-1279
174. Santer R, Hillebrand G, Steinmann B, Schaub J. Intestinal glucose transport: Evidence for a membrane traffic-based pathway in humans. *Gastroenterology* [published online ahead of print: 2003]; doi:10.1053/gast.2003.50009
175. Sansbury FH et al. SLC2A2 mutations can cause neonatal diabetes, suggesting GLUT2 may have a role in human insulin secretion. *Diabetologia* [published online ahead of print: 2012]; doi:10.1007/s00125-012-2595-0
176. Gopalakrishnan A, Kumar M, Krishnamurthy S, Sakamoto O, Srinivasan S. Fanconi-Bickel syndrome in a 3-year-old Indian boy with a novel mutation in the GLUT2 gene. *Clin. Exp. Nephrol.* [published online ahead of print: 2011]; doi:10.1007/s10157-011-0456-7
177. Roy M, Bose K, Paul DK, Anand P. Hypophosphatemic Rickets: Presenting Features of Fanconi—Bickel Syndrome. *Case Rep. Pathol.* [published online ahead of print: 2011]; doi:10.1155/2011/314696
178. Yamada K, Saito M, Matsuoka H, Inagaki N. A real-time method of imaging glucose uptake in single, living mammalian cells. *Nat. Protoc.* [published online ahead of print: 2007]; doi:10.1038/nprot.2007.76
179. Gaudreault N, Scriven DRL, Laher I, Moore EDW. Subcellular characterization of glucose uptake in coronary endothelial cells. *Microvasc. Res.* [published online ahead of print: 2008]; doi:10.1016/j.mvr.2007.04.006
180. Hato T et al. Novel application of complementary imaging techniques to examine in vivo glucose metabolism in the kidney. *Am. J. Physiol. - Ren. Physiol.* [published online ahead of print:

2016]; doi:10.1152/ajprenal.00535.2015
181. Pérez MD, Calvo M. Interaction of β-Lactoglobulin with Retinol and Fatty Acids and Its Role as a Possible Biological Function for This Protein: A Review. *J. Dairy Sci.* [published online ahead of print: 1995]; doi:10.3168/jds.S0022-0302(95)76713-3
182. Yang MC, Chen NC, Chen CJ, Wu CY, Mao SJT. Evidence for β-lactoglobulin involvement in vitamin D transport in vivo- role of the γ-turn (Leu-Pro-Met) of β-lactoglobulin in vitamin D binding. *FEBS J.* [published online ahead of print: 2009]; doi:10.1111/j.1742-4658.2009.06953.x
183. Power O, Jakeman P, Fitzgerald RJ. Antioxidative peptides: Enzymatic production, in vitro and in vivo antioxidant activity and potential applications of milk-derived antioxidative peptides. *Amino Acids* 2013; doi:10.1007/s00726-012-1393-9
184. Li M, Ma Y, Ngadi MO. Binding of curcumin to β-lactoglobulin and its effect on antioxidant characteristics of curcumin. *Food Chem.* [published online ahead of print: 2013]; doi:10.1016/j.foodchem.2013.02.099
185. Tai CS, Chen YY, Chen WL. β -Lactoglobulin Influences Human Immunity and Promotes Cell Proliferation. *Biomed Res. Int.* [published online ahead of print: 2016]; doi:10.1155/2016/7123587
186. Badr G, Ebaid H, Mohany M, Abuelsaad AS. Modulation of immune cell proliferation and chemotaxis towards CC chemokine ligand (CCL)-21 and CXC chemokine ligand (CXCL)-12 in undenatured whey protein-treated mice. *J. Nutr. Biochem.* [published online ahead of print: 2012]; doi:10.1016/j.jnutbio.2011.11.006
187. Belford DA et al. Milk-derived growth factors as serum supplements for the growth of fibroblast and epithelial cells. *Vitr. Cell. Dev. Biol. - Anim.* [published online ahead of print: 1995]; doi:10.1007/BF02634116
188. Teng Z, Xu R, Wang Q. Beta-lactoglobulin-based encapsulating systems as emerging bioavailability enhancers for nutraceuticals: A review. *RSC Adv.* 2015; doi:10.1039/c5ra01814e
189. Tojo A, Endou H. Intrarenal handling of proteins in rats using fractional micropuncture technique. *Am. J. Physiol. - Ren. Fluid Electrolyte Physiol.* [published online ahead of print: 1992]; doi:10.1152/ajprenal.1992.263.4.f601
190. Tojo A, Kinugasa S. Mechanisms of glomerular albumin filtration and tubular reabsorption. *Int. J. Nephrol.* 2012; doi:10.1155/2012/481520
191. Birn H, Christensen EI. Renal albumin absorption in physiology and pathology. *Kidney Int.* 2006; doi:10.1038/sj.ki.5000141
192. Russo LM et al. Impaired tubular uptake explains albuminuria in early diabetic nephropathy. *J. Am. Soc. Nephrol.* [published online ahead of print: 2009]; doi:10.1681/ASN.2008050503

193. Wagner MC et al. Proximal tubules have the capacity to regulate uptake of albumin. *J. Am. Soc. Nephrol.* [published online ahead of print: 2016]; doi:10.1681/ASN.2014111107
194. Endres BT et al. Intravital imaging of the kidney in a rat model of salt-sensitive hypertension. *Am. J. Physiol. - Ren. Physiol.* [published online ahead of print: 2017]; doi:10.1152/ajprenal.00466.2016
195. Eddy AA. Molecular basis of renal fibrosis. *Pediatr. Nephrol.* 2000; doi:10.1007/s004670000461
196. Goulam Houssen Y, Gusachenko I, Schanne-Klein MC, Allain JM. Monitoring micrometer-scale collagen organization in rat-tail tendon upon mechanical strain using second harmonic microscopy. *J. Biomech.* [published online ahead of print: 2011]; doi:10.1016/j.jbiomech.2011.05.009
197. Strupler M et al. Second harmonic imaging and scoring of collagen in fibrotic tissues. *Opt. Express* [published online ahead of print: 2007]; doi:10.1364/oe.15.004054
198. Luo Z et al. Widefield optical imaging of changes in uptake of glucose and tissue extracellular pH in head and neck cancer. *Cancer Prev. Res.* [published online ahead of print: 2014]; doi:10.1158/1940-6207.CAPR-14-0097
199. Rajaram N et al. Delivery Rate Affects Uptake of a Fluorescent Glucose Analog in Murine Metastatic Breast Cancer. *PLoS One* [published online ahead of print: 2013]; doi:10.1371/journal.pone.0076524
200. Kreshuk A, Zhang C. Machine learning: advanced image segmentation using ilastik. In: *Methods in Molecular Biology*. 2019: